Investigation of industrial gear oils: insights from complementary surface and subsurface characterisation

A thesis submitted to the University of Manchester for the degree of Doctor of Philosophy in the Faculty of Science and Engineering

2018

Aduragbemi J. Adebogun

School of Materials

Contents

List of Tables

List of Figures

Investigation of industrial gear oils: insights from complementary surface and subsurface characterisation

Abstract

A traditional approach to investigating gear oils involves running a tribo-test followed by characterisation of the tribofilm formed and the surface topography of the worn surface generated. While this provides insights into how gear oils minimise friction and wear, there has been much less focus on how gear oils influence the near-surface microstructure which plays a crucial part in the generation of wear debris.

Three industrial gear oils with different base oil-additive combinations were investigated under boundary lubrication sliding conditions. The aim was to understand how these gear oils and their associated tribofilms influence the near-surface metal layer of spheroidised and hardened AISI 52100 steels. Secondly, the study sought to understand how oil temperature and variable contact pressure influences the respective performance of the gear oils. Oil A contains molybdenum dithiophosphate (MoDTP) friction modifier, Oil B contains an amine molybdate complex friction modifier along with zinc dithiophosphate (ZDDP) antiwear additive. Oil C contains an antiwear/extreme pressure phosphonate additive combined with an ashless commercial gear oil package. To achieve this we evaluated the respective frictional performance of the oils by running sliding friction test using HFRR and SRV tribometers, followed by wear measurement on the wear scars generated. The nature of tribofilm formed was evaluated using complementary EDX and Raman spectroscopy techniques. To understand how the gear oils influence the near-surface layer, we measured the hardness-depth profile of the worn surfaces generated using the nanoindentaton technique and the near-surface microstructure was characterised using SEM-FIB.

The results showed that the gear oils and the tribofilms they formed influenced the degree of strain-hardening and the extent of grain refinement below the steel surfaces. Significant amount of strain-hardening and grain-refinement in the near-surface of the spheroidised AISI 52100 steel corresponded to higher levels of wear; whereas severe wear of the hardened AISI 52100 steel corresponded to friction-induced softening of the near-surface layer and the formation of adiabatic shear bands. The gear oil formulations and their respective tribofilms also influenced how friction-induced deformation is distributed in the near-surface microstructure. In addition, higher oil temperature and contact pressure increased surface-additive interaction and promoted the formation of tribofilms with better frictional performance. However, these conditions also reduced the oil film thickness, hence promoting near-surface hardening, degradation of the near-surface microstructure and ultimately corresponded to lower wear performance. It is also clear from this thesis that the performance of the gear oils depends on the contact pressure range and tribo-pair material, in particular the starting microstructures and hardness ratio. This reiterated the importance of testing gear oils with operating conditions similar to those of their industrial application.

Declaration

I, Aduragbemi Adebogun, declare that no portion of the work referred to in the thesis has been submitted in support of an application for another degree or qualification of this or any other university or other institution of learning

Copyright Statement

Acknowledgments

My Sincere appreciation goes to Professor Philip J. Withers for his excellent supervision and most importantly honest and sincere feedback aimed at ensuring that I perform at my highest potential. To Robert Hudson, your patience, guidance and mentorship throughout this period has been priceless, I'm truly grateful. To Prof. Allan Mathews, I was extremely glad you joined my supervisory team, thanks for your wonderful support ever since, excellent research advice and belief in my abilities. I would also thank Bart Winiarski, Etienne Bousser and Joanna Walsh for their mentorship and moral support particularly in the earlier years of my PhD studies. I would like to thank the following experimental officers in the school of materials: Ken Gyles, Ali Gholinia, Mike Faulkner, Andrew Forrest, John Warren and Gary Harrison. I'm grateful for the immense support I have received being a part of the BP-ICAM. I have had very useful conversations and received experimental help from ICAM researchers and BP mentors. The team at the ICAM hub have also been very supportive.

My time in Manchester as a PhD student has been wonderful thanks to my church family at the DLBC, Manchester and across the UK. To my pastor and my dear friends I appreciate you all for your care and concern throughout these years.

To my parents, you both have believed in me from the very beginning and being my biggest cheer-leaders. Words are not sufficient to express the depth of my gratitude to you two. Dr. Oluwarotimi Ismail, you've supported me in my academic journey over the past 10 years and played a vital role in my success. I'm eternally grateful.

My biggest appreciation goes to my maker, in whom I've always put my faith in, and from whom I have received the ability and courage to complete this PhD, to you be all the glory.

1 Introduction

1.1 Research motivation and objectives

Engineering systems such as wind turbines and heavy mining equipment such as transfer lines utilize industrial sized gearboxes. Gearboxes are designed to convert speed and torque between rotating parts. For example in wind turbines, the low speed/torque of the turbine blades are converted to high speed through a gearbox contained in the wind turbine nacelle. One of the common causes of downtime in wind turbines is due to failure of the gearbox. The main cause of gearbox failure is often bearing initiated [1]. Although wind turbines are designed to last for up to 20 years, often component failures (such as the bearings) happens well before then. The financial losses due to downtime for maintenance and repairs can be quite substantial.

Due to operating load and duty cycle, gears and bearings housed within the gearbox often have to withstand high loads, wide range of operating temperatures and varying ambient conditions (e.g. humid, dry, wet, dusty etc.). Modern industrial gear oils which lubricate both gears and bearings in the gearbox are formulated to handle extreme operating conditions. Under high load, low speed conditions, gears and rolling element bearings can experience direct metal to metal contact as opposing surfaces sliding against each other and causing micropitting [2]. Industrial gear oils have been designed to deal with extreme load contact and possess excellent antiwear properties. The key development focus for these lubricants over the last decade has been enhancing surface protection in rolling and sliding contact and extending a lubricant's life cycle. With increasing demands for smaller gearboxes with higher power rating, the performance demand on industrial gear oils is even higher. The gearbox components have to withstand higher loading conditions and operating temperatures. Higher temperature conditions can promote oxidation and thermal instability, yet the oils are expected to remain thermally stable and maintain high anti-oxidation performance.

The typical process of investigating industrial and automotive lubricants involves: evaluation of the friction and wear performance of the lubricant using a tribometer

and subsequent evaluation of wear. Forensic characterisation of the wear scar is conducted to investigate the wear mechanism(s) and the tribofilm generated on the surfaces. This approach has proven to be a reliable iterative method for improving lubricant formulation through empirical re-formulation and additive investigation.

In the boundary lubrication condition, where direct metal-to-metal contact occurs, the metal subsurface layer may potentially be transformed during the tribo-process. Earlier studies [3-5] using dry contact conditions have shown that surface transformation is accompanied by subsurface modification. A plastically deformed subsurface layer has been observed with most metals, depending on the original microstructure and severity of contact, the plastic layer usually consist of a gradient structure of nanocrystalline grains near the surface to micro-size grains towards the bulk (original) microstructure [6,7].

Formulated industrial oils usually contain friction and wear additives in addition to other additive classes such as anti-oxidants, detergents and dispersants. These additives are added to improve different aspects of the base oils. The friction and wear additives in particular play a dominant role in boundary lubrication conditions. Typically they interact with the surface to form a protective layer during a tribo-process which reduces metal-to metal contact and adhesion between the surface asperities of the opposing surfaces. Reduced surface interaction will reduce the transformation of the subsurface layer.

This project seeks to investigate how industrial gear oils and their associated tribofilms influence the nature and extent of subsurface transformation. Three industrial gear oils (Oil A, Oil B and Oil C) have been selected for this study. The research objectives include:

- Investigating the friction and wear performance of the gear oils by carrying out friction sliding test and examining the extent of wear forensically from the wear scar generated.
- Utilizing a combination of complementary chemical characterisation techniques to investigate the nature of tribofilm formed on the surface for the gear oils.

- Investigating how the gear oils and the nature of tribofilms they form influence the nature and extent of transformation (mechanical and microstructural) beneath the worn surface.

The research work has been divided into three research papers and tries to answer the following questions:

Paper 1 - Do the gear oils and their associated tribofilms influence the nature of transformation (mechanical and microstructural) beneath the metal surface?

Paper 2 - How does bulk oil temperature and varying contact pressure influence the nature of tribofilm formed for the different gear oils and how does this influence the extent of subsurface transformation?

Paper 3 - How does contact pressure range and tribo-pair material, in particular the starting microstructures and tribo-pair hardness ratio influence the tribological performance of the gear oil and the way they affect the transformation beneath the metal layer?

1.2 Structure of the thesis

This thesis is divided into seven chapters. Chapter 2 contains the literature review which can be sub-categorized in five sections. The first three sections cover tribology as a scientific field, the nature of surfaces and bearing steel. The fourth section contains a review of friction and wear additives, their associated tribofilms and tribological performance. The fifth section is a review on the influence of tribofilms on subsurface deformation.

Chapter 3 contains information on the lubricants used, the tribotests and the materials used. This chapter also describes the techniques and the procedure used to evaluate wear, characterize the tribofilms formed and also the subsurface changes.

Chapter 4, 5 and 6 are results chapters. They have been written up as manuscripts for journal publication and contain an abstract, introduction, materials and method section, results and discussion as well as a concluding section. The three result

chapters all contain information about the lubricant's tribological performance, the nature of tribofilms formed and their influence on the subsurface microstructures observed. Chapter 4 investigates the influence of the gear oils on the subsurface transformation. Chapter 5 investigates influence of oil temperature and contact pressure on tribological performance and subsurface transformations of spheroidised AISI 52100 steel. Chapter 6 investigates the performance of the gear oils in a higher contact pressure range (1.3 GPa - 2.8 GPa) and how they influence hardened AISI 52100 steel microstructure.

The overall conclusions of the whole thesis and potential further works to be carried out are outlined in Chapter 7.

2 Literature review

2.1 Tribology as a scientific field

Tribology is the study of interacting surfaces in relative motion and broadly covers the field of friction, wear and lubrication. When any two surfaces come in direct contact, friction occurs between the surfaces. Friction is the force opposing the relative motion between two surfaces. Wear is the gradual degradation of two surfaces in relative motion and manifested as material loss from one or both surfaces. There are different wear types or mechanisms as well as different factors that can influence the extent of wear. Lubricants are often primarily used to minimise friction and wear between interacting surfaces whether they are sliding or rolling relative to each other. They also serve other functions such as the removal of heat and wear debris. Tribology is multidisciplinary in nature; in most cases it requires some understanding of mechanical engineering (relating to engineering components such as bearings, gears, and engine pistons functionality), materials science (development of wear resistant materials) and also chemistry to design optimal lubricants for specific applications [1]. There is a constant need to advance our understanding of tribology with increasing demands such as development of novel materials, refractory operating conditions, and stringent environmental legislations.

2.2 Nature of surfaces

2.2.1 Surface layer

The surface of a solid material is the boundary between the solid and the environment. Metal surfaces consist of the different zones as shown in Figure 2.1 and can be divided broadly into two parts, the inner boundary layer and the outer boundary layer [8]. The inner boundary layer consists of a deformed layer and below this layer lays substrate or bulk material. The extent of deformation and the layer depth is determined by the final finishing step. The inner boundary layer is very important as its properties (such as hardness and residual stress) can be very different to the bulk material. There is also the outer layer which can be simply

categorized into reacted layer and adsorbed layer. The reacted layer refers to oxide layer that forms immediately after the final surface finishing step and results from reaction of the metal or alloy with oxygen in air. In environments containing sulphur or chlorine other layers can be formed; sulphide and chloride respectively. Following the formation of the reaction layer, molecules from the environment such as water molecules and other hydrocarbon molecules can adsorb unto the surface. The adsorbate is bonded weakly to the surface via weak van der Waals forces in which case they can be easily removed. Molecules can also attach strongly to the surface via covalent bond; more energy is required to break this bond.

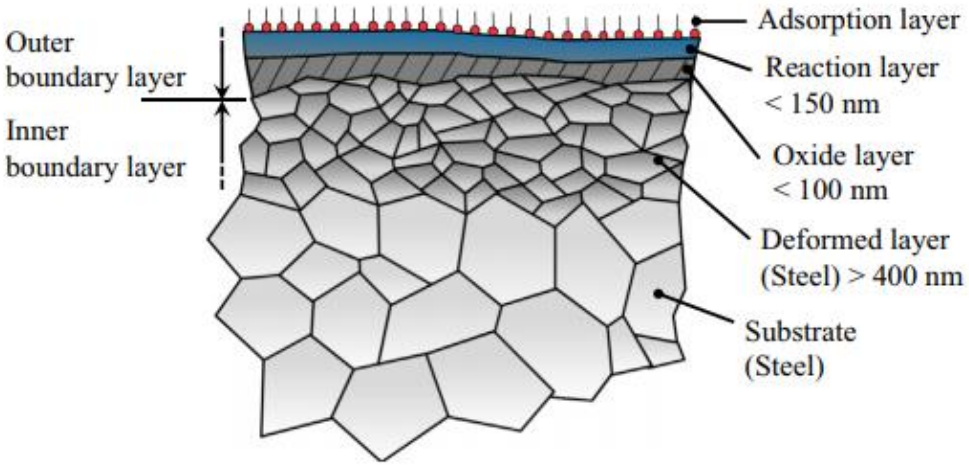

Figure 2.1: Simple schematic of metal surface layers [8]

2.2.2 Surface finishing

One of the final steps in manufacturing of engineering components such as gears and bearing involves surface machining. Figure 2.2 shows the typical manufacturing process sequence in which raw material is transformed to a finished product [9]. The raw material is formed or forged into the desired shape and size this is followed by machining process such as drilling and milling. Thereafter the near-finished component is heat treated to achieve the appropriate mechanical properties and microstructure. These processes are followed by the finishing stages which begin with grinding or hard turning; these processes are used to achieve the design dimensions and tolerance. Subsequently, the surface is 'super-finished'. Some of the common super-finishing techniques include: honing, lapping, polishing and isotropic finishing.

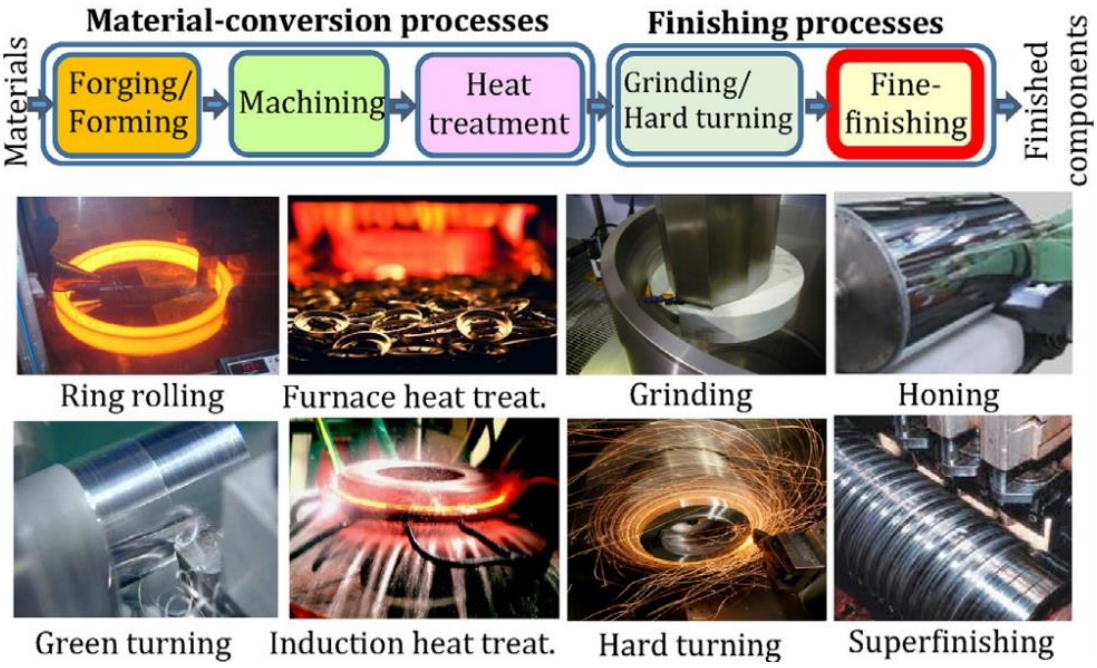

Figure 2.2: Typical manufacturing process sequence from raw material to finished product [9]

2.2.3 Surface texture

Surface texture can be defined as "the local deviations of a surface from a perfectly flat plane" [10] and it includes (1) roughness (2) waviness (3) lay and (4) flaw. These four terms helps to better distinguish surfaces which can look very different depending of the surface finishing process used. Figure 2.3 shows a schematic illustration of surface texture (roughness, waviness, lay and flaw), the top part (a) shows a *'flaw'* which is any unintended interruption of the surface profile this could be material defects or inclusion from prior processing stages. Part (a) also shows the surface *'lay'* which the direction of the predominant surface pattern. Surface *'waviness'* as shown in part (b) of Figure 2.3 is a periodic surface pattern with longer wavelength than surface *'roughness'* which is also a periodic surface pattern but with shorter wavelength and is super-imposed on the waviness. Surface roughness as illustrated in part (c) of Figure 2.3 is characterised by peaks or asperities and valleys. There are many different ways of defining surface roughness; this is discussed in the next section.

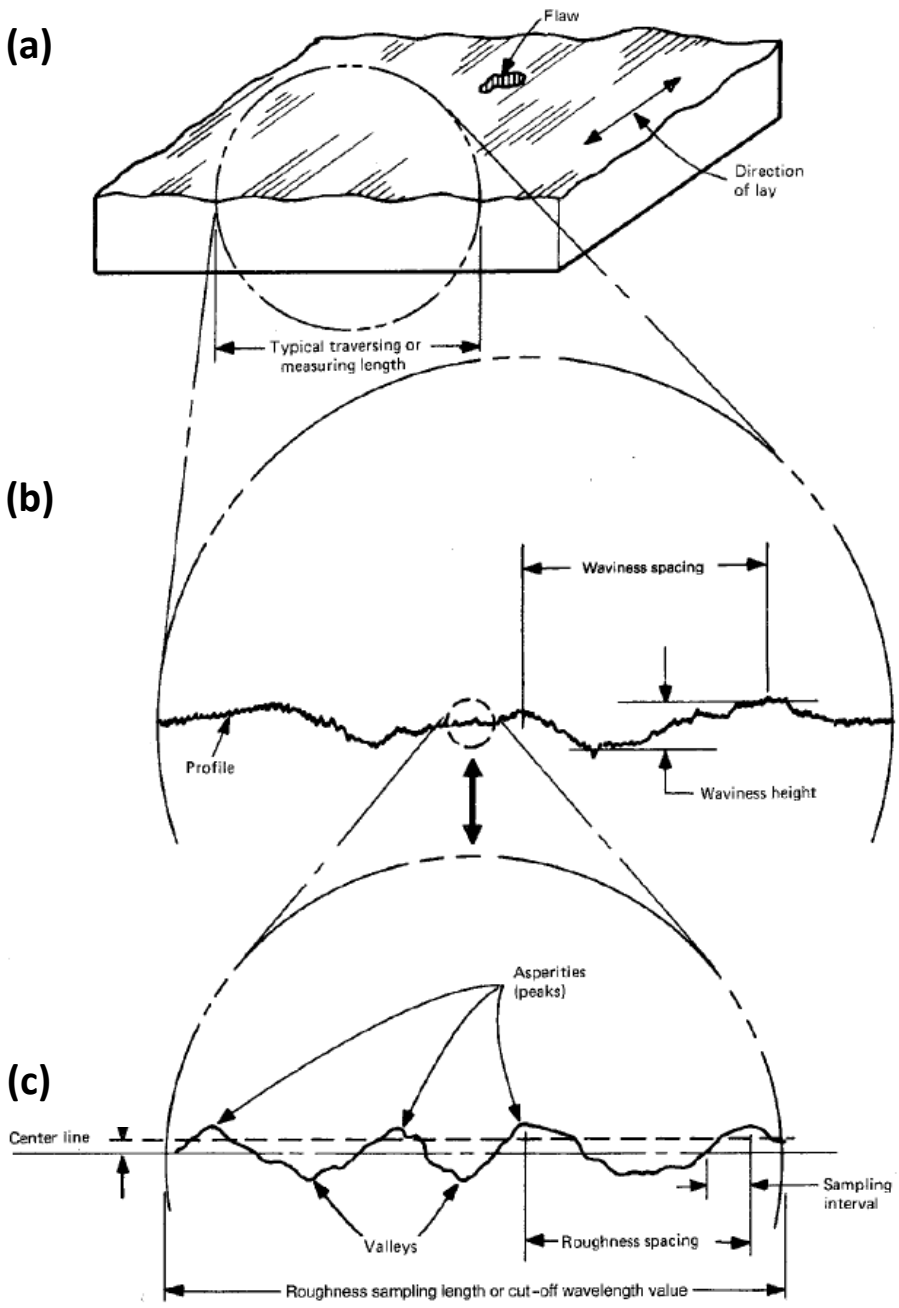

Figure 2.3: Schematic illustration of surface texture showing (a) surface flaw and lay (b) surface waviness (c) surface roughness [11]

2.2.3.1 Surface roughness parameters

Short-order deviations (roughness) can be defined in three major ways: using amplitude, spacing and hybrid parameters. The amplitude parameters measure the vertical characteristics of the surface deviation, the spacing parameter measures the horizontal characteristics and the hybrid simply combines the horizontal and vertical characteristics of the surface deviation. The amplitude parameters are

probably the most commonly used to describe surface roughness and are more relevant in this study. They include:

(a) Centre-line average roughness (R_a)
(b) Root-mean square roughness (R_q) and
(c) Ten-point height average roughness (R_z)

Centre-line heights average roughness (R_a) – is also known as centre line average (CLA) and is one of the most commonly used roughness parameter. It can be defined as the arithmetic mean of the absolute vertical deviation from a mean/centre line over one sampling length (l) as shown in Figure 2.4.

It can be represented mathematically as shown in Equation 2.1 below:

$$\mathbf{R_a} = \frac{\mathbf{1}}{\mathbf{l}} \int_{\mathbf{0}}^{\mathbf{l}} |\mathbf{y(x)}|\, \mathbf{dx} \qquad \textbf{Equation 2.1}$$

Although R_a is easy to define and measure, it is not sensitive to spatial distribution of surface height and as such could be misleading.

Root mean square roughness (R_q) – is the standard deviation of the surface height distribution (illustrated in Figure 2.4). Although similar to R_a, it is more sensitive to large deviation from the centre line.

It can be mathematically represented as shown in Equation 2.2 below:

$$\mathbf{R_q} = \sqrt{\frac{\mathbf{1}}{\mathbf{l}} \int_{\mathbf{0}}^{\mathbf{l}} \{\mathbf{y(x)}\}^{\mathbf{2}}\, \mathbf{dx}} \qquad \textbf{Equation 2.2}$$

Ten-point height average roughness (R_z) – Rz parameter illustrated in Figure 2.4 is the difference in height between an average of five highest peaks and the average of five lowest valleys in the assessment length of the profile. R_z parameter reduces error from the presence of random scratches on the surface.

The mathematical representation of R_z is shown in Equation 2.3 below:

$$\mathbf{R_z} = \frac{\mathbf{1}}{\mathbf{n}} \left(\sum_{\mathbf{i=1}}^{\mathbf{n}} \mathbf{p_i} - \sum_{\mathbf{i=1}}^{\mathbf{n}} \mathbf{v_i} \right) \qquad \textbf{Equation 2.3}$$

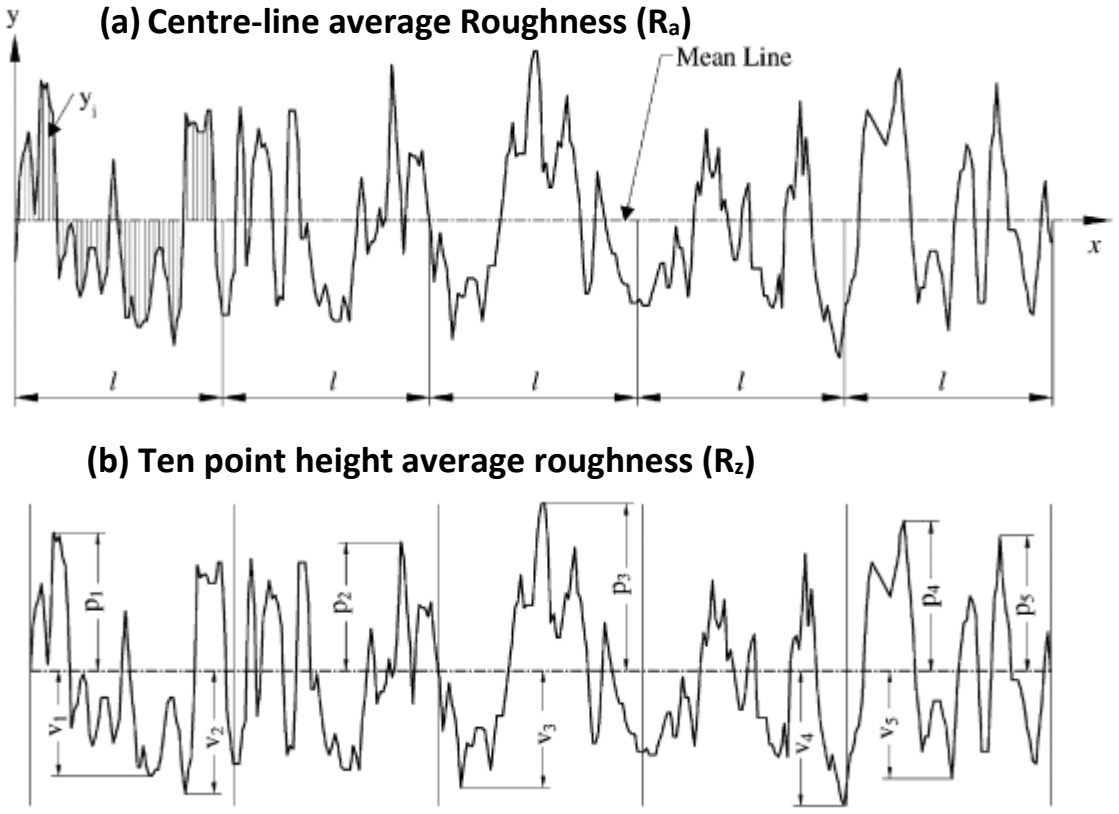

Figure 2.4: Definition of roughness parameters (a) centre-line average height roughness (R_a) and (b) ten-point height average roughness(R_z) [12]

2.3 Bearing steel

2.3.1 Introduction to bearings and material requirements

Industrial gear oils lubricate both gears and bearings in gearboxes. Focus is given here to the bearing steel since gearbox failures have been reported to initiate at the bearing in the majority of cases [1].

Bearings are tribological components that serve the purpose of separating machine parts and minimising contact between them as they rotate or move in contact with one another. In addition to reducing friction between surfaces, bearings also function to transmit/support load.

Bearing assemblies generally consists of four main components (See Figure 2.5). These are inner and outer rings (including the raceways on which the balls or roller roll), the rolling element (either balls or rollers) and the cage that separates the

rolling elements. Rolling element bearings are possibly the most widely used type of bearing, and are characterised by little or no sliding motion [13]. Roller bearings in comparison to ball bearings can have greater load carrying capacity due to the greater contact cylindrical roller make with the rings as opposed to balls. There are several types of rolling bearings: cylindrical roller bearings, tapered roller bearings, spherical roller bearings and cylindrical roller thrust bearings. Cylindrical roller bearings are the simplest of the roller bearing types and typically comprised of a pair of parallel thrust plates (washers); a row of cylindrical rollers sitting between the thrust plates and a cage retaining the rollers. This bearing type experiences a greater amount of sliding between the rollers and the raceway due to spin motion.

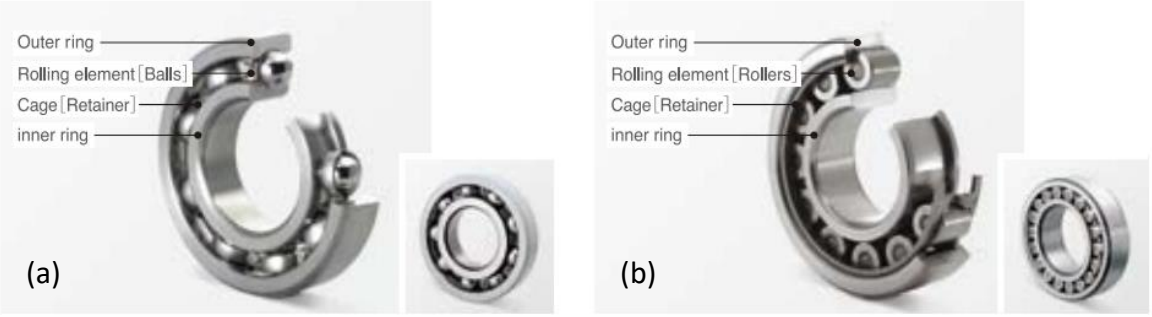

Figure 2.5: Main components of a (a) ball and (b) roller type bearings [14]

Bearing rings/raceways and rolling elements experience high stresses with small amount of sliding. Also the cages are subjected to tensile and compressive stresses and sliding contact with the rolling elements and either or both of the bearing rings. Therefore, the materials used for bearing rings, rolling element and cages are expected to have certain characteristic. They include:

Material characteristics required for bearing rings and rolling

- High rolling contact fatigue strength
- High hardness
- High wear resistance
- High dimensional stability
- High mechanical strength

Characteristics required for cage

Other important characteristics are shock and heat resistance and corrosion resistance. Steels are good candidates based on the requirements listed above and currently represent the materials of choice in the manufacturing of bearings [15].

100Cr6 and AISI 52100 steel alloys with basic composition of 1 wt.% C and 1.5 wt.% Cr are probably the most extensively used bearing materials [16,17]. They are used for the bearing rings (raceways) and the roller elements, while high strength brass or stainless steel is used for the cage. The chemical compositions of high-carbon bearing steels typically used for small and medium-size bearings are shown in Table 2.1.

Table 2.1: Chemical compositions of high-carbon bearing steels typically used for small and medium-size bearings [13]

	Chemical Composition (wt %)						
Grade	C	Si	Mn	Cr	Mo	P	S
DIN-100Cr6	0.90-1.05	0.15-0.35	0.25-0.40	1.40-1.65	0.30	≤0.025	≤0.025
NF-100Cr6	0.95-1.10	0.15-0.35	0.20-0.40	1.35-1.60	≤0.08	≤0.030	≤0.025
ASTM-A295-94 (52100)	0.98-1.10	0.15-0.35	0.25-0.45	1.39-1.60	≤0.10	≤0.025	≤0.025
ASTM-A535-85 (52100)	0.95-1.10	0.15-0.35	0.25-0.45	1.39-1.60	≤0.10	≤0.015	≤0.015

2.3.2 Manufacturing

The raw material used in the manufacturing of bearing rings and rollers is commonly supplied in a hot-rolled condition with pearlitic microstructure with proeutectoid cementite (emphasized by white line in Figure 2.6a), which forms at the prior austenite grain boundaries [15]; this is followed by annealing to spheroidise the cementite (Figure 2.6b). Subsequently, the material goes through forming processes before it is heat treated to enhance its mechanical properties.

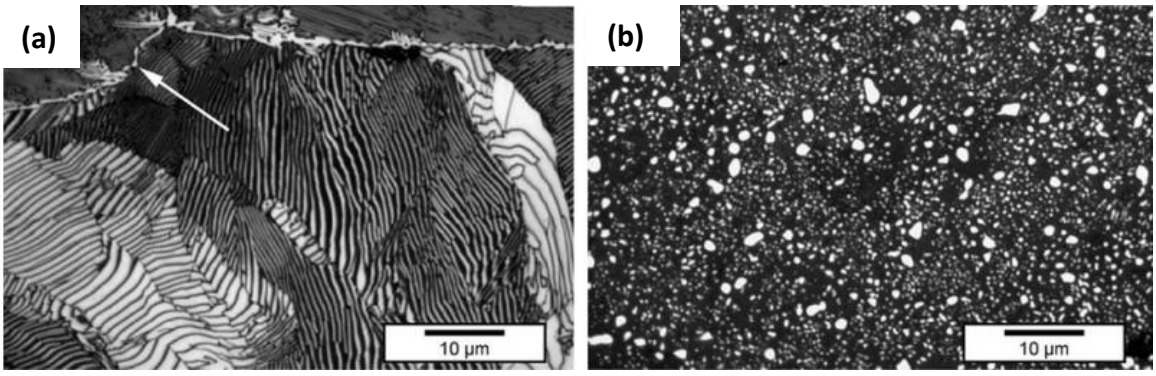

Figure 2.6: (a) Microstructure of 52100 steel as supplied, in a hot-rolled condition (white arrow indicates the presence of grain boundary cementite). (b) spheroidised structure after heat treatment [18].

The as-supplied material with a pearlitic microstructure has poor machinability. The aim of spheroidised annealing is to facilitate the forging and machining processes involved in making bearing raceways and rollers. Spheroidised annealing reduces the hardness of the material and results in a microstructure of relatively coarse cementite particles in a soft ferrite matrix (Figure 2.7b).

Bearings are usually through-hardened i.e. possessing sufficient hardness (Rockwell hardness of 58 to 64 HRC) such that the bearing is martensitic or bainitic through-out, from the surface to the core of the material. Alternatively some bearings are case or induction hardened; this is common with larger bearings, where the surface layer must be carburised to produce a martensitic case. In case-hardening, the carbon content of the surface layer of the steel alloy is increased, by prolonged exposure of the surface to a chemically reactive source at high temperature. Therefore on subsequent quenching, the surface layer is hardened. The soft core helps to slow down cracks emanating below sub-surface, from propagating to the surface while the hardened surface layer provide high contact load-carrying capability [19].

2.4 Sliding condition in industrial gears and bearings

Industrial gears and bearings experience both rolling and sliding conditions. Gears experience rolling and sliding contact along the gear tooth faces. Different sources of friction exist in a rolling element bearing. One of which is sliding friction between the rolling element and the raceway. For example, the axial cylindrical roller bearings in Figure 2.7 consisting of a housing and shaft washer, rollers mounted in a brass cage; the rollers are constrained to move on a circular running track, as a result, pure rolling condition exist only at the centre of the cylindrical rollers, with rising slippage zone towards the roller ends (Figure 2.8) [20]. Sliding wear arises in the slippage zone (positive and negative) during boundary lubrication regime, where direct contact exists between the rollers and the washer (or raceway). The amount of wear in the centre where pure sliding occur is significantly smaller than the slippage zone, also maximum wear occurs at the roller end, where sliding is greatest.

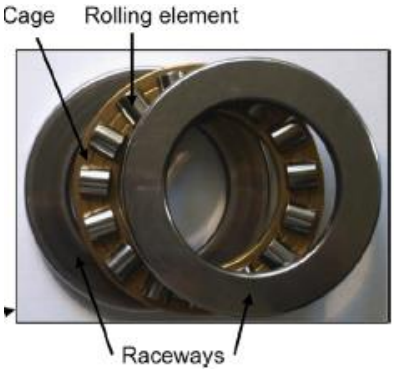

Figure 2.7: An Axial cylindrical roller bearing [20].

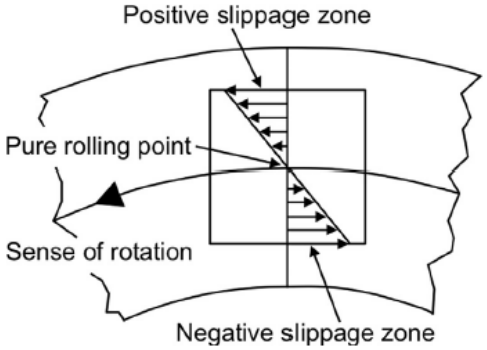

Figure 2.8: Illustration of slippage situation between a axial cylindrical roller thrust bearing drawn on a washer [20].

2.5 Surface and subsurface deformation wear mechanisms

This section elaborates on the process of wear debris generation in boundary sliding contact.

2.5.1 Surface ploughing

Ploughing is one of most dominant wear mechanisms in boundary sliding of metals [21-24]. Regardless of how highly polished or finely finished a surfaces is, it will inevitable still have asperities or peaks and depending on the application, some surfaces will have remnant grinding marks on them. In boundary lubrication contact, the original grinding marks and high asperities will support contact load. As sliding begins and progresses, the asperities and grinding marks deform plastically and can even fracture. During this stage often referred to as running-in, the asperities are flattened leaving a relatively smoother surface[21]. Akagaki observed that with several more passes, the flattened asperities can become extruded

forming a thin film layer[21]. This film layer becomes even more extruded and eventually breaks off to generate small wear particles of a few micrometres in length. Wear debris generated in the running-in stage can attach/lodge on the surfaces or remain in contact. Either way these wear debris and remnant asperities can generate ploughing marks or tracks usually on the softer surface. Komvopoulos, Saka and Suh found that ploughing grooves were formed on a smooth surfaces at the very beginning of sliding[22]. They also found that with more sliding passes, the number of ploughing tracks and track width increased [22].

2.5.2 Delamination wear

Another sliding wear mechanism that explains wear particle generation in metals is delamination wear proposed by Suh [3,25]. The wear process can be described in stages including: plastic deformation of the surface layer, crack nucleation and crack propagation. During sliding of surfaces, normal load and tangential loads are transferred through the surface by ploughing action. With more sliding cycles plastic shear deformation is induced and accumulates on the surface, particularly the softer one. Crack eventually nucleates below the surface and propagates as the deformation process continues. As cracks grow and join together, they propagate parallel to the surface at a depth which is a function of the material and the amount of surface friction. Eventually the crack shears to the surface and a long thin sheet "delaminates"[26,27].

Voids nucleation can occur around hard particles during sliding of surfaces; Jahanmir and Suh investigated delamination wear and found that voids can occur at a particular depth which is a function of the subsurface stress state, normal load and friction coefficient during sliding [5]. They postulate that in materials were void nucleation occurs readily around hard particles, it is likely crack propagation becomes the wear controlling mechanism. However, in some materials void nucleation is extremely difficult but crack propagation occurs easily. In this case, void nucleation is likely to be the controlling mechanism [5].

2.5.3 Micropitting wear

Micropitting is a contact fatigue damage in gears and bearings that reduces their lifetime and lead to expensive downtime and high maintenance costs [28].The Micro-pits are formed by the initiation and growth of micro-cracks as asperities between surfaces (e.g. bearing raceways and rollers) interact [29,28]. They alter the micro-geometry of gears, altering contact stress distribution. Figure 2.9 shows micropitting on a spherical roller bearing where low cycle micropitting starts off as two distinct wear track at the centre of the raceway (Figure 2.9a). Micropitting continues and more material is removed leading to severe wear (Figure 2.9b) and eventually the loss of design contact geometry. Low-cycle micropitting described in Figure 2.9 is caused by high amount of sliding between roller and raceway of the spherical roller main shaft bearing in a wind turbine gearbox [28]. There are many factors that influence micropitting and they include: surface finish, lubricant, load, material type, temperature, slide-to-roll ratio and speed. However Oila and Bull [30] found that applied load was the biggest effect on micropitting initiation whereas speed and slide-to-roll ratio played a major role in micropitting propagation.

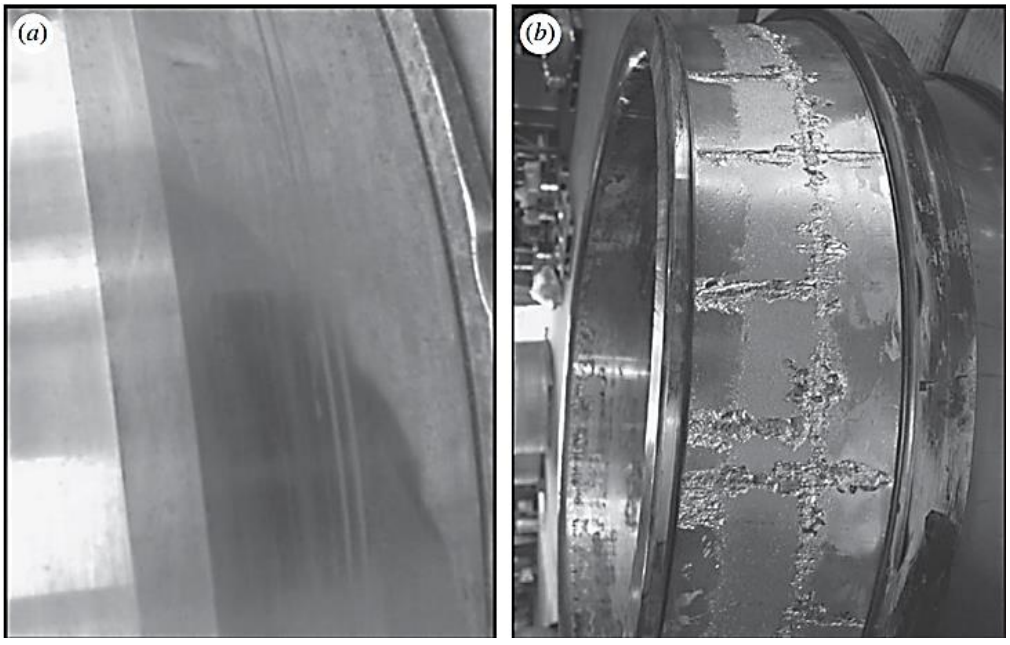

Figure 2.9: Micropitting of a spherical roller main shaft bearing (a) onset of micropitting wear at the centre of the inner raceway (b) advanced micropitting wear [28]

2.6 Industrial oils: their tribofilms and tribological performance

The scope of this section is on friction and wear additives: Antiwear/Extreme pressure additives and friction modifiers.

2.6.1 Antiwear and Extreme pressure additives

Antiwear (AW) and extreme pressure (EP) are commonly used in the formulation of a range of lubricants (including automotive and industrial applications) where there's a possibility of wear perhaps due to high loads creating a boundary lubrication situation. The term "antiwear" is used to refer to wear reduction at moderate loads and temperatures, while "extreme pressure" is used in high load and temperature conditions. They are jointly discussed here as they work with a similar mechanism in that they chemically interact with the metal surface to form a sacrificial film that prevents direct metal- to metal contact. These films are usually thick and tough and such are able to minimise wear, (compared to friction modifiers that form a soft film that can be easily sheared and serve the primary purpose of reducing friction between the rubbing surfaces). There are active and non-active AW/EP additives. Active AW/EP additives chemically react with the surface to form a sacrificial film and the non-active AW/EP additives form a film by deposition or deposition of by-products at the interface of the two surface [31]. Active AW/EP additives include compounds of sulphur, phosphorous. The non-active ones include compounds of boron, silicon and lead. One of the most common antiwear additives used in formulating industrial lubricants is zinc diakyldithiophosphate (ZDDP), to be discussed to a greater depth (vide infra). There are other classes of additives that serve more than one function, for example, overbased detergents such as calcium carbonate often perform well as antiwear additives [32]. In general, antiwear and extreme pressure additives adsorb unto surfaces, break up and react with nascent surface generated due to direct metal to metal sliding. The frictional heat and nascent surface facilitates the formation of protective film (tribofilm). Lubricant formulation containing sulphur based AW/EP additives typically form sulphides such as FeS, and $FeSO_4$, whilst those containing phosphorous compounds tend to form iron phosphates such as $FePO_4$ and $FePO_3$.

Zinc dialkyldithiophosphate (ZDDP)

One of the most effective and widely used anti-wear additives is zinc dialkyldithiophosphate (ZDDP), which also finds use as an anti-oxidant. ZDDP additives react with ferrous metal surfaces to form a tribofilm in mixed and boundary lubrication regimes, where wear is prevalent. ZDDP additives can act as extreme pressure additives (EP) under severe condition to form metal sulphides, which helps to reduce friction in sliding contact [33]. The interaction (rubbing) of ferrous metals with ZDDP additive results in the formation of a glassy phosphate film (Figure 2.10). The tribofilm is formed in sliding contact and does not develop in rolling contact or when the hydrodynamic film thickness exceeds the surface roughness. Research has shown that the films grow to about 50-150 nm thick on steel surfaces before they stabilise [34,35].

ZDDP films formed on steel surfaces appear initially as separate islands or patches which gradually grow with time and temperature to form an almost continuous, yet pad-like, structure (separated by deep valleys). The pads (Figure 2.10) have a layered structure comprising of a thin outer layer of zinc polyphosphate grading to a bulk film of pyro- or orthophosphate [36,37]. The outer layer of the pad contains Zn cations, however, more Fe and shorter chain phosphates can be observed directly on the metal surface [37]. Underneath the pads lies a sulphur-rich layer of zinc or iron sulphides (ZnS, FeS, FeS_2) [38,37,39].

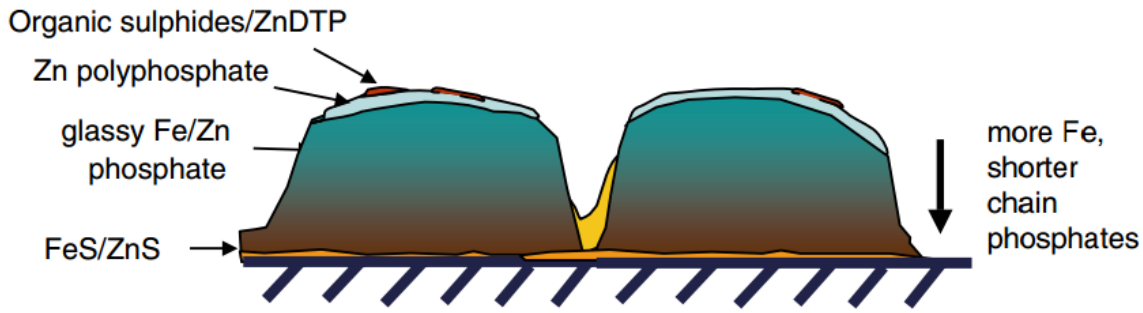

Figure 2.10: Structure and composition of a ZDDP glass film [33]

The mechanism of formation of ZDDP tribofilm is accepted to be thermal decomposition, where temperature plays a major role and the rate of decomposition of ZDDP is proportional to temperature [36,40,41,33,38]. However

more recent research studies have shown that formation of ZDDP tribofilm is promoted by shear stress [42,43]. Yin et al. [36] studied the chemical nature of tribofilms formed on steel surfaces lubricated by ZDDP using X-Ray absorption near edge structure (XANES) spectroscopy. They found that the higher temperature and load both increase the rate of ZDDP decomposition. ZDDP decomposed faster as temperature was increased from 100 ^{o}C to 150 ^{o}C and 200 ^{o}C. Also unchanged ZDDP present in the oil initially, completely decomposed at 150 ^{o}C. Similarly, increased load, from 40 N to 400 N also lead to decomposition of all the ZDDP detected on the film surface. Chao et al. [40] explains that with increase in temperature, chemical reactivity causes the film formation rate to increase, at the same time the film removal rate is also increased. However, when the rate of film formation exceeds the removal rate, the film grows, but becomes thinner when removal rate exceeds the formation rate. At low bulk oil temperature, a thin durable film is formed, at moderate temperatures; the film grows (due to lower durability) but then diminishes above a certain load due to lower durability. At higher temperature, a thin film is formed and is not able to sufficiently reduce friction and wear even at low loads. In the same study conducted by Yin et al. [36], the chemical nature of tribofilm found by ZDDP additive varies with temperature. At low temperature of about 100 ^{o}C, low chain phosphate and sulphide (Sulphur species) are formed in the film and on the other hand at 200 ^{o}C, shorter chain phosphate and sulphates are formed on the surface.

Onodera et al [44] modelled the effect of pressure and shear on ZDDP tribochemical reaction and their result showed that besides temperature the other key driving force was increase in molecular shearing and entropy. Zhang and Spikes [43] in their investigation of ZDDP tribofilm formation found that ZDDP film can form without solid-solid rubbing contact in which case film formation is driven by applied shear stress. Their work concluded that shear stress present in high-pressure contact can reduce the thermal activation energy for ZDDP by at least half. This highlight the role of shear stress in ZDDP tribofilm which have since been confirmed by studies conducted by Dorgham et al [42] in which they concluded that

the formation of ZDDP tribofilm is a thermally activated process accelerated by shear.

Attributes of ZDDP tribofilm

- Morphology of ZDDP tribofilm - ZDDP tribofilm is patchy in a nature. Aktary et al [45] describes the evolution of ZDDP tribofilm morphology on steel in three stages: (a) nucleation of an active surface which leads to the formation of segregated islands. (b) With further tribo-action, the islands join together causing the film to spread over a larger fraction of the surface. (c) In the third stage, following further rubbing, the islands are divided into smaller densely packed structures.
- ZDDP tribofilm has a graded structure. Ye et al [46,47] demonstrated that ZDDP tribofilm is friction-functionally graded. Scratch test was conducted on a surface containing ZDDP tribofilm. Friction coefficient was measured as a function of scratch depth. The result showed that friction coefficient measured was highest at the film surface and decreased with depth.
- Stability and durability – Once formed on the rubbing surfaces ZDDP tribofilms are stable and durable [48]. Parsaeian et al found that the durability of ZDDP tribofilm evolves in time, becoming more durable [49]. The increased durability was linked to the change in the chemistry of the tribofilm with time. Longer chain polyphosphates are converted to shorter chain derivatives which also accounts for their increased durability [49]. However, the tribofilm's durability was also found to be influenced by the operating temperature; as temperature increases the tribofilm becomes less durable.
- ZDDP tribofilms comprised of longer alkyl chain length, have been linked to an increase in friction and lower wear[50].
- Tribofilm induction time – ZDDP tribofilms form relatively quickly, which might contribute to its excellent wear performance [45,51]. For example in the study conducted by Zhang et al, ZDDP phosphate film was formed after a short rubbing time of 10s, however the film was barely uniform. After 30 s of rubbing, antiwear pads were formed and a well-developed film was formed after 30 min of rubbing time [51].

2.6.2 Friction modifiers

Friction modifiers as their name implies are chemical compounds added to lubricants with the goal of achieving excellent frictional performance. Detailed reviews of friction modifiers have been published by Tang and Li [52] in 2007 and by Hugh Spikes [53] in 2015. There are three main types of friction modifiers: oil-soluble organomolybdenum compounds, organic friction modifiers and nanoparticles. However, this review will focus on organomolybdenum compounds.

Organomolybdenum compounds can be further classified into:

1. Sulphur and phosphorus containing (e.g MoDTP)
2. Sulphur containing and phosphorus free (e.g MoDTC)
3. Sulphur and phosphorous free (e.g Molybdate ester)

The friction-reducing ability of organomolybdenum friction modifiers is commonly attributed to the formation of MoS_2 on the contacting surfaces [54,55]. Friction coefficient values recorded with Mo-based friction modifiers are in the range of 0.04 – 0.075 [54]. Organomolybdenum decompose during rubbing of surface to form MoS_2. MoS_2 forms on load bearing asperities and as such is not always evenly distributed on the rubbing surface. Organomolybdenum compounds interact with the surface to form nanosized 'single' sheets on the surface and friction reduction happens as a result of sliding between the sheets[56]. Using high resolution TEM, Grossiord et al [56] showed that the tribofilm formed contained highly-dispersed MoS_2 sheets in a carbon matrix.

Molybdate ester friction modifiers without the sulphur and phosphorous are not able to effectively reduce friction however, when combined with ZDDP additive which contains sulphur and phosphorus, their friction and wear properties have been shown to significantly improve.

The effect of combining organomolydenum friction modifiers with antiwear additive, ZDDP have been investigated, most of these studies [57] have reported a synergistic effect with regards to friction and wear performance. With formulated containing Mo-based friction modifier and ZDDP, the additives are bound to compete for adsorption on the metal surface. Muraki et al [58] showed that during

the running in process, ZDDP preferentially forms decomposition products and coexists with decomposition products of MoDTC. The synergy between MoDTC and ZDDP may be attributed to the ability of ZDDP to promote the formation of MoS_2 and enhance wear resistance [57].

Increasing temperature and pressure of formulated oils containing a molybdenum based friction modifier increases the rate of formation of low friction tribofilm formation form lubricant containing MoDTC and hence thicker tribofilm [48]. At low temperature (30 °C), MoDTC is not very effective in reducing friction; one reason for this could be due to the formation of high friction Mo oxides formed in the wear scar [50]. Poor frictional performance at low temperature has been attributed to the presence of MoO_3[50]. Khaemba et al [55] attributed high friction at low temperature (20 °C) to the formation of MoS_x and $FeMoO_4$. Low friction tribofilms formed from MoDTC once formed need continuous replenishment of MODTC additive to maintain low friction and are not stable otherwise [48]. Morina and Neville found that compared with ZDDP tribofilm, MoS_2 tribofilm formed from MoDTC is much less stable and can be easily removed from the contact [48].

2.7 Influence of industrial oils and their tribofilms on subsurface deformation

The previous section discussed friction and wear additives particularly organomolybdenum friction modifiers and ZDDP additives. Section 2.9 was focused on their tribological performance and the nature of tribofilms they form. In addition the influence of temperature and pressure on tribofilm formation and tribological performance was discussed.

One of the main goals of this project is to investigate the influence of surface films (tribofilms) on the nature of subsurface transformation. The following questions are explored based on outstanding questions in the current knowledge:

(a) Can surface films influence the nature and extent of subsurface deformation?

AND

(b) What are the mechanisms by which surface films influence the extent of subsurface deformation?

In boundary lubrication conditions, tribofilm formation plays a vital role in minimising friction and wear. The combination of additives in a gear oil determines several aspects of the tribofilm formed including: chemistry, mechanical properties (shear strength and hardness) and how quickly it forms in the contact. This section discusses the influence of formulated oils on the near-surface microstructure.

The idea that surface films can influence the subsurface structure of metals dates back as far as the early 1990s. One of the earliest researchers to propose this idea was Rehbinder [59]. He and his colleagues found that a non-polar paraffinic lubricant containing oleic acid increased the plastic flow of a metal under stress. Likewise, Buckley [60] also found that the presence surface active species such as oleic acid and dimethyl sulfoxide increased resistance to sliding deformation of calcium fluoride.

There have been more recent studies on the effect of formulated oils and their associated tribofilms on subsurface deformation. These studies show that the tribofilm formed during boundary lubrication influences the metallurgical response of metal surfaces [61,62]. Wear protection is jointly influenced by the protective surface film and the near-surface layer (sometimes referred to as tribo-mutation layer), both of which are influenced by the lubricant additive formulation. [62,63]

Other mechanisms have been proposed by which surface films influence subsurface deformation [61,64]. Cao et al [61] reported that the boundary film influenced the plastic deformation (hindering or promoting grain rotation) and thus influencing the extent of wear. The authors suggests that a softer film would allow for grain rotation, whereas a harder film will hinder grain rotation hence more strain is accumulated in the near-surface and consequently more wear. The reverse is the case when a softer film is formed which allows grain rotation and less strain accumulated in the metal. They investigated two formulated oils with different tribofilms (iron-zinc oxide film and calcium rich film) which produced similar level of friction coefficient in boundary lubrication sliding but had different metallurgical

response below the metal surface. Wang et al [64] propose that stable tribofilms that suppress or reduce annihilation of stacking faults promotes strain accumulation in the subsurface and consequently more severe wear occurs.

Another mechanism by which surface films have been proposed to influence subsurface deformation and wear is the level of friction they provide on the surface. The magnitude of friction coefficient provided by a formulated lubricant can determine the level of subsurface deformation and wear mechanism [24]. Jahanmir [24] proposed the idea of a specific threshold of friction coefficient determining the wear mechanism. Below this threshold, wear mechanism was primarily by deformation of surface asperities but above this threshold hold, wear was driven by ploughing, and delamination wear. Frictional energy generated in boundary lubrication is dissipated mostly as heat and raises the surface temperature. The rest is used up in the generation of wear particles, tribofilm formation and shearing, and transformation of subsurface structure (plastic deformation) [65]. Although two different oils might generate the same level of friction coefficient at the surface, under the same tribosystem condition, the energy might not be partitioned into the other simultaneous processes taking place (wear, tribofilm formation and subsurface deformation) in the same way [61,63].

2.8 Conclusions

In boundary lubrication condition, the friction modifiers and antiwear/extreme pressure additives play a vital role in lowering friction and preventing excessive wear. Additives added to formulated oils influence the chemistry of tribofilm formation and thus friction and wear performance. The tribofilm chemistry and tribological performance of gear oils are influenced by operating temperature and the applied load/pressure. Many of the studies on industrial gear oils have been focused on tribofilm formation, tribological performance and the influence of operating temperature and pressure. While these studies have led to better understanding of the oils, there have been limited studies on the influence of gear oils, their associated tribofilms on subsurface changes. The idea that surface films could influence surface and subsurface transformation dates back to the early 1900s, however, only few studies have focused on this since then.

From the studies reviewed on the influence of tribofilms on subsurface transformation, two main premises emerge. One is that the mechanical properties and the stability of the tribofilm (hardness in particular) could influence the process of plastic strain accumulating below the surface. The other premise is that the tribofilm form influence the level of frictional energy generated at the surface and that less friction would limit damage to the surface and greater levels of friction would translate to plastic deformation at the surface and significant plastic strain accumulating subsurface leading to a more severe wear.

This thesis explores the premise that industrial gear oils and their associated tribofilms influence the extent of subsurface deformation and consequently wear. In addition, we investigate the influence of oil temperature and contact pressure on subsurface deformation of AISI 52100 steel in both spheroidised and hardened states.

3 Materials and methods

3.1 Lubricants

The lubricants studied in this thesis are three industrial gear oils provided by BP International Ltd. The lubricants are commercially available industrial gear oils used in different applications. For the sake of confidentiality, the gear oils have been given generic name: Oil A, Oil B and Oil C. Figure 3.1 shows the as-received oils.

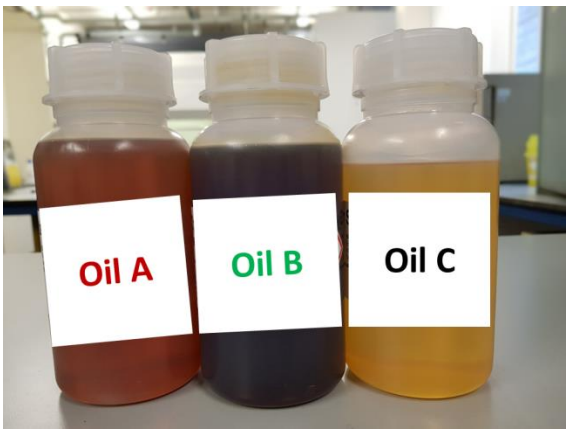

Figure 3.1: Investigated gear oils: Oil A, Oil B and Oil C

3.1.1 Application

Oil A is typically used in wind power gearboxes, Oil B in heavy industrial applications such as mining gearboxes and Oil C is multifunctional gear oil that can be used in different applications.

3.1.2 Lubricant formulation and rheological properties

The three oils are of the same viscosity grade of 320 and have the same kinematic viscosity of 320 ± 32 mm^2/s at 40 °C. Oils A, B and C all have different base oil-additive mix as shown in Table 3.1 and as were chosen with the expectation that they will form different protective films (tribofilm) with distinct tribological performance (friction and wear). Oil A and C were formulated using synthetic base oil consisting mainly of the polyalphaolefin (PAO) type, whereas Oil B was formulated using a group 1 mineral base oil.

Table 3.1: Base oil and additive combinations for oils A, B and C

	Oil A	Oil B	Oil C
Base oil	Polyalphaolefin (> 90%)	Group 1 base stock mix (> 85%)	Polyalphaolefin (> 80%) Alkylated Naphthalene (5-15%)
Additives	Molybdenum Dithiophosphate (MoDTP) - (< 5%)	Amine Molybdate complex (< 5%) ZDDP (< 5%) Sulphurised - extreme pressure additive	Phosphonate (< 1%) Commercial gear oil package (< 5%)
	Mixed sulphonates – corrosion inhibitor (< 0.5%) Copper - corrosion inhibitor (< 0.5%)	Sulphonate mix – corrosion inhibitor (< 5%)	
	Antifoam –trace	Antioxidant (< 1%) Methacrylate polymer – pour point depressant (< 5%)	Antifoam -trace

3.2 Tribotesting

The frictional performance of the gear oils were tested using two different tribometers: High Frequency Reciprocating Rig (HFRR) and Schwing–Reib–Verschleiss (SRV®). The HFRR tribometer was used to conduct sliding tests with results presented in Chapters 4 and 5. The SRV tribometer was used to conduct sliding tests with results presented in Chapter 6. Although the HFRR and SRV are both used to conduct reciprocating sliding tests, they were used complementarily to perform a wider range of contact pressure tests. Low contact pressure tests (0.44 GPa – 0.94 GPa) were performed using the HFRR tribometer and higher contact pressure tests (1.3GPa – 2.8 GPa) were performed using the SRV tribometer.

3.2.1 HFRR (high frequency reciprocating rig)

The HFRR tribometer is a product of PCS instruments, London, England. The AutoHFRR software provided by the manufacturer is used to program the

experiments. Images of the HFRR unit and the test specimens used are shown in Figure 3.2. The ball and disks are firmly secured in the upper and lower specimen holders respectively. The disk is fully submerged by the test lubricant. The lower specimen holder seats on a heating block and raises the temperature of the lubricant to the set temperature. A weight is applied on the ball via a string and oscillates on the disk at the set frequency and stroke length. The main properties of the HFRR specimens and the testing parameters are shown in Tables 3.2 and 3.3 respectively.

Table 3.2: Main properties of HFRR specimens

	Material	Diameter (mm)	Hardness (GPa)	Surface roughness (μm)
Ball	AISI 52100 steel	6	3.3 ± 0.2	≈ 0.02
Disk	AISI 52100 steel	10	11.7 ± 1	< 0.05

Table 3.3: Testing parameters for the HFRR tests.

Load (N)	0.98 – 9.8
Average contact pressure (GPa)	0.44 – 0.94
Temperature (°C)	30 - 120
Stroke length (mm)	1
Frequency (Hz)	50
Test duration (min)	5 - 120

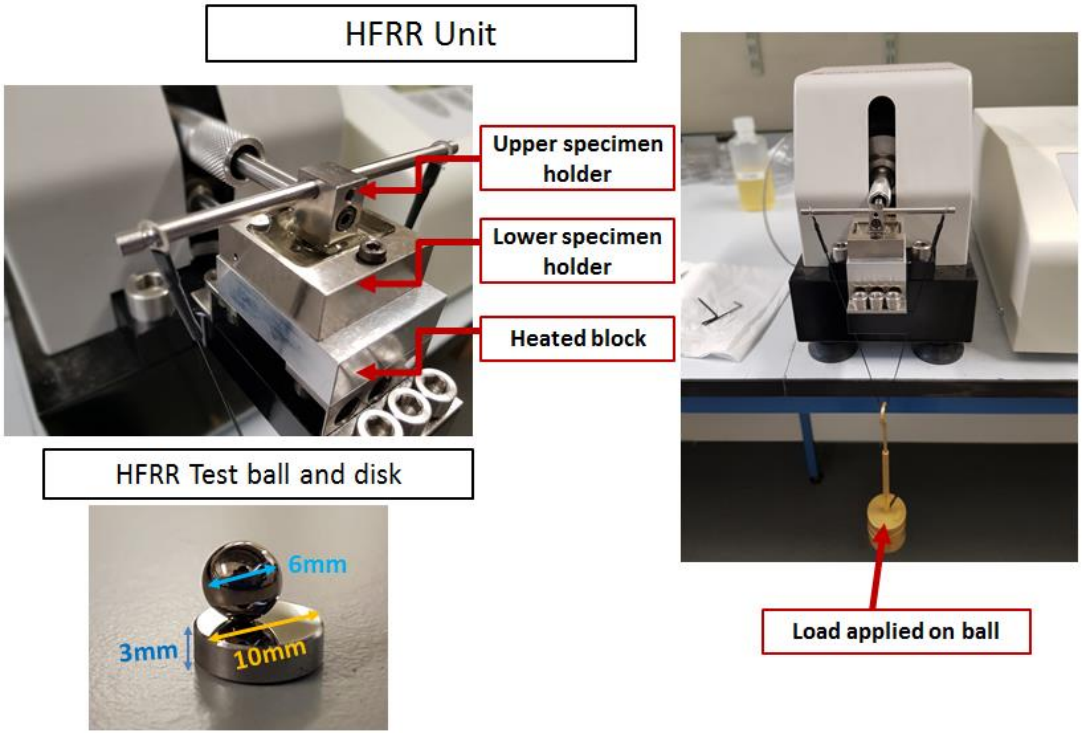

Figure 3.2: HFRR unit and test specimens (ball and disk)

3.2.2 SRV tribometer

The Schwing–Reib–Verschleiss (SRV®) tribometer (Optimol Instruments Prüftechnik GmbH, Munich, Germany) is a ball-on-disk test which has a higher contact pressure range compared to the HFRR test. The SRV test unit and specimen are shown in Figure 3.3. The main properties of the SRV test specimens and the testing parameters are shown in Tables 3.4 and 3.5 respectively.

Table 3.4: Main properties of HFRR specimen

	Material	Diameter/thickness (mm)	Hardness (GPa)	Surface roughness (µm)
Ball	AISI 52100 steel	24 ± 0.5/7.8± 0.5	3.3 ± 0.2	0.46 ± 0.14
Disk	AISI 52100 steel	17.3	11.7 ± 1	0.75± 0.06

Table 3.5: Testing parameters for the HFRR tests.

Load (N)	200 – 2000
Average contact pressure (GPa)	1.3 -2.8
Temperature (°C)	30 - 120
Stroke length (mm)	1.5
Frequency (Hz)	33
Test duration (min)	120

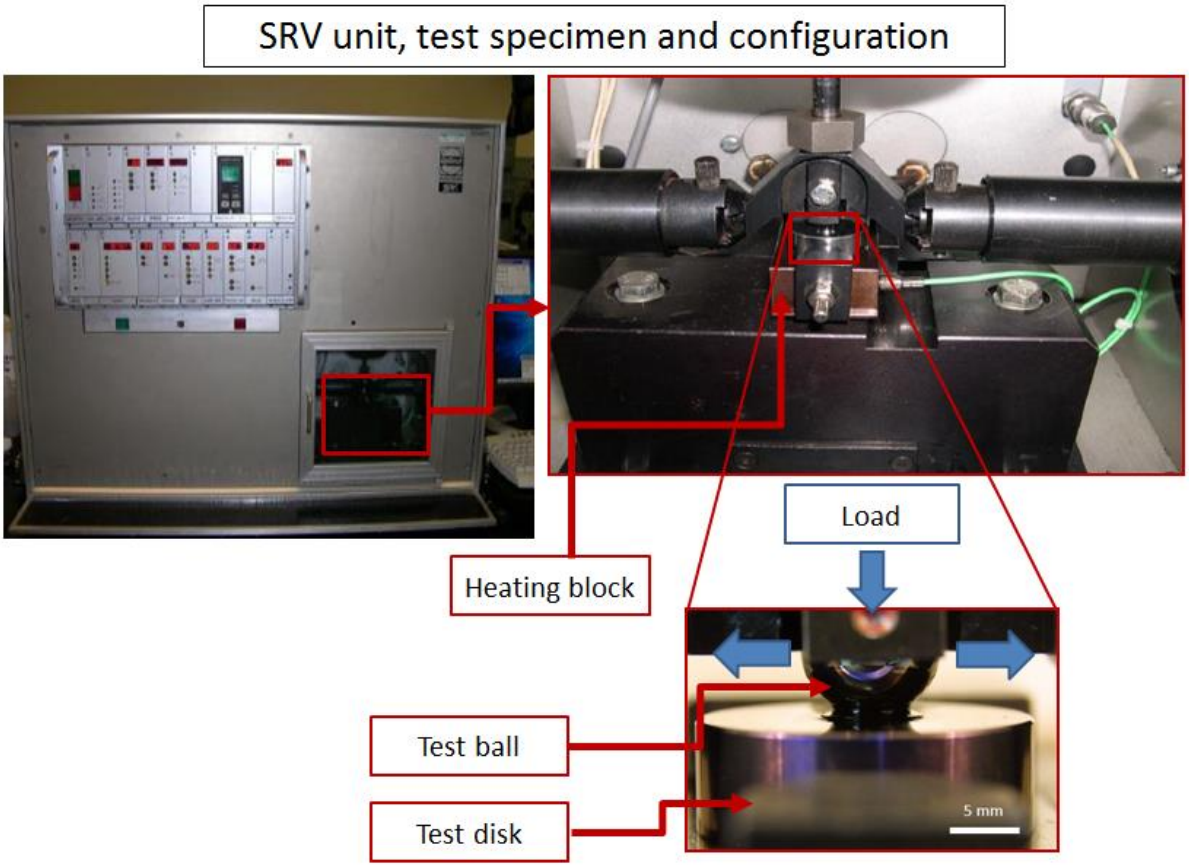

Figure 3.3: SRV unit, test specimens and configuration

3.3 Wear and surface roughness measurement

Following sliding test with the tribometer, the wear performances of the gear oils is evaluated by carrying out wear measurements on the wear scars generated.

A Keyence VK- X200 3D confocal laser microscope was used so scan the wear scar 3D profile from which post processing software VK analyser (provided by the manufacturer of the instrument – Keyence) was used to calculate wear volume. In addition, the Keyence system was used to calculate surface roughness of the test balls and disks prior to sliding test and after the sliding test. The setup of the KEYENCE LSM is shown in Figure 3.4.

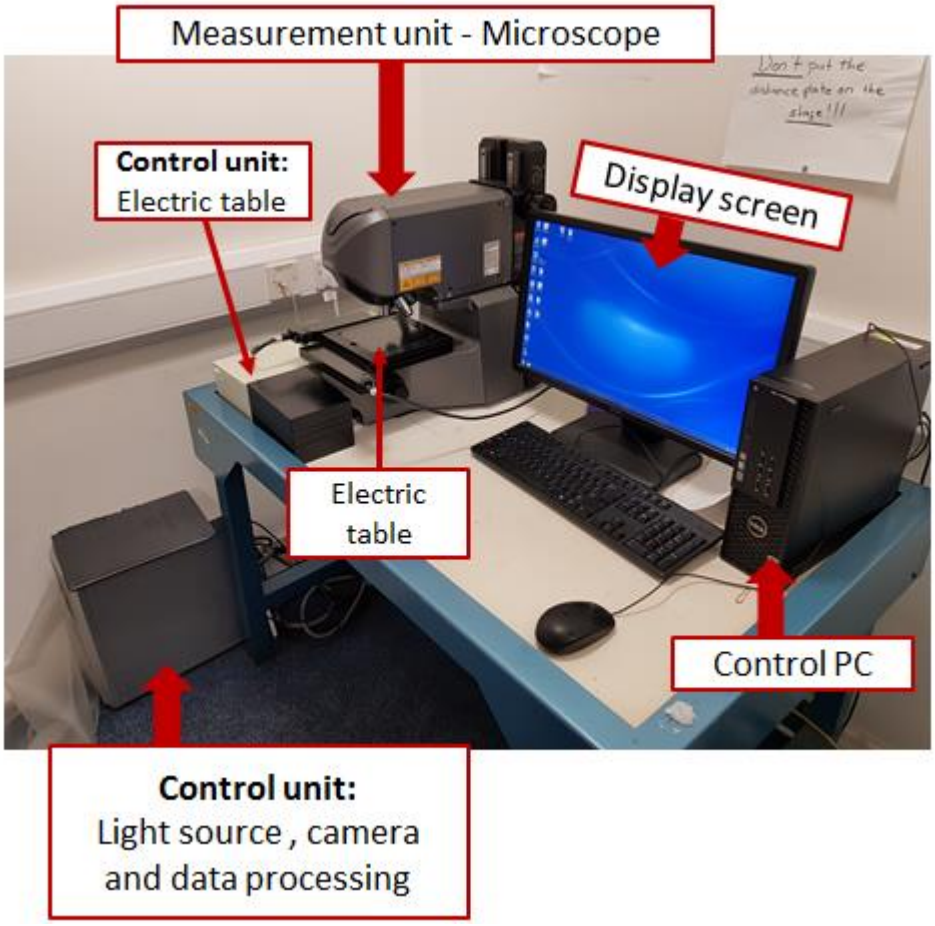

Figure 3.4: Image of the Keyence VK X-200 confocal laser scanning microscope unit.

3.3.1 Wear measurement and wear volume estimation

For the results in Chapters 3 and 4, wear measurements were taken from the scars generated on the test disk. The HFRR ball was three times harder than the test disk hence the scars on the disk were very visible. For the result in Chapter 6, wear measurements were carried out on the test ball since they were more visible in comparison to the scars generated on the test disk. For wear measurement, the sample is mounted on the electric table. Using the $10\times$ or $20\times$ objective lenses the wear scar is captured in 3D. Once the image of the wear scar is generated it is then post-processed using the VK analyser software. Firstly, the image is tilt-corrected. To calculate the wear volume from the scar, 10 cross-sectional areas cutting across the track and spaced out 140 ± 20 µm apart were measured as shown in quadrant A and B of Figure 3.5. The wear volume was obtained by multiplying the wear scar length by the average of the 10 cross-sections. Specific

wear rate was then calculated by dividing the wear volume by the normal load and sliding distance.

3.3.2 Surface roughness measurement

In Chapter 4, surface roughness on the worn surface was measured. The VK Analyzer software was used to estimate the line roughness across the track. 10 lines with spacing of 140 ± 20 µm (see quadrant A in Figure 3.6) were used to estimate surface roughness. The waviness of the profile was eliminated in the measurement. An appropriate cut-off wavelength, λ_C was selected according to the British Standard BS ISO 4288:1998 [66]. Table 1 contained in the standard [66] was used as a guide to selecting the cut-off wavelength and is based on the cut-off on the evaluation length and the sampling length (see quadrant B of Figure 3.6).Cut-off wavelength λ_C used in estimating the average roughness (R_a) on the worn surfaces was 0.025µm.

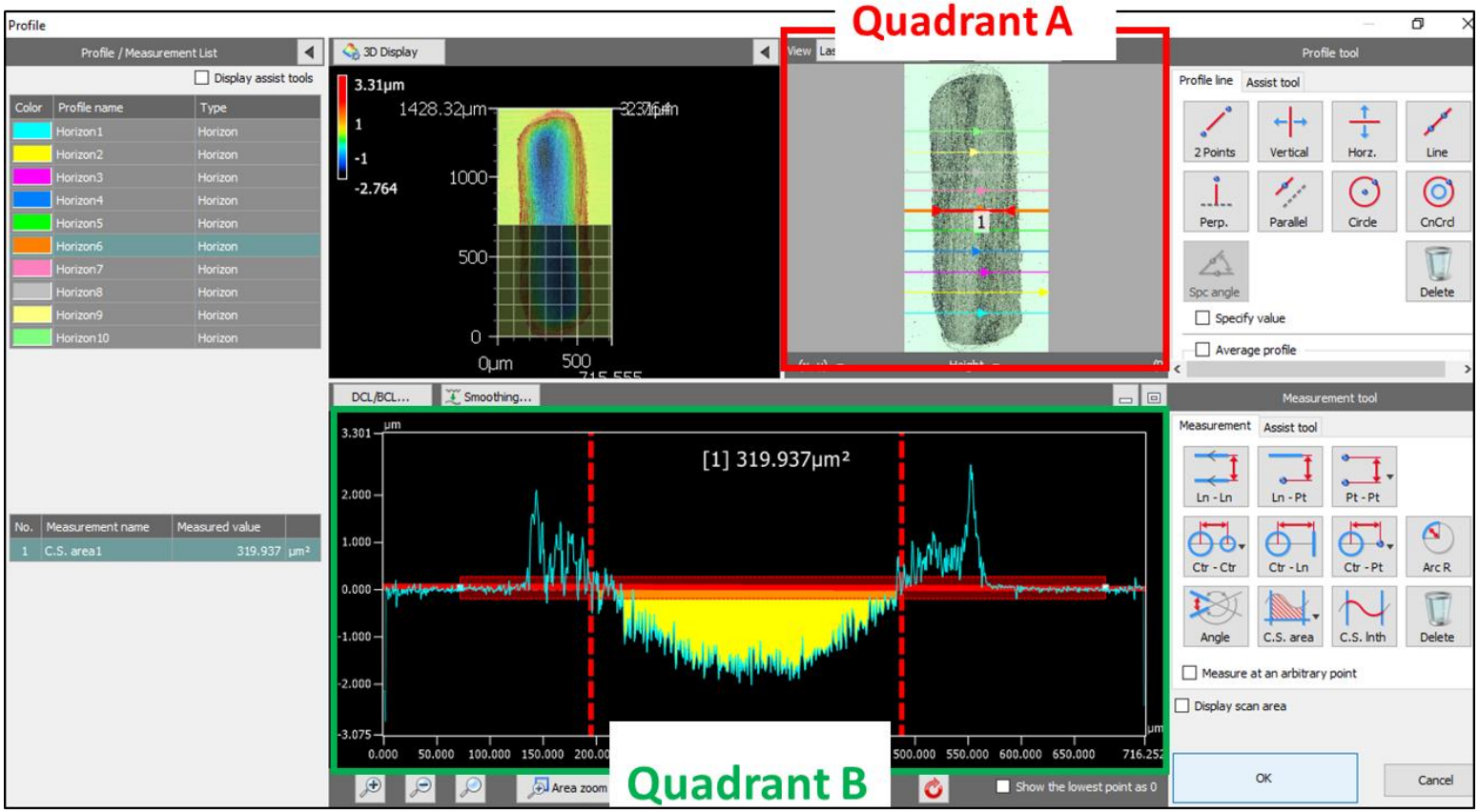

Figure 3.5: Screen view from VK analyser software showing how wear scar volume was estimated.

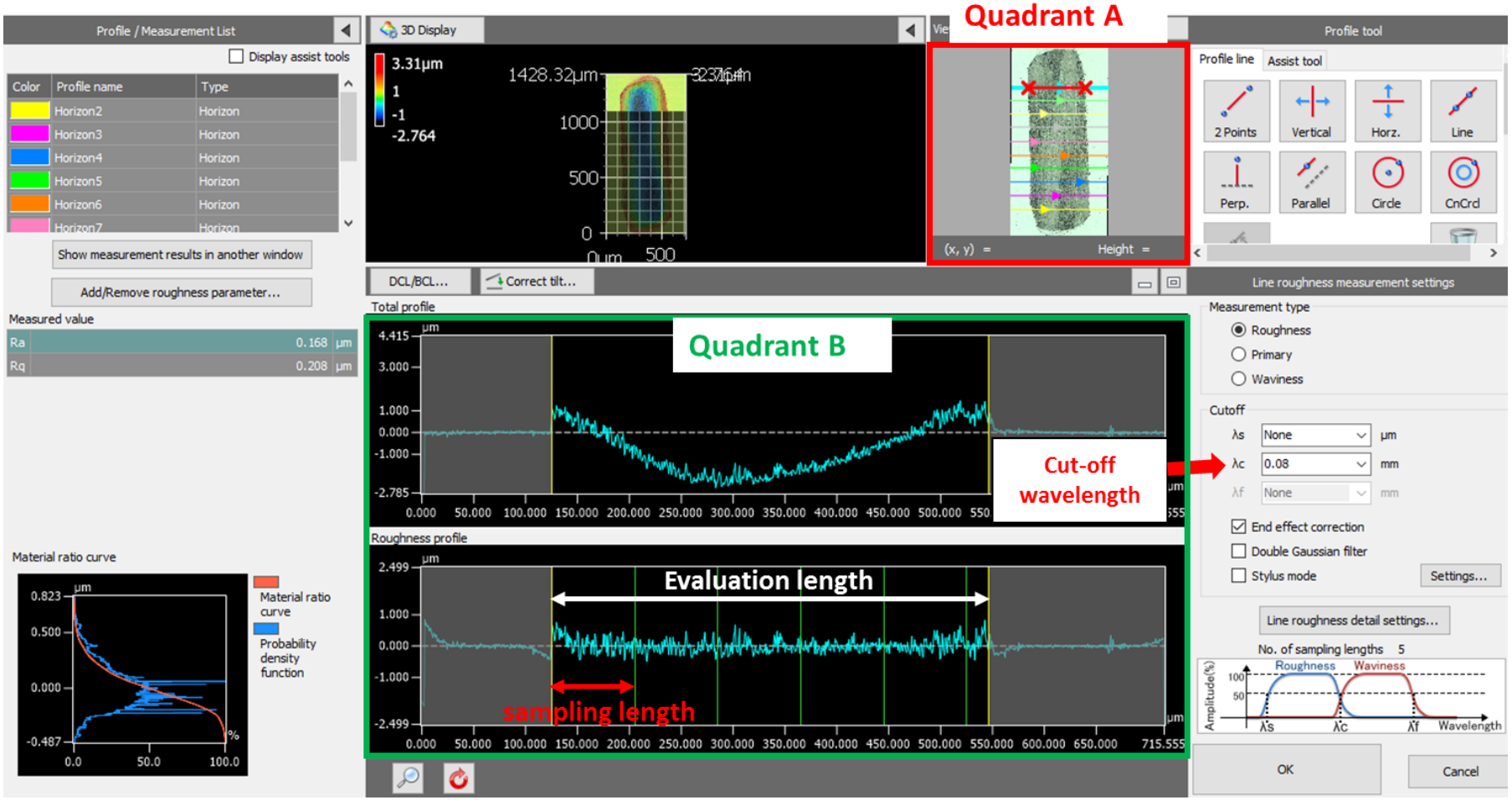

Figure 3.6: Screen view from VK analyser software showing how surface roughness was estimated.

3.4 Nanoindentation

Nanoindentation technique was used to measure the near-surface hardness of the unworn and worn test surfaces. The hardness of the bulk material is related to the microstructure [67]; hence this technique was chosen to complement the cross-sectional microstructures in understanding how tribological performance of the gear oils influence subsurface structure.

Hardness measurement was carried out with the MTS Nano Indenter XP. The continual stiffness measurement (CSM) mode allows for continuous measurement of the mechanical response during the loading portion of the indentation test [68]. Hence we can obtain the hardness-depth profile outside and inside the wear scar. One of the limitations experienced with this technique is the limited probing depth of 2 μm. This means we can only evaluate the microstructure very close to the surface (< 2 μm).

A diamond Berkovich indenter tip was displaced into the material at a constant rate of 0.05 s^{-1} to a depth of 2 μm. For the worn surfaces, measurements were taken at 15-30 points within the wear scar. Likewise outside the worn surface, hardness values reported are an average of values obtained from 15 – 40 points.

3.5 Raman spectroscopy

Raman spectroscopy is a non-destructive technique based on Raman scattering. Figure 3.7 shows a schematic of a Raman spectroscopic microscope system. The excitation source generates a monochromatic laser light usually in the visible range. Light travels through the optical mirror and microscope objective lens, forming a laser beam on the sample surface. When laser beam hits the sample the light is either absorbed, transmitted or scattered. Most of the scattered light usually has the same frequency as the incident beam and is filtered by the Rayleigh filters; the remaining few have a different wavelength. This is what is referred to as Raman scattering (inelastic scattering). In Raman scattering where, the scattered light has a different wavelength, the light either absorbs or emits energy; hence the scattered light will have wavelength,$\nu_0 \pm \nu_m$, where ν_0 is the vibrational frequency of the incident light and ν_m is the vibrational frequency of a molecule. The positive or

negative sign will depend on whether the incident light absorbs or emits energy. The shift in wavelength signifies the excitation of molecular vibration modes and can be used to determine the presence of Raman active molecules on a surface or with a material. Not all materials are Raman active (i.e. able to scatter light inelastically) and is a slight drawback with this technique. Raman measurements results are usually presented as spectra by plotting a graph of intensity of the scattered light (y-axis) against energy (frequency) of light (x-axis). The x-axis is usually presented as number of waves per cm (cm^{-1}).

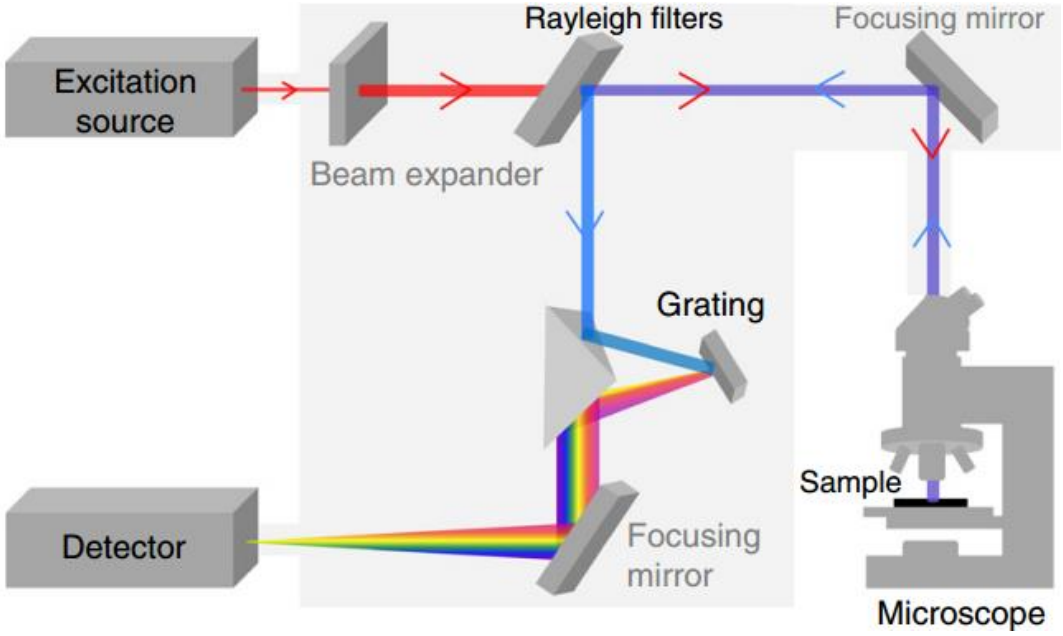

Figure 3.7: Schematic diagram of a Raman spectroscopic microscope system working process [69]

3.5.1 Raman procedure and parameters

A Renishaw 1000 microscope was used to chemically characterise the tribofilm formed on the worn surfaces. An Argon laser source with wavelength of 514 was used. A 50 x Olympus objective lens was used in scanning the surface and gives a beam spot size of about 1 µm. The exposure time was 1 s to minimise the chances of excessively heating the sample surface. In addition, 20 accumulations were taken to reduce the signal-noise ratio.

3.6 Scanning Electron Microscopy (SEM)

3.6.1 SEM principle and surface imaging

SEM is commonly used to resolve and analyse sample surfaces. Figure 3.9 shows a schematic of the main components in an SEM. A high energy (primary electron) is generated in an electron source, accelerated through the vacuum column and focused unto the sample. The primary electron interacts with the sample and electrons are reflected off the surface mainly secondary electron (SE) and back scattered electrons (BSE) as shown in Figure 3.8. Secondary electrons are backscattered and detected, processed and used to form the image of the scanned area. The secondary electrons originate from the surface, whereas, the backscattered electron interact with a larger volume of the sample. In this thesis, SEM was used to image the wear scars generated from the sliding tests in secondary electron mode. The SEM system used was FEI Quanta 650 surface. Surface imaging was carried out with accelerating voltage of 5 kV.

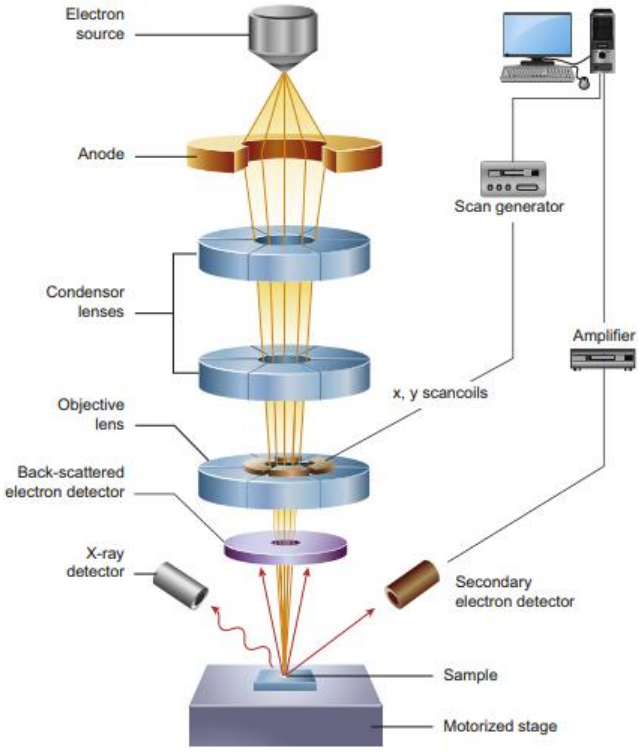

Figure 3.8: schematic diagram of the main components in an SEM microscope [70]

3.6.2 Scanning electron microscopy - energy dispersive X-Ray spectroscopy (SEM-EDX)

EDX analytical technique was used to carry out elemental analysis of the tribofilm generated on the wear scars. This technique relies on X-ray emission from the sample surface. The interaction of high energy (primary electron) with a sample surface can also lead to X-ray emission in addition to secondary electron and backscattered electron. When the primary electron knocks off an electron from the electron shell around the nucleus, a positive hole is generated. Since this state is unstable, an electron from a higher shell fills this hole. This process emits X-Rays. The X-ray released is characteristic of the energy difference between the two shells. The X-rays are detected by an X-ray detector and used to determine the elemental composition of the sample. The Quanta 650 SEM used for imaging of the wear scars was also equipped with an EDX detector. The accelerating voltage used was 15 kV.

3.6.3 Scanning electron microscopy – focused ion beam (SEM-FIB)

In the SEM, electrons are generated with an electron sources in an electron column. However, some SEMs also have within them a second column for generating ions from a liquid metal ion source (such as Gallium) and a column where an ion beam can be directed on the sample surface. These systems are commonly referred to as dual beam (electron and ion) system. At low beam currents, FIB gallium (Ga^+) is used for imaging and for milling or sputtering at higher beam currents. In this thesis, ion beam was used for milling the surface to reveal the near-surface microstructure as well as for imaging the microstructure. Figure 3.9 shows the process of revealing the cross-sectional microstructure below the wear scar. Using secondary electrons, the sample surface is imaged which allows us to find the wear scar. A region of interest is then selected (in the middle of the wear scar). One of key reasons SEM-FIB was chosen instead of the conventional approach of sectioning, grinding and polishing is due to the small of the wear scar (approximately 1.5 mm x 0.5 mm). Using SEM-FIB, we able to analyse the cross-section in roughly the same location (middle of the wear scar) and minimise the chances of inconsistence arising for analysing different sections of the wear scar. Once the region of interest is located, a platinum layer is sputtered to protect the

region from excessive contamination of the surface with the ions and edge rounding during the milling process. Using high current and voltage, a trench of 60 µm x 40 µm x 15 µm is generated, revealing the near-surface microstructure. A two-step cleaning process is conducted with low current to enhance to remove milling artefact (curtaining) and accentuate the microstructure. The cross-sectional microstructures were imaged using Ion channelling contrast imaging (ICCI). It simply using ion beam to create a (grey) contrast image. The (channelling) contrast mechanism relates to the crystallographic orientation in the material. The grains appear bright or dark depending on their orientation.

In this thesis, FIB milling and imaging was conducted with a FEI Nova NanoLab 600i system. Ion imaging was taken with voltage of 30 kV and beam current of 9.7 pA.

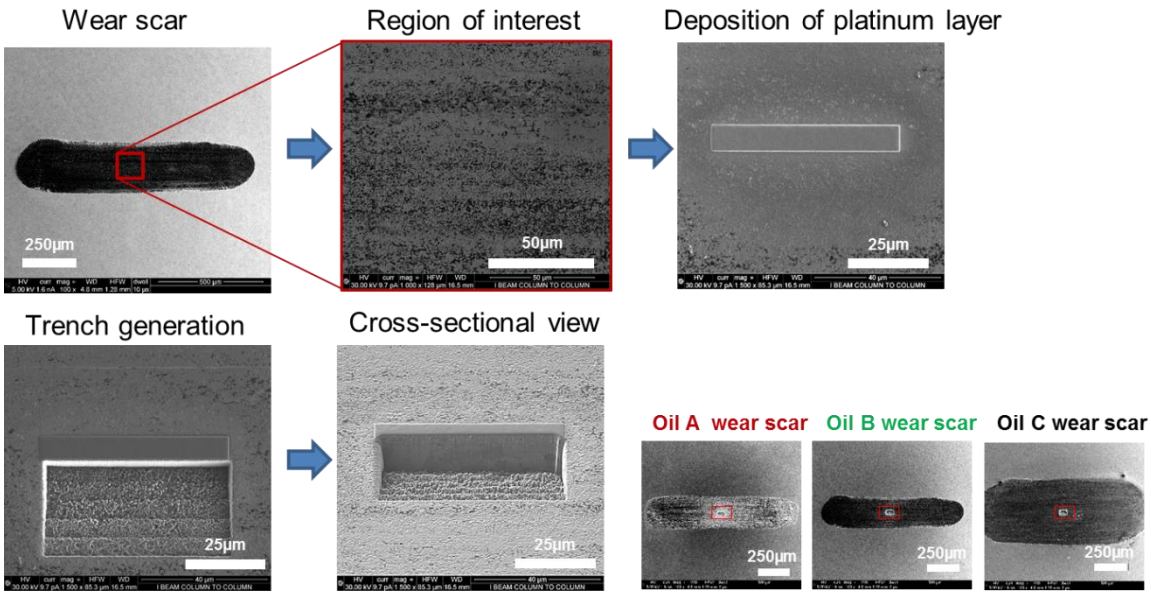

Figure 3.9: SEM micrographs showing the process of subsurface microstructural examination using SEM-FIB technique

Chapter 4

Paper 1: Industrial gear oils: tribological performance and subsurface changes

This paper was submitted to 'Tribology Letters' journal in December 2017. It was peer-reviewed and accepted for publication in April 2018.

Contributions:

Aduragbemi Adebogun – is the lead author of this article and conducted all the experiments (except for the Transmission EBSD experiment which was conducted by **Ali Gholinia**), analysed and interpreted the results.
Robert Hudson, Allan Matthews and Philip Withers gave advice on the experimental design, gave suggestions on data interpretation and also contributed to reviewing the article along with **Angela Breakspear and Chris Warrens.**

4 Industrial gear oils: tribological performance and subsurface changes

Aduragbemi Adebogun[1, 2, a], Robert Hudson[3], Angela Breakspear[4], Chris Warrens[4], Ali Gholinia[2], Allan Matthews[1, 2], Philip Withers[2]

[1] International Centre for Advanced Materials (ICAM, Manchester Hub)

[2] School of Materials, The University of Manchester, Manchester, M13 9PL, United Kingdom

[3] BP Europa SE - Castrol Industrial Monchengladbach, Germany

[4] BP Technology Centre, Whitchurch Hill, Pangbourne, RG8 7QR, United Kingdom

[a] **Corresponding Author**: Aduragbemi Adebogun, aduragbemi.adebogun@postgrad.manchester.ac.uk

Abstract

This study examines the tribological performance of three gear oils (Oils A, B and C), in relation to surface and microstructural changes. Oil A contains molybdenum dithiophosphate (MoDTP) friction modifier, Oil B contains amine molybdate combined with zinc diakyl dithioposphate (ZDDP) antiwear additive, while Oil C contains phosphonate and a commercial gear oil package. Following sliding tests of a hardened AISI 52100 steel ball on a spheroidised AISI 52100 steel disk, the worn surfaces were chemically studied using Raman and energy dispersive X-ray (EDX) spectroscopy. The tribological performance for each oil was different, likewise the nature of the tribofilm formed. After a 5 min sliding test, the hardness-depth profile of the worn surfaces was measured; also the cross-sectional microstructure was examined using scanning electron microscopy (SEM) combined with focused ion beam (FIB) preparation and transmission-electron back scattered diffraction (t-EBSD) techniques. With Oil A, there was a relatively small increase in surface hardness (33% of the original surface) whereas with Oils B and C, the average hardness near the surface was 100% greater than that of the unworn surface. The cross-sectional microstructure using Oil A also differs from oils B and C, which are quite similar. The result shows that the plastic deformation below the surface of Oil

A spreads deeper into the material (>10 μm), whilst that of oils B and C was largely limited to 2-3 μm below the surface. It is concluded that lubricant formulation and its associated tribofilm influenced the extent of deformation in the subsurface layers and consequently influenced the wear performance. Tribosystems are complex due to the inter-relationship between simultaneously occurring processes such as generation of frictional heat, tribofilm formation and shearing, plastic deformation and wear. This makes it difficult to make direct correlations for example between frictional performance and subsurface changes.

Keywords: Boundary lubrication, gear oils, surface chemistry, subsurface microstructure, mechanical properties

4.1 Introduction

Formulated oils used in mechanical systems such as gears and bearings are primarily designed to sustain low friction and wear of moving parts. Minimizing friction and wear improves energy efficiency and extends the lifetime of the systems. To achieve this, friction and wear additives are included in the formulation of industrial lubricants. This class of additives are particularly important in boundary lubrication conditions whereby surfaces come in direct contact as a result of a high load and low speed combination. In this case, the lubricant is too thin to prevent surface asperities from touching. Without these additives functioning properly in the formulated oils, gears and bearings can fail in catastrophic ways.

During sliding of surfaces, these additives are surface active and contribute to the formation of a protective layer or tribofilm that prevents direct metal contact and lowers friction between the metal surfaces on the bases of its low shear strength relative to that of the metal [71]. Friction and wear additives can be sub-divided into subcategories. These include friction modifiers, antiwear and extreme pressure additives. Other classes of additives usually added to formulate oils include corrosion inhibitors, antifoam, dispersants and detergents. The focus of this study will be on the friction and anti-wear additives. The formation mechanism of these tribofilms and their properties determines the level of friction and wear protection that they provide initially and over time.

Friction modifiers such as organomolydenum compounds (OMCs) react with metal surfaces to form molybdenum disulphide (MoS_2) and other compounds such as sulphides and oxides [72-75]. Transmission electron microscopy (TEM) characterisation of tribofilms formed on surfaces worn in the presence of OMCs has shown that they contain nanosheets of MoS_2 [76,77] which adhere well to the surfaces. Low friction observed with these friction modifiers is attributed to the ease of sliding between single layers of MoS_2 in the tribofilms formed [76]. MoS_2 is Raman active and the first order Raman mode are $E^{\,2}_{2g}$,E_{1g}, E^{1}_{2g} ,A_{1g} observed around 34 cm^{-1} , 287 cm^{-1}, 383 cm^{-1} and 409 cm^{-1} respectively [78]. The $E^{\,2}_{2g}$ and A_{1g} modes have peaks with the highest intensity and can easily be used to identify the presence of MoS_2. Commonly used antiwear and extreme pressure additives in industrial applications include Sulphur-Phosphorus compounds, Molybdenum-Sulphur compounds and ZDDP (zinc dialkyldithiophospate). ZDDP additive is the most widely used antiwear additive. A comprehensive review of the history and mechanism of ZDDP has been reported by Spikes [33]. ZDDP was decomposed on rubbing surfaces to form a rough pad-like tribofilm of glassy zinc phosphate/polyphosphate [79,37] material with thickness of 50-200 nm. This tribofilm is effective at reducing wear by acting as a sacrificial layer with a faster rate of formation than the rate of removal. During sliding of surfaces under high load, surface asperities cannot be completely separated. Plastic deformation and/or fracture of the asperities are inevitable. Tribofilms are able to reduce friction and can influence plastic deformation of the surface asperities depending on their properties. Lower friction at the surface will reduce the level of frictional strain induced in the subsurface and play a significant role in wear reduction [24]. Frictional strain during sliding is usually localised very near the surface and continues to accumulate with more cycles of sliding. Under significantly high load and sufficient number of sliding cycles, most ferrous metals form a refined grain structure a few nanometres in depth [80]. This layer can eventually delaminate to form plate-like wear debris [81].

Friction and wear performance of different industrial oils have been widely studied and reported in the literature. An established approach to understanding the

mechanisms by which industrial oils perform in boundary lubricated sliding is examining the properties of the tribofilm formed and surface topography. There is a limited amount of studies that have investigated the relationship between tribological performance, the nature of tribofilm formed and the subsurface changes. One of those who have studied this relationship is Reichelt et al. [62]. They studied the surface film formed during triboaction and the subsurface layer (or tribomutation layer) that formed beneath the surface film. Their work showed that the wear protection provided by formulated oils is a function of the combined properties of the induced surface film and the underlying tribomutation layer. Cao et al. [61] reported in a recent study that tribofilms had an effect on wear by influencing the plastic flow of the nano-grained structures generated near-surface of the contacts. Two different oils produced very different tribofilms. Although they produced similar levels of friction coefficient in a 2 hrs sliding test, there was a large disparity in the level of wear protection. The difference in the level of wear protection was attributed to the ability of the tribofilm to hinder or promote grain rotation. A softer film would allow for more degrees of rotation of the nano-crystalline layer, as a result reducing wear significantly. The concept of surface films influencing the deformation behaviour of surfaces dates back to early 1990's. One of the earliest research was conducted by Rehbinder [82] who observed that the presence of a lubricant can significantly affect changes that take place in a solid contact. The presence of Oleic acid on the surface increased the ability of a mineral crystal to deform in a plastic manner. Similarly Buckley and co-workers [60] showed that the mechanical behaviour of a Calcium fluoride crystal was sensitive to extremely small concentrations of surfactant. Although this concept has been investigated in recent times [62,61,63] there is still more room for exploration particularly in the development of industrial lubricants and with the advent of advanced electron microscopy.

The aim of this study was to investigate the relationship between tribological performances of three industrial gear oils (via their tribofilm) on subsurface mechanical and microstructural changes.

4.2 Materials and methods

4.2.1 Lubricant

The test lubricants were three ISO VG 320 gear oils, which all have the same kinematic viscosity of 320 ±32 mm^2/s at 40 °C. Oil A is used in wind power gearboxes, Oil B in heavy industrial applications (such as mining) and Oil C is a multifunctional gear oil used in a variety of applications. The complete formulation of the lubricants includes the base oil and the complete additive mix are shown in Table 4.1. Oil A is formulated with synthetic polyalphaolefin (PAO) base oil and an additive package that includes molybdenum dithiophosphate (MoDTP) friction modifier, mixed sulphonates and an antifoam. Oil C is also formulated with synthetic PAO base oil with a different additive mix, containing Phosphonate, alkylated naphthalene, antifoam and a commercial gear oil package. Oil B is formulated with a mineral base oil and additive package that combines a friction modifier (amine molybdate), an antiwear additive (ZDDP), extreme pressure sulphurised additive and metal sulphonate (corrosion inhibitor). These three oils with different base oil-additive mix were selected with the intention of generating different types of tribofilms with different tribological properties.

Table 4.1: Base oil and additive combinations for oils A, B and C

	Oil A	Oil B	Oil C
Base oil	Polyalphaolefin (> 90%)	Group 1 base stock mix (> 85%)	Polyalphaolefin (> 80%) Alkylated Naphthalene (5-15%)
Additives	Molybdenum Dithiophosphate (MoDTP) - (< 5%)	Amine Molybdate complex (< 5%) ZDDP (< 5%) Sulphurised - extreme pressure additive	Phosphonate (< 1%) Commercial gear oil package (< 5%)
	Mixed sulphonates – corrosion inhibitor (< 0.5%) Copper -	Sulphonate mix – corrosion inhibitor	

	corrosion inhibitor (< 0.5%)	(< 5%)
	Antifoam –trace	Antioxidant (< 1%) Methacrylate polymer – pour point depressant (< 5%)
		Antifoam -trace

4.2.2 Tribotesting

Sliding test was carried out using an High Frequency Reciprocating Rig (HFRR, PCS Instruments, London, England). The test configuration is a ball-on-disk, where the disk is held stationary, submerged by the test lubricant. Load is applied on the test ball which oscillates linearly on the disk. For the entire sliding test, a load of 9.8 N is applied on the test ball oscillating at a frequency of 50 Hz with a stroke length of 1 mm providing average Hertzian contact pressure of 0.94 GPa. All tests were carried out at 80 $°C$ by heating up the lubricant bath and maintaining the temperature throughout the test. The temperature of 80 $°C$ was selected to match the temperature at which gear oils typical operate in industrial systems. The test duration was varied between 5 min and 2 h. Each test was carried out three times to give the mean friction coefficient. The HFRR system which uses the AutoHFRR software provided by the manufacturer was used to measure and store friction coefficient continuously throughout the test. Additionally, Electrical Contact Resistance (ECR) is monitored. ECR gives an indication of whether or not a separating film is formed between the ball and disk. A 15 mV potential is applied between the ball and disk which form a resistance referred to as the contact resistance; this potential is also applied to a balance resistor which is in series with the contact resistance and forms a potential divider [83]. A resistance of 1000 Ω is selected in the HFRR control software. The change in potential between the contacts (referred to as electrical contact voltage) is a measure of the 'contact resistance' in comparison to the balance resistor. A zero electrical contact voltage indicates a direct metal-metal contact and no electrical contact resistance between

the contact and the formation of a fully insulating film means that the electrical contact voltage reaches a maximum voltage of 15 mV.

4.2.3 Ball and disk

The test ball and disk were made of AISI 52100 steel. The ball is 6.0 mm in diameter with hardness of 11.7 ± 1.0 GPa and surface finish or roughness (Ra) of less than 0.05 μm. The test disk is 10 mm in diameter and 3 mm thick; with a hardness of 3.3 ± 0.2 GPa and surface roughness of about 0.02 μm. Before each test, the test ball and disk were cleaned with toluene and acetone. After experiment, the test samples were cleaned with heptane to get rid of the residual oil. The test disks were further degreased with soapy water and ethanol prior to characterisation in the scanning electron microscope.

4.2.4 Wear measurement

A KEYENCE VK – X200 3D confocal microscope was used to scan the profile of the wear scar on the test disk, followed by post-processing of the measurement with KEYENCE VK Analyser. Tilt correction was applied to adjust for the slight tilt of the sample on the microscope stage. Wear volume was calculated by the product of the wear scar length and the cross-sectional areas. The average of 10 2D profiles along the wear scar was used to determine the cross-sectional area. The R_a of the worn surfaces was measured by applying a cut-off wavelength (λ_c) of 0.025 μm to the primary profile which eliminate the influence of the longer wavelength components.

4.2.5 Raman spectroscopy

A Renishaw 1000 microscope system was used to analyse residual tribochemical products on the wear scars. The wavelength of the laser source was 514 nm. All scans were carried out with Olympus objective lens which gives a laser spot size of about 1 μm. Raman spectra were obtained from the wear scar at 1 sec exposure and 20 accumulations to reduce the signal-to-noise ratio.

4.2.6 Scanning electron microscopy – energy dispersive spectroscopy (SEM – EDX)

A scanning electron microscopy (SEM) FEI Quanta 650 FEG equipped with energy dispersive X-ray (EDX) spectroscopy detector was used to characterize the wear surface topography and map the elements present on the surface. Surface imaging and EDX mapping were performed with accelerating voltages of 5 kV and 30 kV respectively.

4.2.7 Nanoindentation

The hardness of the near surface after sliding tests was measured using the MTS Nano Indenter XP. The Continual Stiffness Measurement (CSM) mode makes it possible to continuously measure mechanical response with depth as an indenter tip penetrates the surface [84,12]. The Diamond Berkovich indenter tip is displaced into the material at a constant strain rate of 0.05 s^{-1} to a depth of 2 µm. Hardness measurement was carried out on the as-received surface and the three worn surfaces.

4.2.8 Scanning electron microscopy – focused ion beam (SEM-FIB)

SEM equipped with FIB was used to characterise the subsurface microstructure of the spheroidised AISI 52100 steel disks before and after sliding test with the three oils. The study was carried out using FEI's Nova NanoLab 600i system. The dual beam system has secondary electron and focused ion beams. Electron images were taken with voltage of 5 kV and current of 16 nA. Ion imaging was taken with voltage of 30 kV and beam current of 9.7 pA. Imaging of the subsurface microstructure was done using ion channelling contrast technique [85]. With this technique, grains appear either dark or bright based on their orientation. The region of interest is set as the centre of the scar for the three worn surfaces. This is one of the advantages of using the FIB technique, as it allows site-specific analysis. The FIB process (Figure 4.1) involves firstly depositing a platinum (Pt) layer on the surface to protect the region of interest; a trench is generated by ion beam milling to reveal the cross-sectional microstructure.

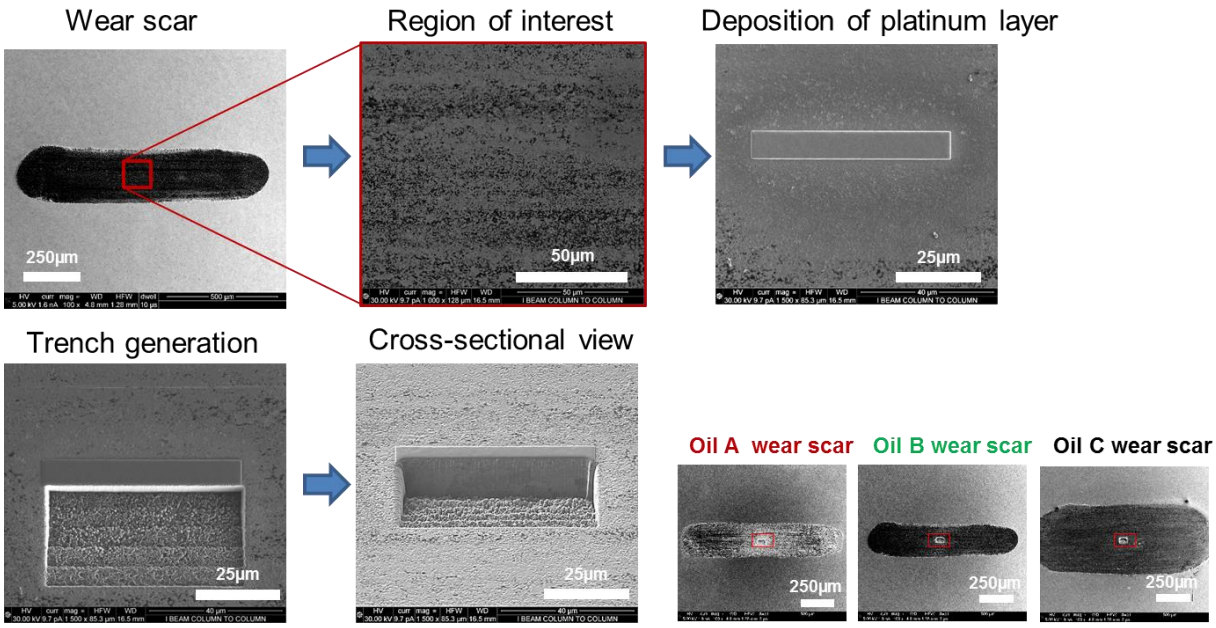

Figure 4.1: SEM micrographs showing the process of subsurface microstructural examination using SEM-FIB technique

4.2.9 Transmission- electron backscatter diffraction (t-EBSD)

T-EBSD in comparison to the conventional EBSD technique provides improved spacial resolution as a result of reduced interaction volume of the electron beam in the sample [86]. This is particularly useful in resolving nano-sized grains. FEI's Magellan 400 XHR SEM equipped with NordlyNano EBSD detector was used to perform EBSD measurements. Using FIB lift-out technique [87] in FEI's Nova NanoLab 600i dual beam system, a thin FIB lamella (<200 nm) was generated from the cross-sections (Figures 4.9b and 4.9c) and mounted in transmission geometry before characterisation with the SEM. An accelerating voltage of 30 kV was used with probe current of 1.6 nA and a step size of 20 nm. The Kikuchi patterns were indexed using Aztec 2.2 software. EBSD data processing was done using Channel 5 software suite developed by Oxford Instruments HKL.

4.3 Results and discussion

4.3.1 Friction and wear performance

In this section, friction and wear performance are discussed in relation to tribofilm formation on the surface. Although all the additives in the mix play a role in the performance of the formulated oils, but this discussion focuses on the role of the

friction and wear additives. Both oils A and B contain organomolybdenum friction modifiers, MoDTP and amine molybdate respectively. Oil B contains ZDDP antiwear additive in addition to amine molybdate friction modifier. Oil C contains Sulphur and phosphorus based antiwear and extreme pressure additives.

The three fully formulated oils were tested in the HFRR tribometer for durations of 5 min and 2 h. Three tests were run for 5 min and another three were run for 2 h continuously. The recorded mean value of friction coefficient at the end of the 5 min tests were averaged and reported in Figure 4.3a. The same as were the 2 hour tests. After friction test, wear measurement was evaluated from the wear scar on the test disks since there was no evidence of wear on the test balls. At the start of the 2 hours sliding test, Oil A provides a low friction coefficient of about 0.08 and this drop slightly to 0.07 within 5 mins (Figure 4.2a). Raman spectroscopy result indicates that MoS_2 is present on the worn surface at this time (Figure 4.4) as evident by $E^{\,2}_{2g}$ and A_{1g} peaks at 378 and 411 cm^{-1} respectively. EDX elemental map shows the surface contains oxygen, sulphur and calcium after 5 mins. One of the additives in Oil A is calcium sulphonate. The presence of Calcium on the wear scar shows that the calcium sulphonate is surface active and contributes to the tribofilm formed. The formation of MoS_2 between sliding metal surfaces is known to be the cause of significant reduction in friction [72,74,75,88]. From 5 mins to the end of the 2 hours test the friction coefficient continues to drop steadily to reach 0.06. MoS_2 remains present on the worn surface after 2 hours of sliding as evidenced by the Raman spectra in Figure 4.4. Elemental map of the wear surface generated after 2 hours of sliding (Figure 4.5) shows an increase in the intensity of oxygen, sulphur and calcium. As the friction coefficient drops, the ECR plot shows the build-up of an unsteady insulating film. At the end of the 2 hours test, wear has increased substantially with Oil A (Figure 4.3b)**.** This suggests that the insulating film was either insufficient to protect against wear or contributed to the increase.

When testing Oil B, the friction coefficient was at 0.1 for the first 10 mins of the sliding test and this was then followed by a sharp drop to 0.065 (Figure 4.2b). This drop in friction coefficient has been attributed to the formation of a low friction film [89,90]. The ECR result for Oil B shows a sharp rise in electrical contact

resistance at the start of sliding suggesting a film forms quickly at the contact. Raman spectroscopy was used to scan the surface for evidence of MoS_2 formation on the surface after 5 mins and 2 hours. The results presented in Figure 4.4 indicate that MoS_2 was formed after 5 mins and remains present at the end of the 2 hours test. The EDX elemental map of the surface shows that oxygen is present on the surface after 5 mins and after 2 hours of sliding, sulphur, phosphorus and zinc are present in addition to oxygen. The presence of zinc and phosphorus after 2 hours of sliding coupled with the relatively low wear obtained with Oil B suggests the formation of zinc phosphate film which is known to play a significant role in the low wear performance when ZDDP is present [79,37].

Similar to Oil A, the friction coefficient of Test Oil C is initially Ca. 0.1, but the friction coefficient profile for Oil C is rougher than that of oils A and B, as evidenced by the short range spikes and dips. This suggests that the tribofilm, if present, is very unstable and this is also implied by the lack of electrical contact signal throughout the 2 hours test. EDX elemental spectrum maps (Figure 4.5) show that oxygen and a smaller proportion of sulphur are present on the surface after 5 mins. After two hours, the surface contains oxygen, sulphur and phosphorus.

The average friction coefficient and wear volume for each of the Oils at 5 mins and 120 mins are presented in Figure 4.3. Oil A provides the lowest friction after both 5 mins and 120 mins of sliding. This can probably be attributed to the formation of low shear MoS_2 tribofilm at the contact, which prevents direct metal to metal contact and reduces friction. However, in the 2 hour test, wear increased considerably. The result shows that Oil A provides relatively good friction performance, but average antiwear performance, particularly over longer periods. Oils B and C provide higher average friction coefficients of 0.087 and 0.089 respectively after 5 mins of sliding test compared to Oil A. After 2 hours of sliding test, Oil B provides the lowest wear and forms an insulating film that covers about 75% of the contact surfaces (Figure 4.2b). Oil B appears to form a complex tribofilm consisting of MoS_2 and a phosphate constituent. This complex tribofilm provides relative low friction and excellent wear performance. The elemental map of the surface worn by Oil C for 2 hours suggests that a S-P based film might have formed

on the surface although this may not have reflected on the ECR plot due to its conductive nature. The roughness of the friction coefficient plot and the substantial increase in wear after 2 hours suggests that any film formed was probably too unstable to adequately protect the surface, as evident by the relatively high wear.

The surface topography of the worn surfaces after two hours is presented in Figure 4.6. The worn surfaces from the three oils (Figures 4.6a – 4.6c) show evidence of plastic deformation caused by ploughing of a hardened AISI 52100 steel balls on the soft AISI 52100 steel disks. Figure 4.7 shows the cross-section profile of the wear scars generated with the three oils which corresponds to the wear result (Figure 4.3b) after 2 hours sliding. For Oil A, the higher magnification micrograph (Figure 4.6a1) shows the softer ferrite matrix organised in a wavy pattern around the hard cementite particles, which has a darker contrast. The surface worn by Oil B (Figure 4.6b1) appears smooth and homogenous, which was confirmed by the surface roughness measurement. For Oil B, the Ra is 0.12 µm, which makes it the smoothest of the three surfaces. On the other hand, the surface lubricated by Oil C appears to be rough with Ra value of 0.21 µm, it is the roughest of the three surfaces (Figure 4.6c1). Also, the surface appears to be densely populated with cementite particles. The cementite particles appear to be sticking-out, which could be the reason for the high surface roughness value measured. This combined with the high density of cementite particles possibly suggests that most of the soft ferrite matrix surrounding the hard cementite particles has been worn away.

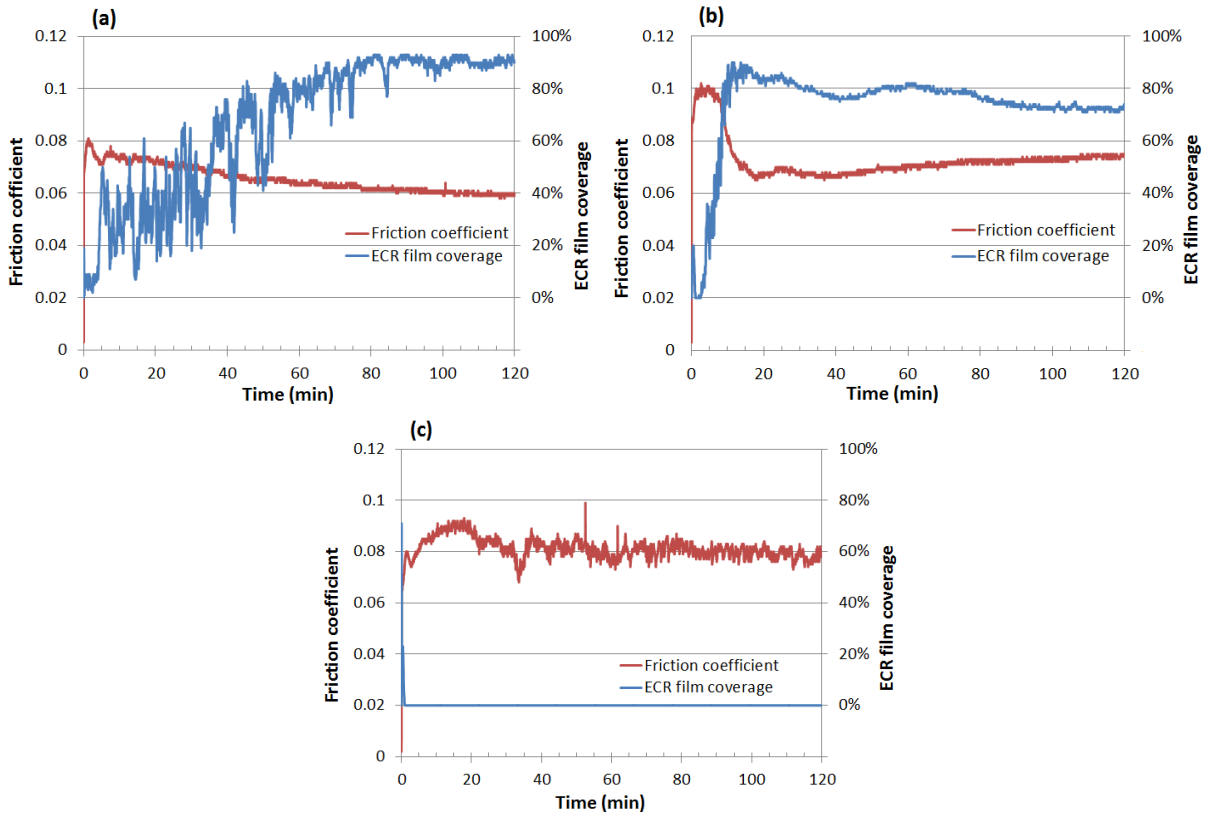

Figure 4.2: Plots of friction coefficient and ECR film coverage for (a) Oil A, (b) Oil B and (c) Oil C during a 2h sliding test at 80°$\boldsymbol{C}$ and 0.94GPa

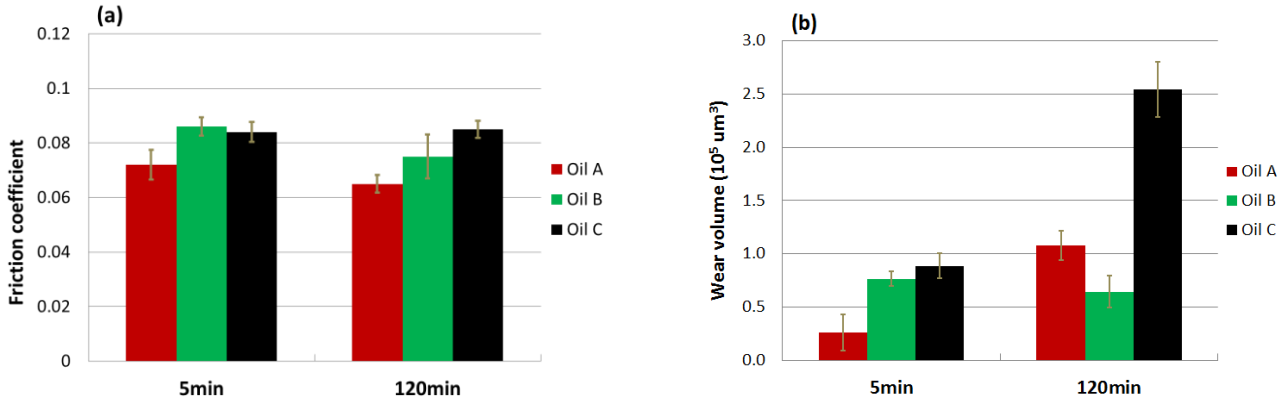

Figure 4.3: Average (a) friction coefficient and (b) wear volume for the three Oils after 5 mins and 120 mins of HFRR sliding test

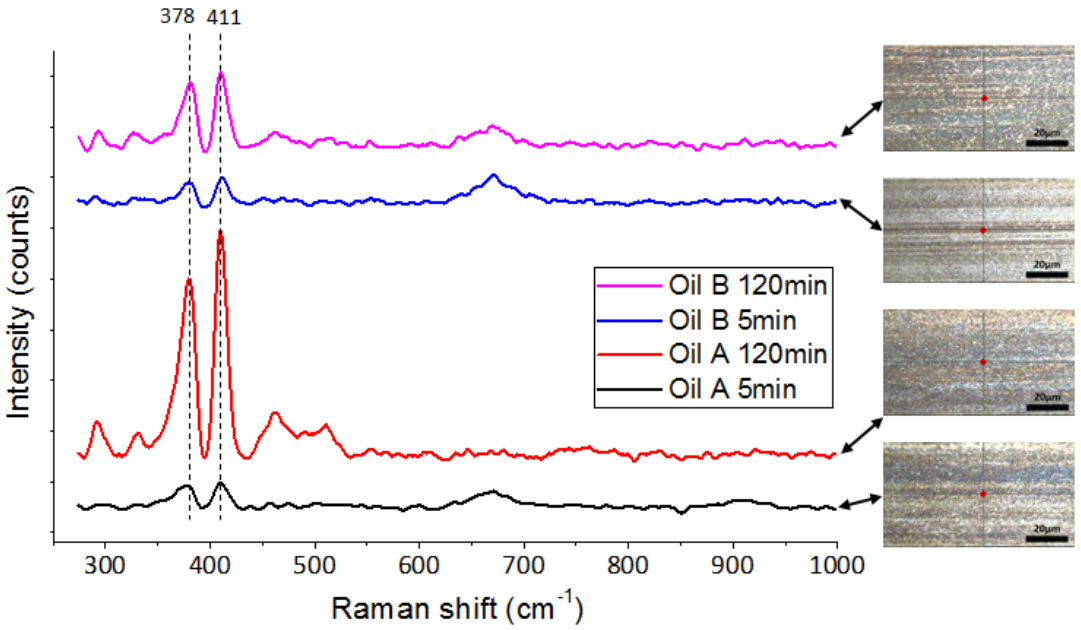

Figure 4.4: Raman spectra obtained from surfaces lubricated by Oils A and B after 5 mins and 120 mins (2 hours). The red dot at the centre of the crosshair in the optical images show the location each spectrum was taken from.

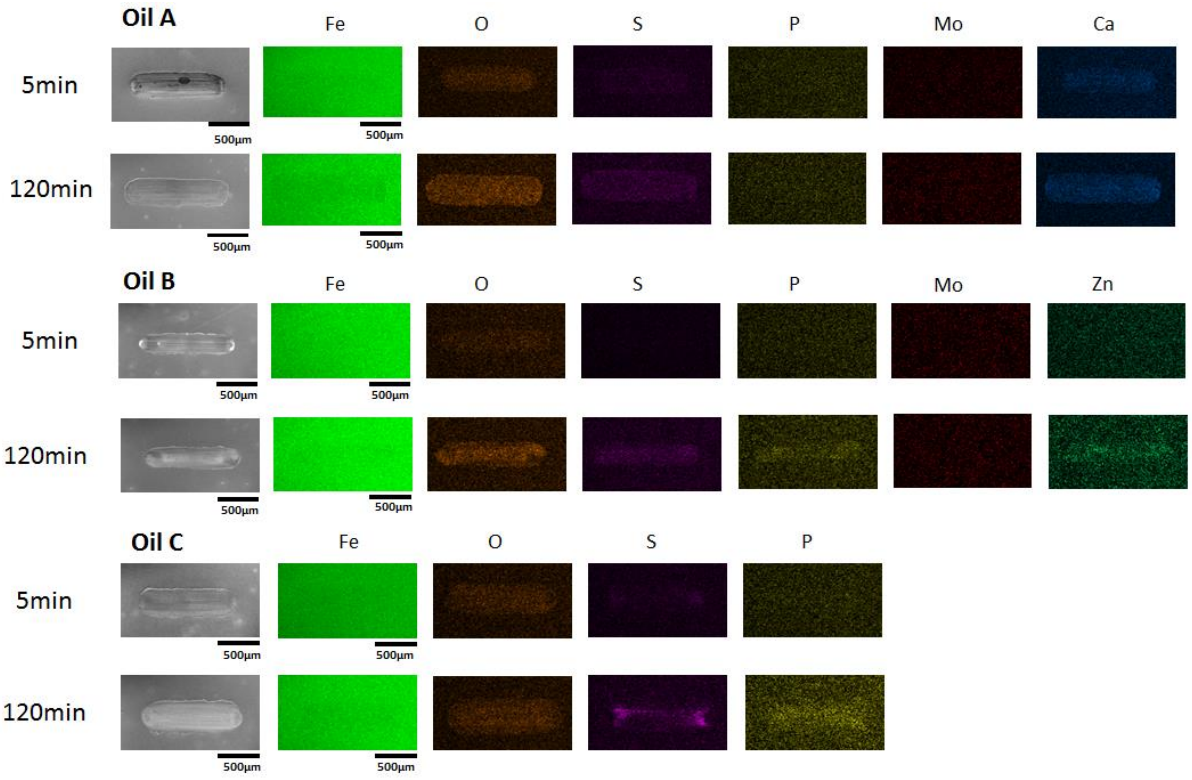

Figure 4.5: SEM images and EDX maps of wear scars lubricated by Oils A, B and C after 5 mins and 2 hours

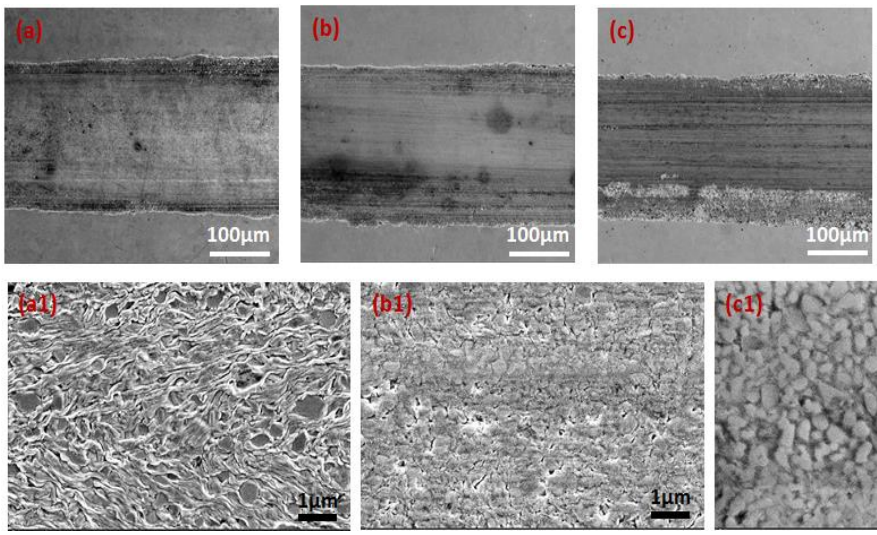

Surface roughness (Ra)	
Oil A	0.14 ± 0.01 µm
Oil B	0.12 ± 0.01 µm
Oil C	0.21 ± 0.05 µm

Figure 4.6: SEM images of wear surfaces generated from 2 hours sliding test with Oil A (a, a1), Oil B (b, b1) and Oil C (c, c1)

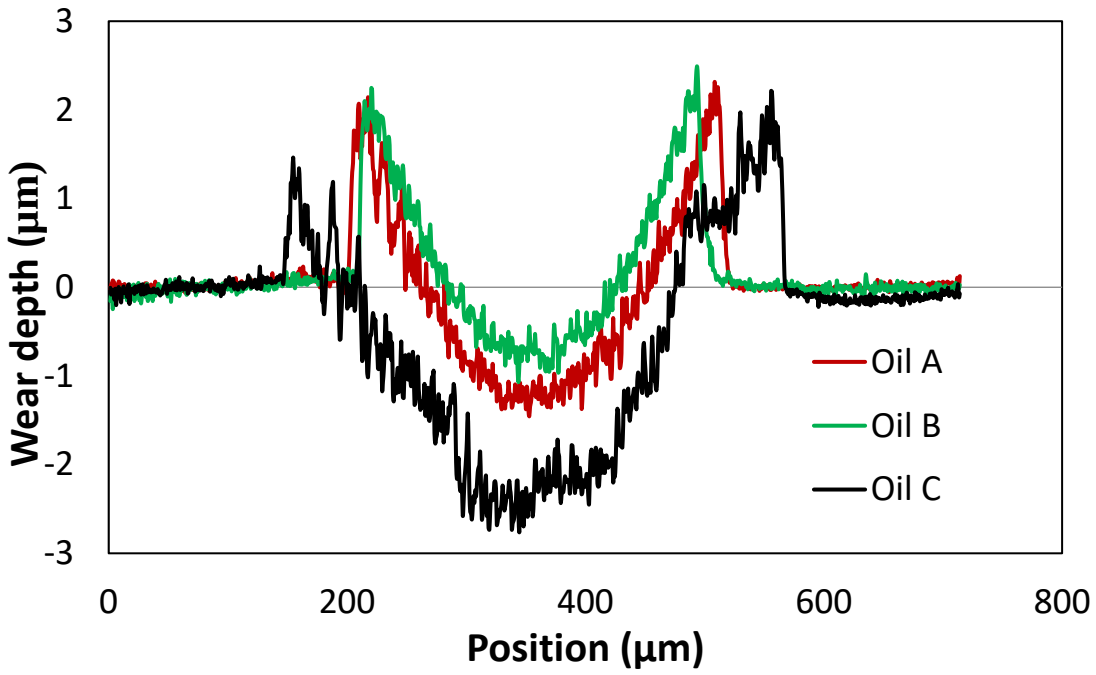

Figure 4.7: Cross-section profiles of the wear scars generated from 2 hours sliding tests with oils A, B and C

4.3.2 Subsurface changes (mechanical and microstructural)

Section 4.3.1 focused on how the tribological performance of the gear oils relates to the nature and extent of the tribofilm formed and also the surface topography. However, the tribological performance of the oils may also be a function of subsurface changes. The aim of this section is to investigate the effect of friction and wear performance on subsurface changes (mechanical and microstructural) and to evaluate any correlation that might exist. Subsurface characterisation was conducted on the surfaces generated after 5 min of sliding wear in the HFRR tribometer. Since the test ball is approximately 3 times harder than the test disk (substrate), plastic deformation and wear is expected to occur entirely on the substrate. No wear was observed on the test ball. Therefore investigation of subsurface changes was conducted on the spheroidised AISI 52100 steel substrate.

The frictional energy generated during sliding of surfaces is dissipated in many ways. Most of the energy is dissipated as frictional heat and will raise the temperature of the surfaces significantly even in well lubricated surfaces [91]. The rest of the energy is partitioned into other processes including: formation and shearing of tribofilm, transformation of the microstructure (plastic deformation) and the process of wear [65]. How frictional energy is dissipated during sliding has been the subject of previous studies [92,93,65]. These studies highlight the importance of considering just how frictional energy is divided into different processes taking place in a system. Evaluating the energy balance in the tribosystem during the sliding test is currently outside the scope of this study. Consequently, analysis of the results in this study have been simplified by assuming that the percentage of frictional energy dissipated to tribofilm formation and shearing, plastic deformation and wear is equal for the three oils. Oil A provided the lowest average friction coefficient of 0.073 ± 0.005 during the 5 min sliding test while oils B and C provided similar levels of friction at 0.087 ± 0.003 and 0.089 ± 0.003 respectively. Based on the assumption made, the higher friction coefficient of oils B and C would equate to higher stored energy in the subsurface layer and wear.

Nano-indentation technique was used to measure the hardness-depth profile for the unworn substrate and those worn in the presence of oils A, B and C to a

maximum depth of 2µm. The hardness-depth profile for the unworn surface in Figure 4.8a shows that the average hardness is approximately 3 GPa and was relatively homogenous up to the measured depth of 2 µm. The hardness-depth profiles for oils B and C in Figures 4.8c and 4.8d respectively are similar and different to that of Oil A. With oils B and C, there is significant rise in hardness towards the top surface from 3.5 GPa – 4 GPa at 2 µm below the surface to 7.5 GPa – 10 GPa at 200 nm. However with Oil A there is a relatively low increase in the hardness from 3 GPa in the unworn substrate to average of 4GPa. Another distinction with Oil A is that the increase in hardness is uniform with depth up to 2 µm. The significant hardening of the subsurface layer with oils B and C in comparison to Oil A is perhaps the first indication that there might be a correlation between the higher level of friction coefficient of oils B and C to the higher level of energy stored in the subsurface layer.

Further examination of subsurface transformation was carried out using FIB technique combined with Ion channelling contrast imaging (ICCI) to reveal subsurface microstructure. This was preferred to the conventional approach of sectioning, grinding and polishing, because of the relatively small size of the wear scar (approximately 1.5 mm by 0.5 mm). Additionally, this technique makes it possible to analyse roughly the same location (centre of the wear scar) for each of the three different samples (Figure 4.1). Figure 4.9a shows the subsurface microstructure of the substrate in the unworn state which consists of cementite (FeC) particles uniformly distributed in large ferrite grains with average grain size of 15 µm. As surface plastically deform during sliding, dislocations or defects are generated and accumulate in the ferrite grains. As sliding progresses these dislocations with strain energy associated with them begin to form dislocation tangles (DT) or dislocation dense walls (DDW)[94]. Intersecting DDW sub-divide the original ferrite grains into dislocation cells or refined blocks and with the accumulation of more dislocations, these cells evolve into sub-grains with small mis-orientations between them. With progressive refinement, of the ferrite grains, the subsurface layer is substantially work-hardened and explains the increase in

hardness in Figure 4.8. The presence of the cementite particles in ferrite facilitates refinement of the large ferrite grains [95].

The cross-sectional microstructures of surfaces lubricated by oils B and C (Figures 4.9c and 4.9d) are similar and different to that of Oil A (Figure 4.9b). With oils B and C the subsurface microstructure reveals a top layer (< 3 µm thick) of refined ferrite grains above large ferrite grains with the cementite particles uniformly distributed. However the subsurface microstructure below the surface worn with Oil A (Figure 4.9b) reveals refined ferrite grains of varying sizes surrounded by cementite particles to a large depth greater than 10µm below the surface. To better characterise the grain structures observed in Figures 4.9b and 4.9c, transmission-Electron Backscatter Diffraction (t-EBSD) technique described in section 2.9 was employed. The process involved extracting out a thin slice of about 100 – 150 nm from the cross-section shown in Figures 4.9b and 4.9c. The thin slice was then examined in transmission mode. This analysis was conducted for the cross-sections of only oils A and B since the cross-sectional microstructures of oils B and C are quite similar. The EBSD inverse pole figure maps (Figures 4.10a and 4.10c) allow clear observation of the grain size, grain orientation which is color-coded and the grain size distribution with depth. One obvious distinction between the microstructures of oils A and B in Figures 4.10a and 4.10c respectively is the difference in the depth of the refined grains. Grain refinement is localised very near the surface with oils B and C and corresponds to the hardness-profiles in Figures 4.8c and 4.8d respectively. However with Oil A grain refinement spreads deeper into the material. Also with Oil A, some of the grains within top 3µm below the surface appear elongated and below 3 µm the average size of the refined ferrite grain appears larger than those in the top layer for Oil B. The subsurface microstructures in Figures 4.9 and 4.10 correspond to the hardness-profiles in Figure 4.8 and yet again there is a similarity between subsurface changes with oils B and C. This is perhaps a second indication that there might be a correlation between higher friction coefficients obtained with oils B and C to the localisation of strain near the surface; whereas with Oil A providing lower friction coefficient the strain accumulated to a larger depth below the surface. Friction coefficient

influences the subsurface stresses during sliding. The zone of maximums stress moves from the subsurface closer to the surface as friction coefficient increases [96,97]. This might explain why with oils B and C with higher friction coefficient strain is localised nearer to the surface as evidenced by the hardness-depth profile and subsurface microstructures. Strain localisation can be induced by stress gradient developing in the subsurface layer during mechanical processes [98].

According to the assumption made earlier that the percentage of frictional energy partitioned into tribofilm formation and shearing, plastic deformation and wear process is equal during sliding with the three oils, higher wear (Figure 4.3b) would be expected with oils B and C which both have higher average friction coefficient (Figure 4.3a) in comparison to oil A after 5min of sliding. Whilst that was the case in this study, it is not always so. It is clear from previous studies [61,63] that although different oils can produce similar steady state friction coefficient during boundary lubricated sliding this does not always correlate to similar levels of wear. Nevertheless, subsurface microstructure generated during boundary lubrication sliding can be related to wear. Nanocrystalline layer typically formed below the surfaces under boundary lubrication play a crucial role in generating wear particles [99] and extent of wear [6,100]. Buscher et al. [99] in their study of nanocrystalline layer and wear particle generation found that the size of wear debris during tribo-process corresponds to the nanocrystalline grain size. Therefore they suggest that the wear particles are generated from nanocrystal torn off from the subsurface layer. Higher wear with oils B and C might be linked to significant localisation of strain very near the surface forming fine ferrite grains near the surface in comparison to oils A where the strain accumulation spreads deeper into the material. Perhaps as the refined grains gets smaller near the surface the boundary between the fine ferrite grains and the hard cementite particles weakens forming voids and eventual delamination of wear debris.

The only variable in the sliding tests conducted for this study was the lubricants and their corresponding additives mix. This will influence the nature and extent of tribofilm formed during sliding as discussed in Section 4.3.1. The tribofilms formed from the different oils during the sliding test influences how much friction is

generated in the tribosystem, how friction evolves and is dissipated into other simultaneous processes such as microstructural transformation and wear. Although it was assumed that the frictional energy generated during sliding is partitioned into other simultaneous processes in the same manner for the different oils; by simply changing the lubricant used the dynamics of how friction is dissipated into heat and other simultaneous process will likely change. There are several characteristics of the tribofilm formed that can influence the dynamics. Some of these characteristics have been investigated by other researchers in the past including: mechanical properties (shear strength, hardness etc.) of the tribofilm [47,46,41,101,102], how quickly forms and stabilizes [103-105]and its durability [106,48,107,108].

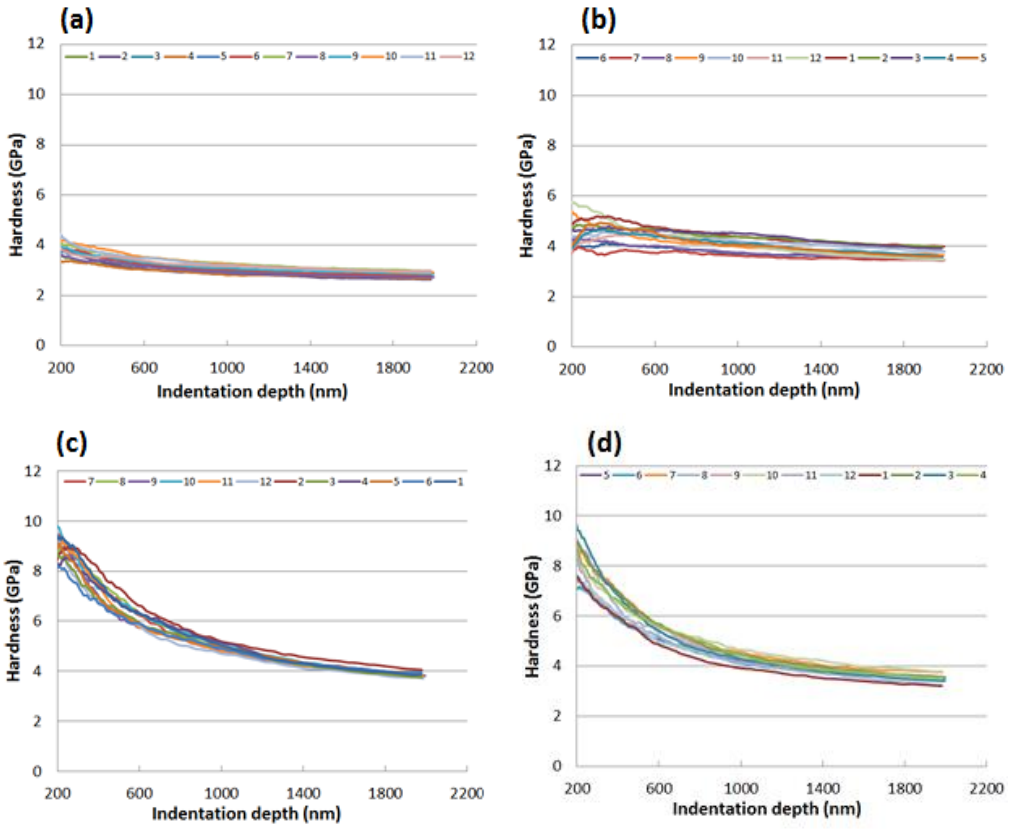

Figure 4.8: Variation of hardness with depth on (a) the unworn surface, and the worn surface after sliding test of 5 mins with (b) Oil A, (c) Oil B and (d) Oil C

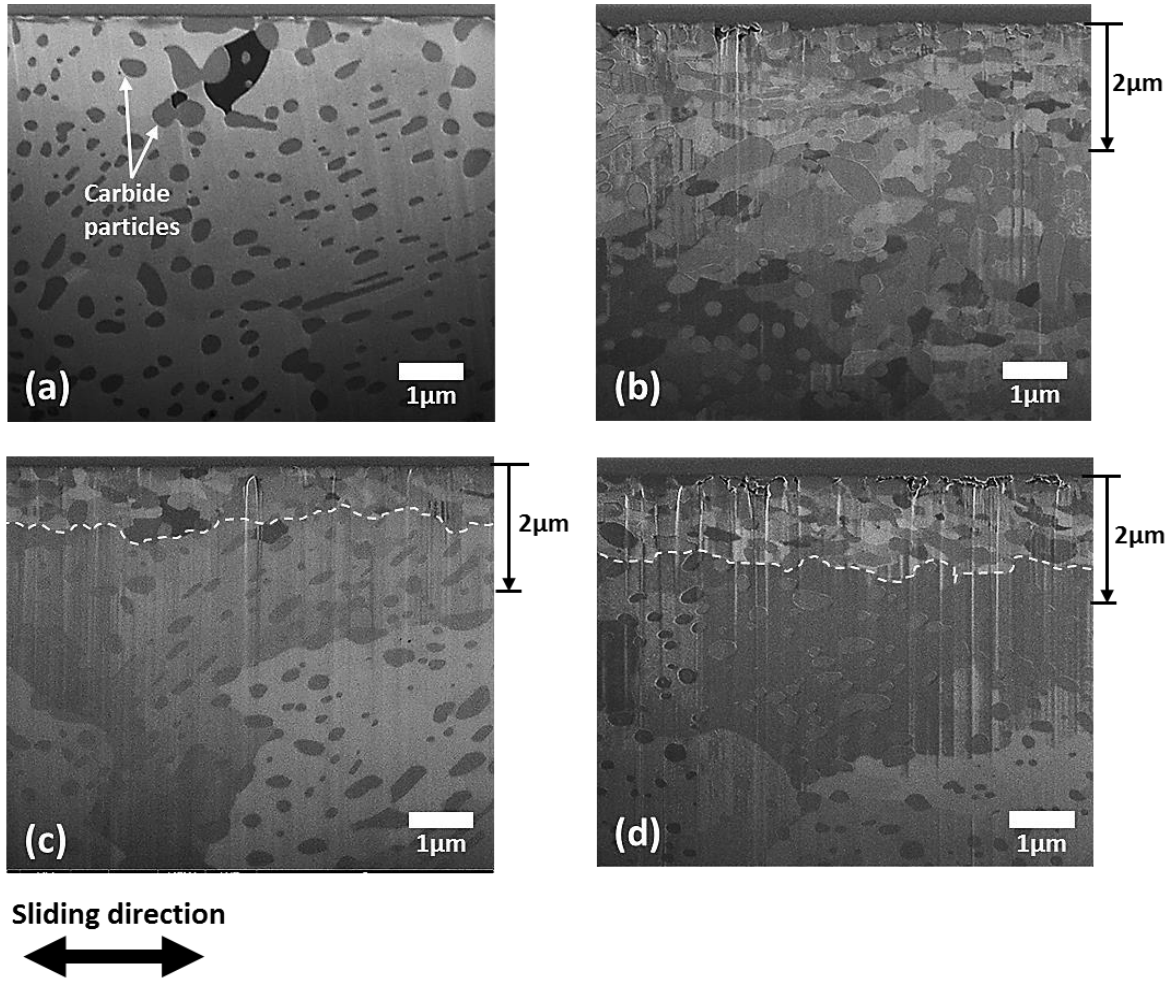

Figure 4.9: Microstructures beneath (a) the unworn surface, and the worn surface after sliding test of 5 mins with (b) Oil A, (c) Oil B and (d) Oil C

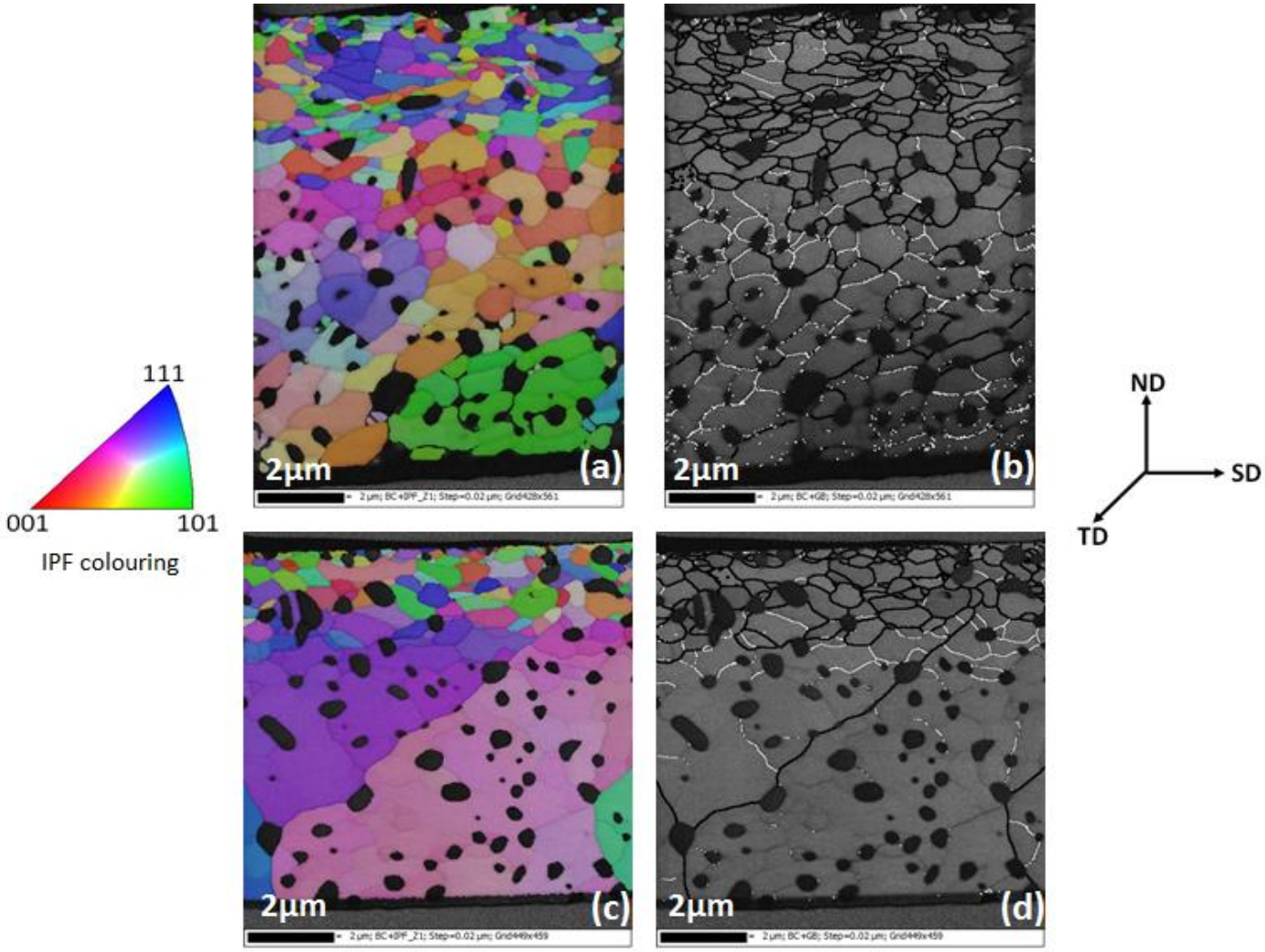

Figure 4.10: Cross-sectional EBSD images of FIB lamella extracted from the centre of the worn surfaces: (a) and(c) Inverse pole figure map for Oils A and B respectively, (b) and (d) Grain boundary superimposed on band contrast map for Oils A and B respectively. Black lines represent high angle GB's (>10°) and white lines represent Low angle GB's (2°≤θ≤10°)

4.4 Conclusions

This experimental paper has investigated the importance of combining surface characterisation (surface chemistry and topography) with subsurface examination (mechanical and microstructural changes) to better understand the mechanisms by which industrial oils perform tribologically in boundary lubricated sliding. Hence, the following conclusions are drawn:

- The combined results of ECR film formation generated by the HFRR tribometer during the sliding test with ex-situ chemical characterisation (Raman and EDX spectroscopy) of the worn surface improve understanding of the tribofilm formation process and its influence on tribological performance.
- The gear oil formulation determines the nature of tribofilm formed on the surfaces during sliding; consequently it influences the type of transformation that takes place in the metal subsurface layer mechanically and microstructurally.
- After 5 mins of sliding, Oil A provided lower friction and wear compared to Oils B and C. When compared to the original surface, Oil A produces a 33% increase in the surface hardness after sliding. Also, the depth of deformation evident by refined grains near the surface is > 10 µm. Conversely, Oils B and C produce over 100% increase in surface hardness and localised deformation to a depth of 2-3 µm below the surface.
- Tribosystems are complex due to the inter-relationship between simultaneously occurring processes such as generation of frictional heat, tribofilm formation and shearing, plastic deformation and wear. This makes it difficult to make direct correlations for example between frictional performance and subsurface changes.
- The nature of subsurface changes in tribological processes influences the extent of wear therefore to better understand how industrial lubricants and the tribofilms they form influence wear it is important to investigate their influence on subsurface changes.

Acknowledgements

The authors would like to gratefully acknowledge the financial support of the Engineering Physical Sciences Research Council UK (EPSRC) through Centre for Doctoral Training in Advanced Metallic Systems and the BP International Centre for Advanced Materials (BP-ICAM). Additionally, the BP-Castrol advisory team (Hocine Faci and Oliver Sfreddo), David Lewis, Aleks Tedstone, Bart Winiarski, Etienne Bousser are sincerely thanked for useful discussions. Appreciations also go to Andrew Forrest for his assistance with nano-indentation experiments.

Chapter 5

Paper 2: Industrial gear oils: influence of bulk oil temperature and contact pressure on tribological performance and subsurface deformation

This paper has not been published yet but has been written up with the intention of publishing it in 'Tribological Transactions' Journal.

Contributions:

Aduragbemi Adebogun – is the lead author of this article and conducted all the experiments, analysed and interpreted the results
Robert Hudson, Allan Matthews and Philip Withers gave advice on the experimental design, gave suggestions on data interpretation and also contributed to reviewing the article.

5 Industrial gear oils: influence of bulk oil temperature and contact pressure on tribological performance and subsurface changes

Aduragbemi Adebogun[1, 2, a], Robert Hudson[3], Allan Matthews[1, 2], Philip J. Withers[2]

[1] International Centre for Advanced Materials (ICAM, Manchester Hub), School of Materials, M13 9PL

[2] School of Materials, The University of Manchester, Manchester, M13 9PL, United Kingdom

[3] BP Europa SE - Castrol Industrial Monchengladbach, Germany

[a] **Corresponding Author**: Aduragbemi Adebogun, aduragbemi.adebogun@postgrad.manchester.ac.uk

Abstract

This study was designed to investigate the influence of oil temperature and contact pressure on the friction and wear performance of three industrial gear oils (oils A, B and C) but also on the corresponding changes taking place beneath the surface. Oil A contains molybdenum dithiophosphate additive friction modifier, Oil B contains amine molybdate complex friction modifier and zinc dithiophosphate antiwear additive. Oil C contains antiwear (AW)/extreme pressure (EP) phosphonate additive combined with a commercial gear oil package. The combination of the electrical contact resistance capability of the high frequency reciprocating rig (HFRR) with ex-situ chemical characterisation with Raman and energy dispersive X-ray spectroscopy provided insight into the influence of oil temperature and contact pressure on the tribofilm formation and tribological performance of the gear oils. The result showed that increase in the oil temperature and contact pressure increased surface-additive interaction, promoting the formation of low friction tribofilms. Subsurface characterisation of the worn surfaces showed that higher oil temperature and contact pressure promotes surface hardening of spheroidised AISI 52100 steel, degradation of the near-surface (< 0.8 μm) microstructural integrity and corresponds to an increase in wear. By combining surface characterisation with subsurface mechanical and microstructural changes, it is clear that the gear oil

formulations and the tribofilms they form uniquely influence the extent of subsurface deformation and wear. It is also clear that the extent of damage in the near surface is minimal with Oil B containing ZDDP antiwear additive and exacerbated with the Oil C containing EP/AW additive. The influence of the gear oils on the nature of subsurface transformation is most likely linked to a number of factors including: how quickly their tribofilm is formed, stability once formed and mechanical properties.

Keywords: boundary lubrication, gear oils, tribofilm formation, subsurface microstructure, surface hardness.

5.1 Introduction

Industrial gearboxes are becoming smaller and expected to produce more power. An Increase in the power density of gearboxes increases the severity of contact in gears and bearings. This places greater demand on the performance of gear oils which are expected to operate under higher contact pressure and wider operating temperature.

Increase in lubricant oil temperature and contact pressure reduces the lubricant film thickness (h) between surfaces, increasing the chances of direct metal contact. The ratio of the lubricant oil film thickness to the combined surface roughness of the contacting bodies is denoted as lambda ratio (λ). Lambda ratio less than one imply that the oil film thickness is less than the surface roughness of the metals in contact and is termed the boundary lubrication regime. In this case direct metal-to-metal contact is inevitable and the gear oil additives play a vital role in minimizing friction and wear. In boundary lubrication regime, the additives in the formulated oil interact with the metal surfaces to form a protective layer usually referred to as tribofilm. It is the nature of the tribofilm formed that determines the tribological performance of the gear oil.

There are several aspects of a tribofilm that contributes to its effectiveness in a tribosystem such as how quickly it forms at the contact [103,104], how stable and durable it is once formed [48,107] and also its mechanical properties (shear

strength and hardness) [47,46,41,101,102]. The combination of these factors determine the friction and wear performance of formulated gear oils.

The nature of the tribofilm formed from a lubricant is in turn influenced by the operating parameters such as temperature, contact pressure, sliding speed, additive mix amongst other factors [55,109,105,110,111]. Temperature generally increases the chemical and physical interaction of the additives with the surface [48,89]. The corresponding effect of this includes: decrease in the time it takes to form a tribofilm, complete decomposition of additive to form a tribofilm with better frictional properties and increase the thickness of the tribofilm formed. Likewise increase in contact pressure can lead to the formation low friction tribofilm, increase the rate of decomposition of friction modifier additive MoDTC [55] and also ZDDP additive [109].

Most studies on formulated oils usually involve a focus on the tribofilm formed using chemical characterisation techniques, examination of wear surfaces generated. Some other studies examine the tribofilm formation using electrical contact resistance technique. This technique makes it possible to track the formation of an insulating film whilst the tribological test is going on in-situ. Tribosystems are complex and require a multi-scale approach as well as a combination of various techniques to better understand the mechanisms of industrial lubricant's tribological performance. One approach that hasn't been well explored in the study of industrial oils is their influence on subsurface transformation and how this might relate to their tribological performance. Friction generated during boundary lubricated sliding of surfaces is mostly dissipated as heat but also induces plastic strain into the subsurface layers as the asperities are plastically deformed. Polycrystalline metals when severely deformed typically form a gradient microstructure as plastic strain decays with depth into the material. The layer just beneath the surface usually consists of micro- or nano- crystalline grains [61,63,62]. Fatigue of this layer can lead to the formation of wear debris. In a previous study [112] we studied the relationship between tribological performance of the industrial gear oils and subsurface mechanical and microstructural changes. The study concluded that the gear oil formulation and their associated tribofilm

influenced the extent of subsurface deformation and consequently influenced the wear performance. However this study aims to extend understanding of the gear oils by investigating the influence of bulk oil temperature and contact pressure on their tribological performance and how this relates to the changes taking place beneath the surface.

5.2 Materials and methods

5.2.1 Lubricants

The lubricants tested in this study are three industrial gear oils under the same ISO viscosity grade 320. The complete formulation of the lubricants includes the base oil and the complete additive mix are shown in Table 5.1. Oil A contains MoDTP friction modifier with mixed sulphonates (including calcium sulphonate). Oil B contains amine molybdate complex friction modifier (With no sulphur or phosphorus), ZDDP antiwear additive, sulphurized extreme pressure additive and sulphonate mix (including magnesium sulphonate). Oil C contains extreme pressure/antiwear additives of phosphonate and a commercial gear oil package.

Table 5.1: Base oil and additive combinations for oils A, B and C

	Oil A	Oil B	Oil C
Base oil	Polyalphaolefin (> 90%)	Group 1 base stock mix (> 85%)	Polyalphaolefin (> 80%) Alkylated Naphthalene (5-15%)
Additives	Molybdenum Dithiophosphate (MoDTP) - (< 5%)	Amine Molybdate complex (< 5%) ZDDP (< 5%) Sulphurised - extreme pressure additive	Phosphonate (< 1%) Commercial gear oil package (< 5%)
	Mixed sulphonates – corrosion inhibitor (< 0.5%) Copper - corrosion inhibitor (< 0.5%)	Sulphonate mix – corrosion inhibitor (< 5%)	
	Antifoam –trace	Antioxidant (< 1%) Methacrylate polymer – pour point	Antifoam -trace

depressant (<5%)

5.2.2 Tribotesting

Sliding test was carried out using High Frequency Reciprocating Rig (HFRR) tribometer (PCS Instruments, London, England). The test configuration is that of a ball-on-disc type where the ball slides reciprocally on the stationary disc with stroke length of 1mm and frequency of 50 Hz. The duration of the sliding test was 2 hours. To study the effect of temperature, the oils were tested at 30 °C, 80 °C and 120 °C. The contact load applied was 9.8 N which corresponds to average contact pressure of 0.94 GPa. For the contact pressure study, the oils were tested with contact load of 0.98 N, 4.9 N and 9.8 N which corresponds to contact pressures of 0.44 GPa, 0.75 GPa and 0.94 GPa respectively. For this study, the tests were run at 80°C. Friction coefficient is measured and stored throughout the sliding test. In Addition, the HFRR is designed to measure electrical contact resistance (ECR) between the test ball and disc. This makes it possible to track the formation of any insulating film formed in the contact.

5.2.3 Ball and Disc.

The test ball and disc used in the HFRR experiment were made of AISI 52100 steel. The balls were 6 mm in diameter with measured hardness of 11.7 ± 1 GPa. The measured surface roughness (Ra) was less than 0.05 µm. The discs were 10 mm in diameter, 3 mm thick and the hardness measured was 3.3 ± 0.2 GPa. The surface roughness of the discs was 0.02 µm on average. The test ball and discs were cleaned using toluene and acetone prior to testing. After the test the residual oil was removed with Heptane. The test discs were further degreased with soapy water and ethanol for further characterisation in the scanning electron microscope.

5.2.4 Wear measurement

A Keyence VK-X200 3D confocal laser microscope was used to scan the profile of the wear scar on the test discs. Thereafter, post-processing of the data was carried out using VK Analyser software. The first step was to correct for slight tilt of the sample on the microscope stage. To calculate the wear volume, 2D profiles across

the wear scar were selected and the cross-sectional area below the surface was calculated. The average of the 10 cross-sectional areas was multiplied by the wear scar length to estimate wear volume. Specific wear volume was then calculated by dividing the wear volume by the normal load and sliding distance of 360 m. Measurement was carried out only on the discs as there was no observable wear on the test balls.

5.2.5 Raman spectroscopy

A Renishaw 1000 microscope system was used to chemically analyse the tribofilm. An Argon laser source with wavelength of 514 nm was used. The scans were carried using 50X Olympus objective lens which gives a laser spot of about 1 µm. An exposure time of 1 s was used to minimize excessive heating of surface and 20 accumulations to reduce the signal-to-noise ratio.

5.2.6 Scanning electron microscopy – energy dispersive spectroscopy (SEM – EDX)

FEI Quanta 650 scanning electron microscope (SEM) equipped with energy-dispersive X-ray (EDX) spectroscopy detector was used to image the wear scar and map out the elements present on the surface. Surface imaging and EDX mapping were carried out with accelerating voltages of 5 and 30 kV respectively.

5.2.7 Nanoindentation

The Hardness of the discs was measured within the wear scar generated after sliding using an MTS Nano Indenter XP system. The continuous stiffness measurement (CSM) mode enables continuous measurement of the hardness with depth up to 2 µm as the Diamond Berkovich indenter tip penetrates the surface at a constant strain rate of 0.05 s^{-1}. Hardness-depth profile of the as-received disc was measured for reference.

5.2.8 Scanning electron microscopy – focused ion beam (SEM-FIB)

To examine the subsurface microstructure, a scanning electron microscope (SEM) with focused ion beam (FIB) was employed. The dual beam system used was FEI Nova NanoLab. Using ion beam a trench is generated within the wear scar to

expose the cross-sectional microstructure and then imaged. Ion beam imaging was carried out with voltage of 30kV and beam current of 9.7 pA.

5.2.9 Calculation of lambda ratio

The minimum film thickness (h_{min}) was calculated using the empirical formula proposed by Dowson and Hamrock [113]:

$$\frac{h_{min}}{R'} = 3.63\left(\frac{U\eta_0}{E'R'}\right)^{0.68}(\alpha E')^{0.49}\left(\frac{W}{E'R'^2}\right)^{-0.073}\left(1-e^{-0.68k}\right) \quad \textbf{Equation 5.1}$$

Where R' is reduced radius of curvature, U is the speed, η_0 is dynamic viscosity, E' is reduced Young's modulus, α is pressure-viscosity coefficient, W is normal load

Table 5.2: Variation of lambda ratio with oil temperature and contact pressure

Variation of oil temperature			
	Oil A	**Oil B**	**Oil C**
0.94 GPa/80 °C	0.91	0.92	0.93
0.94 GPa/120 °C	0.47	0.38	0.45
Variation of contact pressure			
80 °C /0.44 GPa	1.1	1.1	1.1
80 °C /0.75 GPa	0.96	0.97	0.98
80 °C/0.94 GPa	0.91	0.92	0.93

5.3 Results and discussion

5.3.1 Tribological performance and tribofilm formation

In the boundary lubrication regime, friction and wear performance of gear oils is determined by the nature of tribofilms they form. The nature of the tribofilm formed is in turn influenced by the operating conditions in sliding contact such as oil temperature and contact pressure [55,89,109]. There are several aspects of tribofilm formation that can determine the tribological performance of gear oils. These include the induction time of the tribofilm, its stability and the chemical species or compounds formed in the tribofilm. The ECR component of the HFRR tribometer monitors the formation of any insulating film that is formed in the contact. It does not reflect the complete film formed. However, this technique can be used qualitatively to analyse the induction time of the tribofilm formed and the film stability. Raman and EDX spectroscopy are used complementarily to examine

the chemical composition of the tribofilm formed. This section focuses on the influence of oil temperature and contact pressure on the nature of tribofilm formed and the corresponding tribological performance.

5.3.1.1 Influence of bulk oil temperature

The results shows that friction reduction generally occurs with tests conducted at higher oil temperatures of 80 °C and 120 °C (Figure 5.2a) and this corresponds to the build-up of a stable insulating film (Figure 5.1). No friction reduction is observed for the tests at 30 °C (Figure 5.1). Friction coefficient at the start of sliding remains constant throughout the 2 hour test. For oils B and C, the ECR plot for the test at 30°C shows that a film covers 95% of the contact surface for most of the sliding duration. It is not clear if the ECR signal is a response to the lubricant oil film separating the ball and discs or the formation of an insulating tribofilm. It is expected that the viscosity of the oils will be higher at 30 °C. In this case it is likely there will be less direct metal contact between the ball and disc. We could not calculate lambda ratio at 30 °C due to difficulty in measuring the pressure-viscosity coefficient at 30 °C as the oils were highly viscous. Without the pressure-viscosity coefficient it is impossible to estimate the lambda value. However lambda ratio calculated for the three oils at 80 °C was between 0.91 - 0.93 (See Table 5.2). The lambda value at 30 °C can reasonably be expected to be greater than the values measured for 80 °C and 120 °C and could well exceed the boundary lubrication threshold of unity. In this case the lubrication regime would be mixed-lubrication and would support an assumption that the ball and disc are largely separated by the lubricant oil film. With Oil A at 30 °C, an insulating film is formed but is relatively unstable; whilst friction coefficient remained constant for the tests run at 30 °C. Figure 5.1 shows gradual reduction of friction coefficient with time for the tests run at 80 °C and 120 °C. Significant reduction in friction coefficient occurred with Oil A when the oil temperature was 80 °C and 120 °C, with Oil B it occurred only at 120 °C and with Oil C it occurred at 80 °C. Reduction of friction coefficient corresponds to the build-up of a stable film. We observed this to be the case for the three oils. For Oil A, the tribofilm formed at 80 °C and 120 °C is more stable in comparison to the film formed at 30 °C. With Oil B, for the test at 120 °C, there was a significant drop

in friction coefficient from about 0.15 to 0.055 5 min into the sliding test. This drop corresponds to a sharp build-up of an insulating film. For the test with Oil C at 80 °C, significant reduction in friction coefficient began about 40min into the sliding test when the insulating film becomes stable. In addition, the absence of the insulating film for Oil C at 120 °C (Figure 5.1) might be linked to significant rise in average friction coefficient (Figure 5.2a).

Raman characterisation of tribofilm formed on the wear scar indicates that surface chemistry evolves with temperature. Generally, iron oxide was formed at low temperature of 30 °C. However as temperature increases, low friction compound, MoS_2 is formed specifically with Oil A and Oil B containing organomolybdenum compounds while with Oil C, Pyrite (FeS_2) was formed. A Raman peak at 673 cm^{-1} (see Figure 5.3) was measured on the wear scars lubricated by oils A, B and C when tested at 30 °C. This peak corresponds to either iron oxide wüstite (FeO) or magnetite (Fe_3O_4) which both have identical Raman spectra [114]. Thibeau, Brown and Heidersbach [114] proposed that FeO decomposes to more stable Fe_3O_4 when exposed to laser beam. Since Fe_3O_4 is chemically more stable, we assume that the Raman peak measured at 673 cm^{-1} can be likely attributed to the formation of Fe_3O_4. The highest peak intensity of Fe_3O_4 was measured with oils B and C. For the wear scar generated with Oil A at 30 °C, $FeMoO_4$ with Raman peak of 918 cm^{-1} was also measured in addition to Fe_3O_4. Previous study by Khaemba [55] reported that $FeMoO_4$ is formed as a side reaction of iron oxide with molybdenum compounds in low temperature conditions and has been linked to high friction performance [55]. MoS_2 with Raman peaks at 375 cm^{-1} and 410 cm^{-1} was measured on the wear scars generated with oils A and B at 80 °C and 120 °C. Tribofilms containing MoS_2 are known to promote low friction performance [73,56,55]. The presence of MoS_2 on the surfaces lubricated by oils A and B at 80 °C and 120 °C is in agreement with friction reduction observed at these temperatures (Figure 5.2a). This observation is in agreement with previous work that has shown that higher temperature promotes the formation of MoS_2 and friction reduction with oils containing organomolybdenum additives [55,89]. With Oil C, Raman result shows that FeS_2 with peaks at 342 cm^{-1} and 375 cm^{-1} [115] was measured on the surfaces generated

at 80 °C and 120 °C. Oil C contains both sulphur- and phosphorus - based EP/AW additives. Previous studies [116,117] of sulphur based additives have reported the formation of FeS_2 on the wear surface.

EDX spectroscopy was used complementarily to investigate the tribofilm chemistry. Figure 5.4 shows elemental maps of the wear scars for different temperatures. The limitation of this technique is that whilst it tells us the elements present on the wear scar the exact chemical compound remains unknown. Therefore we can only make presumptions. For the three oils, more elements were measured on the wear scar generated at 80 °C and 120 °C when compared to those generated at 30 °C. This suggests increased surface reactivity. Figure 5.4 shows that oxygen is present on all the wear scars possibly due to the oxidation of the nascent surface during rubbing. The three oils contain a combination of different additives mix that interacts with the surface to form distinct tribofilms comprised of different chemical species. The nature of the chemical species in the tribofilm can influence the friction and wear performance of the oils. With Oil A, EDX characterisation shows that oxygen, sulphur and calcium are present on the wear scars generated at 80 °C and 120 °C. Oil A contains MoDTP friction modifier and calcium sulphonate detergent, the presence of calcium strictly on the wear scar implies that the detergent is surface active and contributes to the tribofilm formed. Previous study on the interaction of calcium sulphonate and organomolybdenum compound showed that the tribofilm formed contained MoS_2 and $CaCO_3$ [118]. Wei and Song report a synergistic effect that leads to reduce wear [119]. With Oil B, the wear scars generated at higher contact pressures contains oxygen, sulphur, phosphorus, zinc and magnesium. The presence of ZDDP additive in Oil B could explains the elemental presence of zinc and phosphorus. Formulated oils containing ZDDP additives typically form tribofilms containing zinc phosphate [120,37]. In addition, Oil B also contains magnesium sulphonate detergent which explains the presence of magnesium on the wear scar. The magnesium based additive although included as a corrosion inhibitor is known to provide extreme pressure benefit. EDX map of the wear scars generated with Oil C shows the presence of oxygen, sulphur and phosphorus. Formulated oils containing P- and S- based additives have been

reported to form a multi-component tribofilm consisting of sulphides and phosphate [121-123].

Specific wear increased with tests run at higher temperatures (80 °C and 120 °C) for oils A, B and C. One possible explanation for this trend is that the severity (lambda ratio) of the contact increased as temperature of the oil increased from 30 °C to 80 °C and 120 °C. At higher temperature the viscosity of the oils will be lower, reducing the oil film thickness and increasing metal-to-metal contact. The Lambda ratio calculated for oils A, B and C (Table 5.2) at 120 °C was about 0.38 - 0.47 and is significantly lower compared to the values of 0.91 - 0.93 at 80 °C. This implies increased boundary lubrication and increased metal-to-metal contact. Changes to the nature of tribofilm formed due to increased oil temperature can also have an impact on the wear performance. These changes include those to the chemical species formed, induction time of the tribofilm and the tribofilm stability. At higher temperatures of 80 °C and 120 °C, Oil B provided the best wear performance followed by Oil A, with Oil C providing the worst wear performance. The excellent wear performance of Oil B is likely attributed to the presence of ZDDP additive in the formulation. ZDDP additive is one of the most widely used antiwear additives. The hard phosphate pads within the tribofilm reduce surface interaction and formation of wear debris. MoDTP additive contained in Oil A typically form MoS_2 which have been reported to provide excellent wear performance [124,73]. The poor wear performance of Oil C might be linked to the formation of tribofilm formed containing FeS_2. Najman [116] reported the formation of FeS_2 as the main constituent of tribofilm formed from tribo-testing of organo-sulphur EP additive. The tribofilm formed consisted of “small, smooth and randomly oriented heterogeneous features”. The author argues that the absence of large pad-like structure which is typically of ZDDP tribofilm for example explains the poor wear performance.

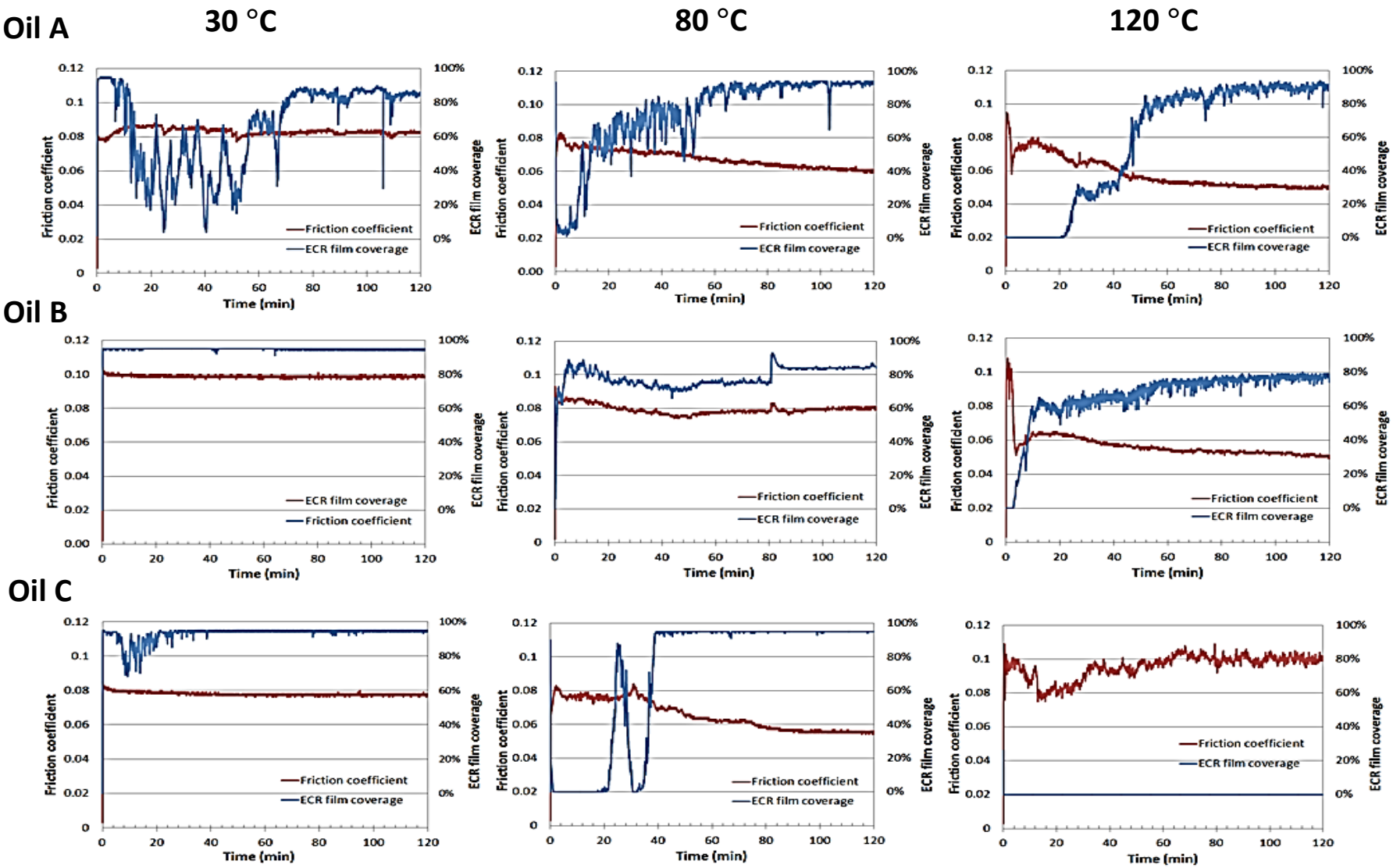

Figure 5.1: Friction coefficient and ECR film coverage for oils A, B and C at 30 °C, 80 °C and 120 °C with contact pressure of 0.94 GPa

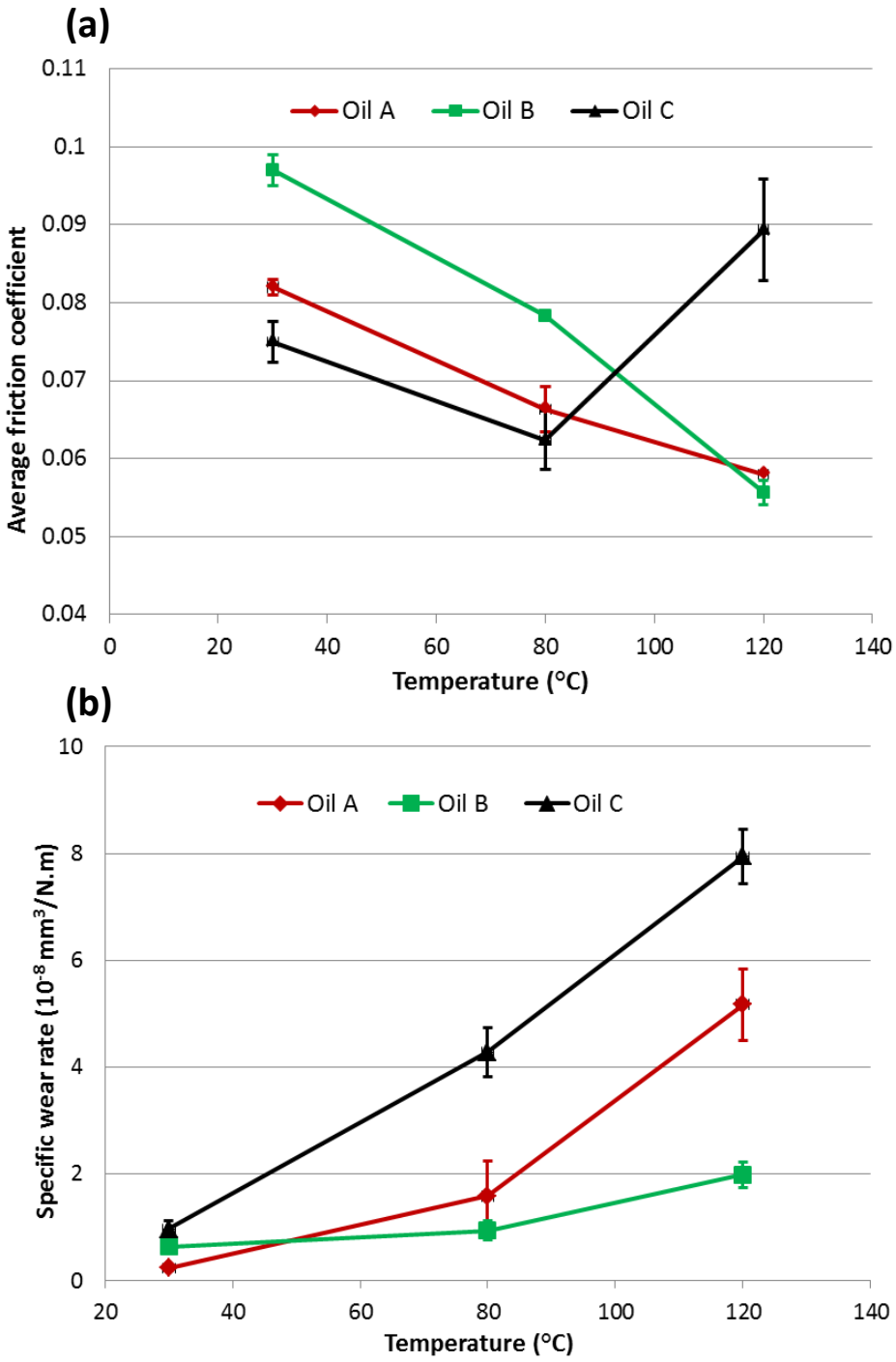

Figure 5.2: Effect of temperature on (a) average friction coefficient and (b) specific wear rate of Oil A, Oil B and Oil C. Each data point shown on graphs (a) and (b) represents the average friction coefficient (N = 3) and average specific wear rate (N = 3) respectively. The error bars represent the standard deviation.

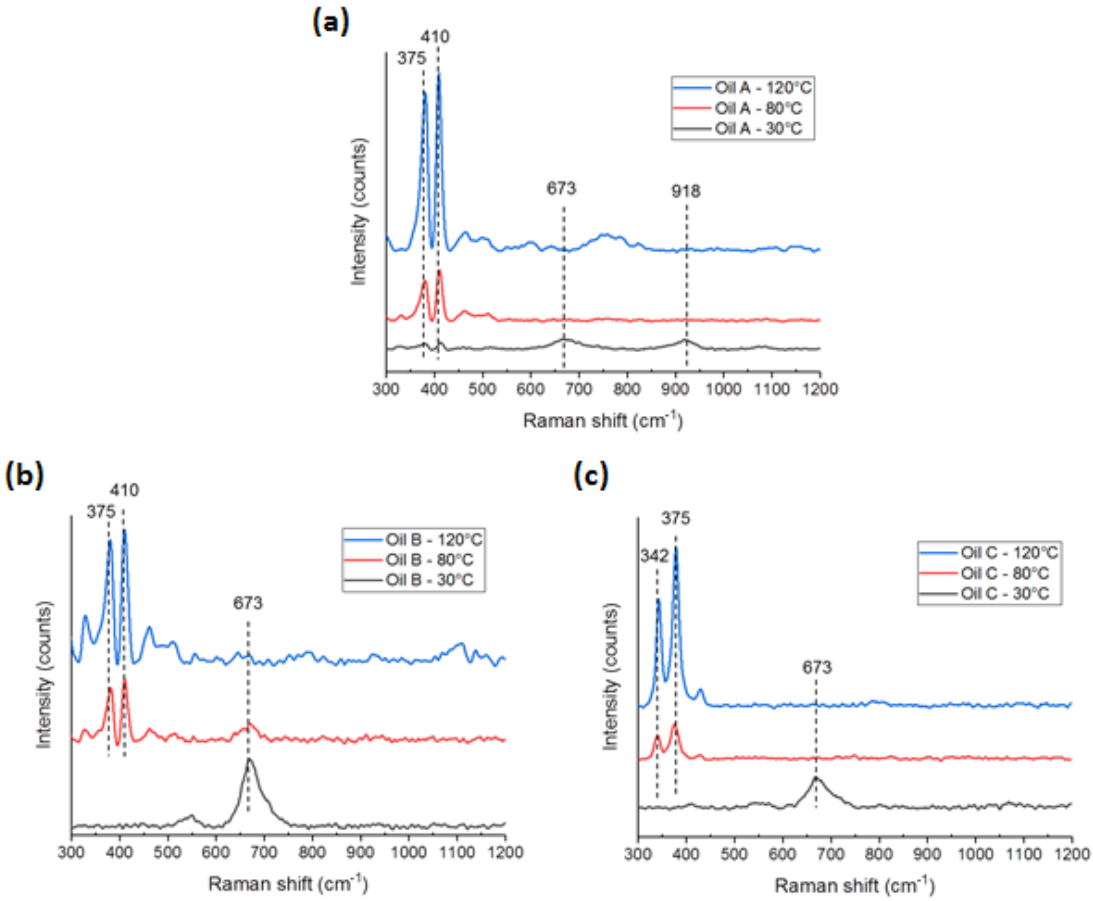

Figure 5.3: Effect of temperature on the Raman spectra measured on wear scars lubricated with (a) Oil A (b) Oil B (c) Oil C

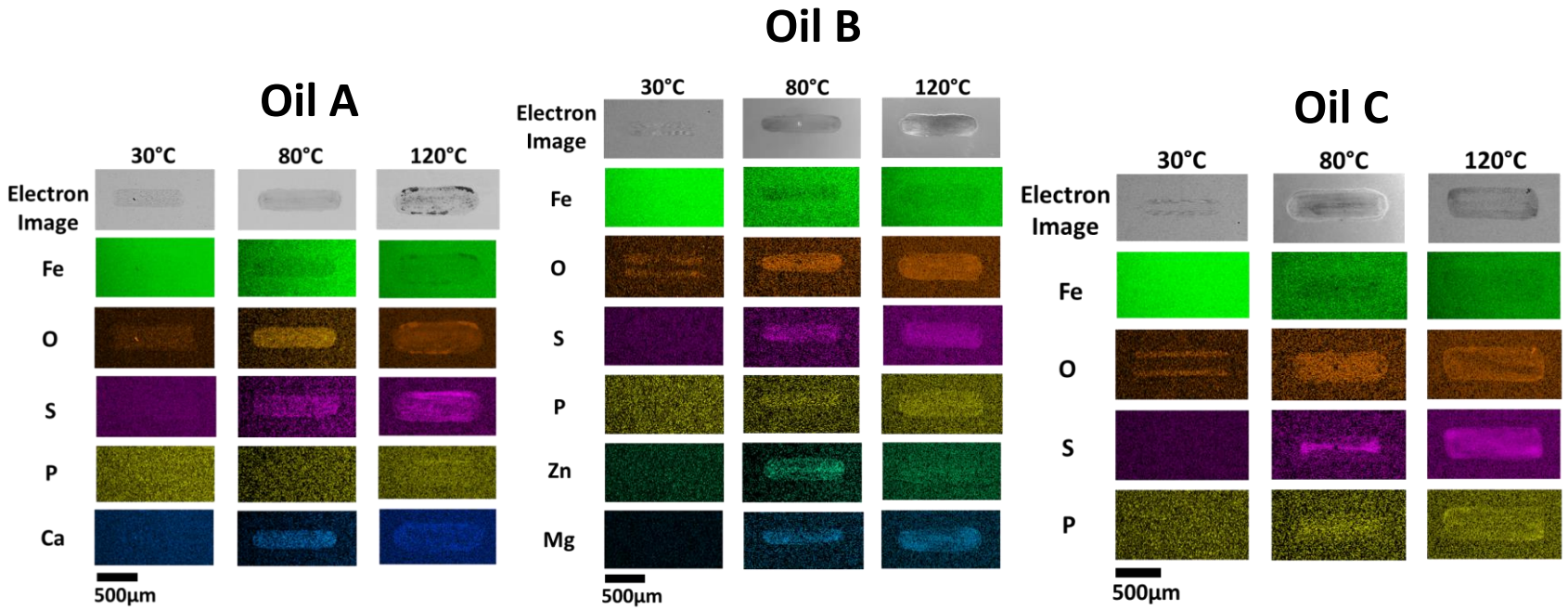

Figure 5.4: SEM images and EDX maps of wear scars lubricated by oils A, B and C after a 2 hour sliding test at temperatures of 30 °C, 80 °C and 120 °C

5.3.1.2 Influence of contact pressure

Three different loads of 0.98 N, 4.9 N and 9.8 N were used to obtain varying contact pressures of 0.44 GPa, 0.75 GPa and 0.94 GPa respectively. For these tests, the oil temperature was 80 °C. Friction reduction was observed at higher contact pressures of 0.75 GPa and 0.94 GPa and corresponds to the build-up of stable insulating films as observed with the aid of in-situ ECR measurements. In the tests conducted with low contact pressure of 0.44 GPa, friction coefficient is relatively high for the three oils and is between 0.08 - 0.12 (Figure 5.5). In addition, the friction coefficient plot is very unstable. This also corresponds to a fully insulated contact with about 95-97% film coverage with oils A, B and C. The unsteady friction is probably caused by the inability of the low load (100 g/0.98 N) to keep the ball steady on the disk as it oscillates reciprocally at 50 cycles per seconds. This also implies that for the most part, the ball is hardly in direct contact with the disk hence the ball and disks are separated by the oil film. This is likely to be the reason for high film coverage (95-97%) measured at 30 °C. However, at higher contact pressures of 0.75 GPa and 0.94 GPa, friction drops as sliding progresses particularly with Oil A and Oil C and correspond to the build-up of insulating tribofilm in the contact. Figure 5.6a shows clearly a significant drop in friction as contact pressure increases from 0.44 GPa to 0.75 GPa, and increases slightly when contact pressure increases to 0.94 GPa.

Surface chemistry measured on the wear scars evolved as contact pressure increased. Raman results are presented in Figure 5.7. With Oil A containing MoDTP, Raman peaks of MoS_2 (375 cm^{-1} and 410 cm^{-1}) , Fe_3O_4 (673 cm^{-1}) and $FeMoO_4$ (918 cm^{-1}) were measured at low contact pressure of 0.44 GPa, at higher contact pressures of 0.75 GPa and 0.94 GPa, only MoS_2 was measured. As previously mentioned, $FeMoO_4$ has been linked to high friction performance [55]. MoS_2, Fe_3O_4 and $FeMoO_4$ were also measured on wear scar lubricated with Oil B (containing amine molybdate) for test conducted at 0.44 GPa. However, at higher contact pressures, $FeMoO_4$ peak was not measured. In this study, $FeMoO_4$ was measured for tests conducted at low contact pressure of 0.44 GPa and corresponds to higher friction. This is in agreement with study by Khaemba [55]. With Oil C containing S- and P- based AW/EP additives, Fe_3O_4 was measured on wear scar lubricated at low

contact pressure (0.44 GPa); however at higher contact pressures FeS_2 peaks were measured.

Increasing contact pressure corresponds to increase in surface chemical reactivity and formation of a multi-component tribofilm. EDX characterisation of the wear scars generated at different contact pressures (Figure 5.8) shows that the wear scar contains more elements at 0.75 GPa and 0.94 GPa compared to 0.44 GPa. This suggests increased surface chemical reactivity. Increasing the contact pressure leads to a reduction in the lambda ratio (Table 5.2) from 1.1 at 0.44 GPa to 0.96-0.98 at 0.75 GPa and 0.91-0.93 at 0.94 GPa. Although the reduction in lambda ratio due to increasing contact pressure is relatively small, it is expected that there is increased contact between surfaces at higher contact pressure. This probably contributed to the increased surface reactivity. The elements identified by EDX characterisation on the wear scars generated at high contact pressures (0.75 GPa and 0.94 GPa) is similar to those generated at high temperatures (80 °C and 120 °C) for oils A, B and C. Generally, oxygen is present on the wear scars generated at all contact pressures for the three oils. The implication of the elements presents on the wear scars for oils A, B and C has been discussed in section 5.3.1

The wear response of the three oils was noticeable different as contact pressure increased. For Oil C, the wear rate continuously increased as contact pressure increased. With Oil B, the wear rate decreases and then increases at 0.94 GPa. Lastly with Oil A, wear rate increases and then stays roughly the same at 0.94 GPa. The exact reason for the different wear response is not known, however it could be that the wear regimes in operation as contact pressure increases is specific to individual formulation design and componentry.

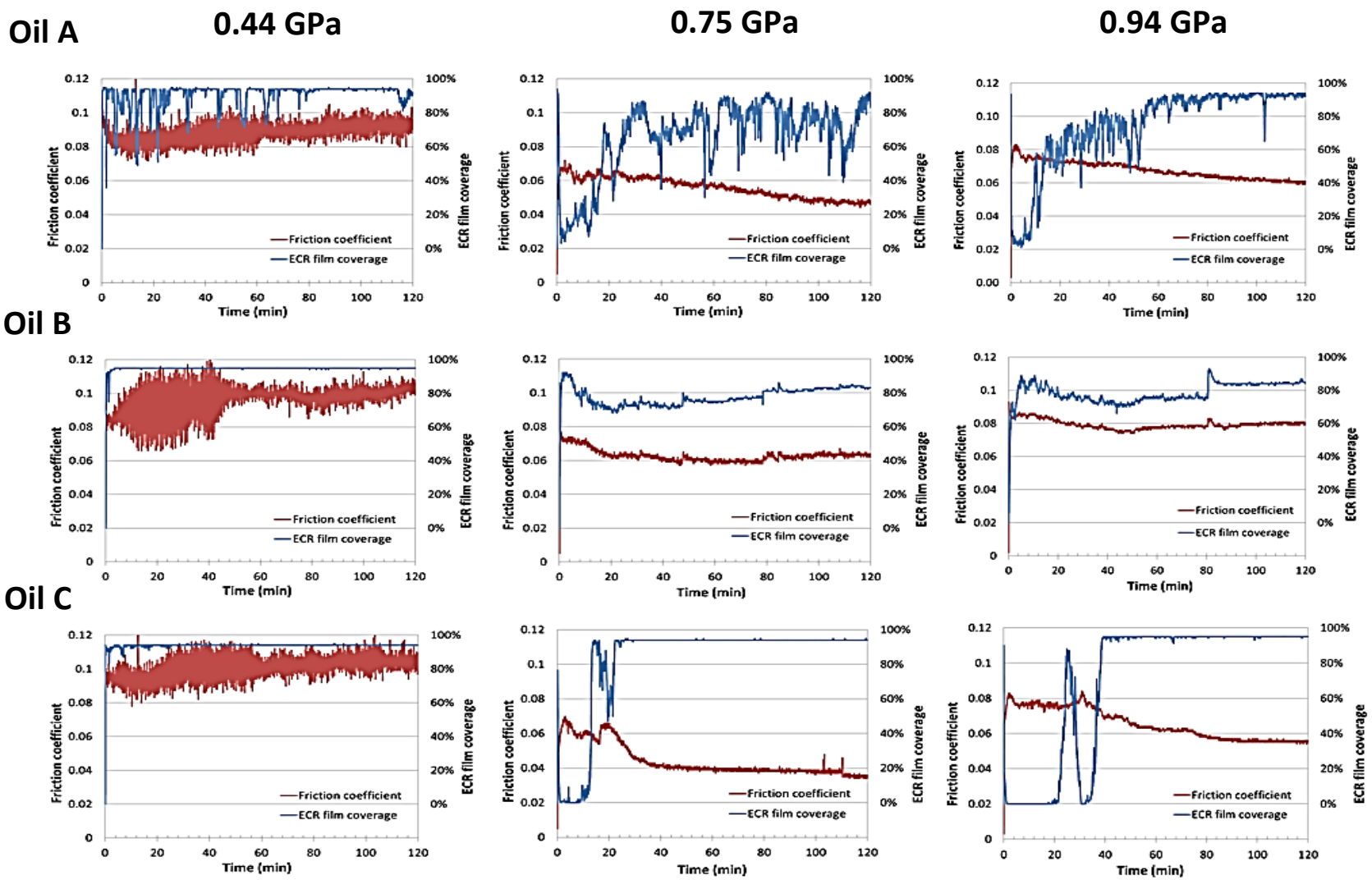

Figure 5.5 friction coefficient and ECR film coverage for oils A, B and C at 0.44 GPa, 0.75 GPa and 0.94 GPa all tested at 80 °C

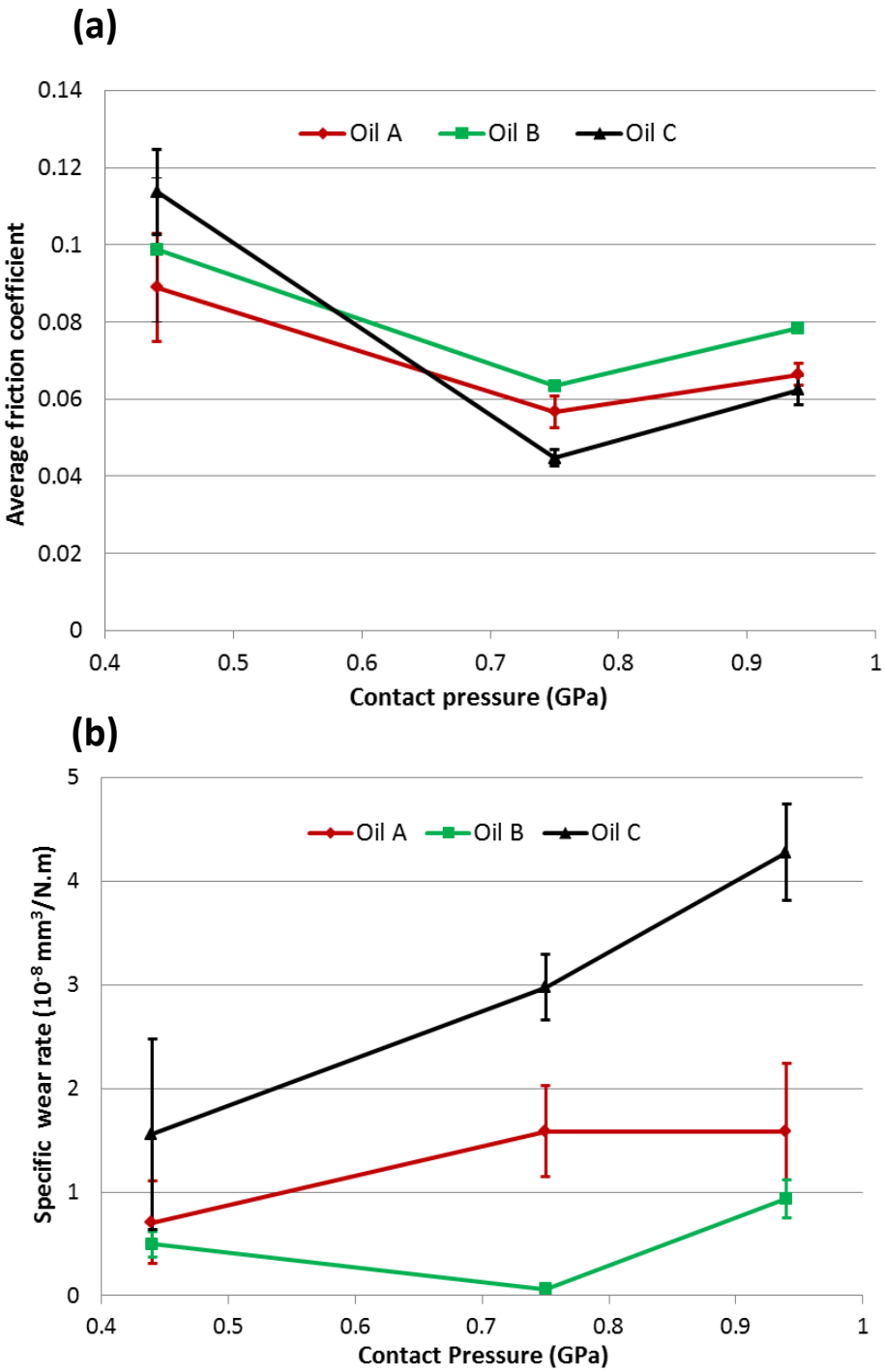

Figure 5.6: Effect of Contact pressure on (a) average friction coefficient and (b) specific wear rate of Oil A, Oil B and Oil C. Each data point shown on graphs (a) and (b) represents the average friction coefficient (N =3) and average specific wear rate (N = 3) respectively. The error bars represent the standard deviation.

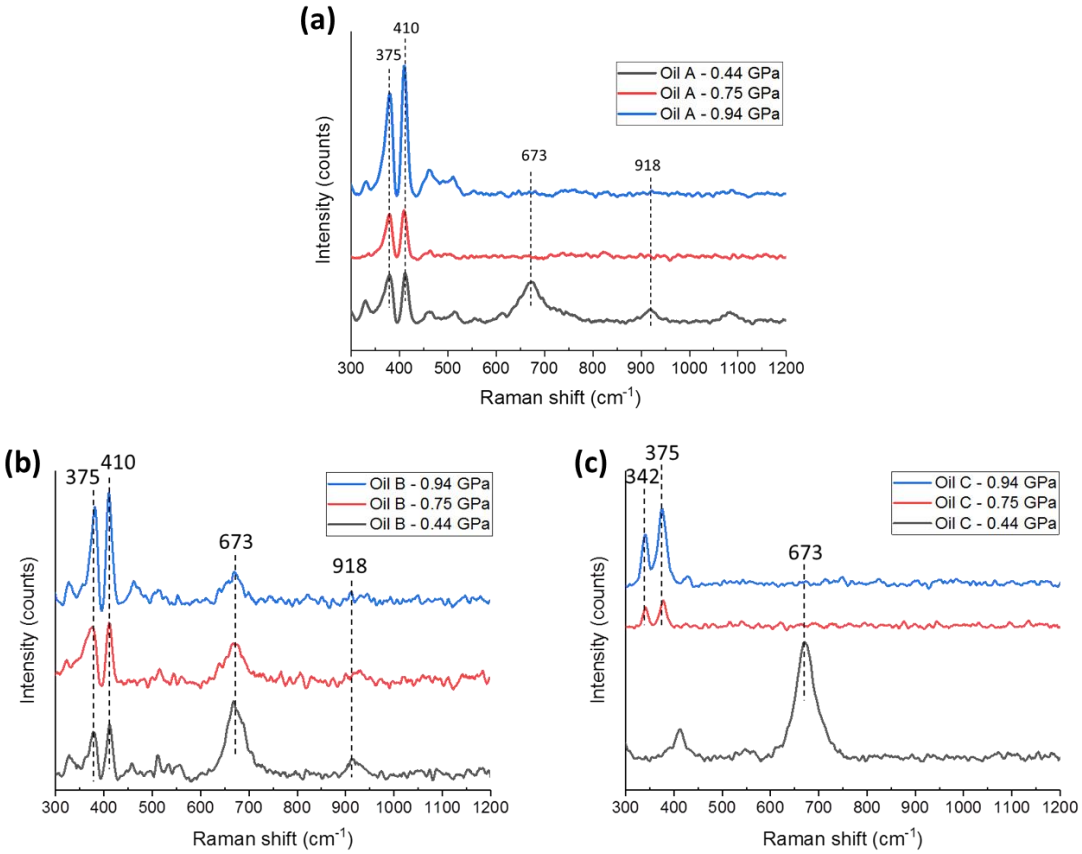

Figure 5.7: Effect of contact pressure on the Raman spectra measured on wear scars lubricated with (a) Oil A (b) Oil B (c) Oil C

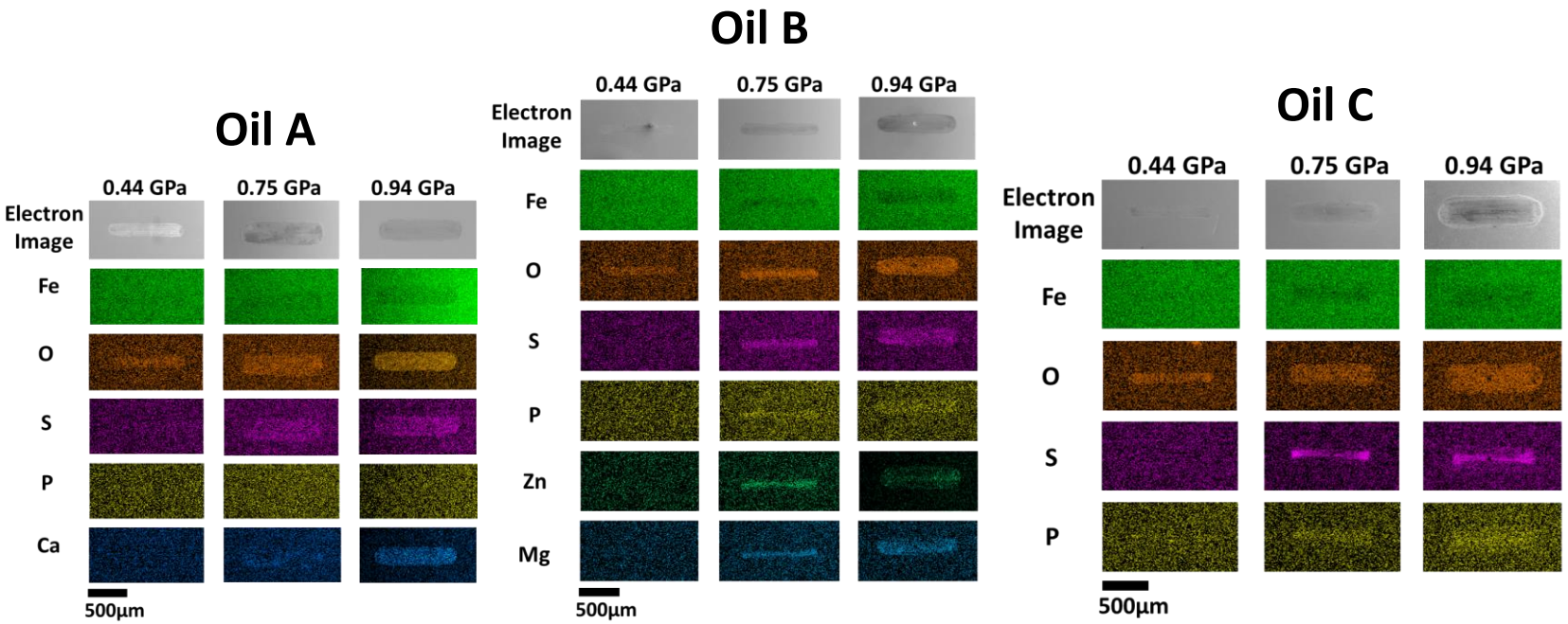

Figure 5.8: SEM images and EDX maps of wear scars lubricated by oils A, B and C after a 2 hour sliding test at contact pressures of 0.44 GPa, 0.75 GPa and 0.94 GPa

5.3.2 Subsurface changes and links to tribological performance.

Section 5.3.1 focused on the influence of oil temperature and contact pressure on the tribofilms formed for the different oils and how these affect tribological performance. It was established that increasing temperature and contact pressure increased surface-additive reactivity, hence improving the frictional performance of the oils. However, increase in oil temperature and contact pressure increased wear. This section reports the influence of oil temperature and contact pressure on subsurface mechanical and microstructural changes. In addition, the differences and similarities in the subsurface transformation for the different oils are highlighted. To examine changes taking place in the subsurface during the sliding test, the hardness-depth profile was measured for the as-received disk and within the wear scars (Figure 5.9). In addition, the cross-sectional microstructures of the worn surfaces were examined using SEM-FIB technique (Figures 5.10 - 5.14).

5.3.2.1 Influence of bulk oil temperature

The degree of subsurface hardening increased for sliding tests conducted at higher temperatures of 80 °C and 120 °C for oils A, B and C. The result for the tests conducted at 30 °C shows that the hardness-depth profile (up to 2 µm below the surface) for oils B and C was relatively unaffected i.e. the hardness-depth profile closely matches that of the unworn surface. However, with Oil A at 30 °C the subsurface was significantly hardened. For oils A, B and C, the subsurface structure was hardened to a greater extent for the tests at 80 °C and 120 °C. To aid the discussion of subsurface hardness-profile, the subsurface region examined (up to 2 µm below the surface) can be sub-divided into two regions: near-surface (< 0.8 µm below the surface) and mid-section (0.8 µm - 2 µm). With Oil A, the hardness-depth profile increased uniformly with depth, whereas with oils B and C, there is a gradient in the hardness profile in the near-surface region. The near-surface (< 0.8 µm) structure of Oil C at 80 °C and 120 °C is significantly harder than that of Oils A and B. Besides the general increase in surface hardening with temperature, hardness profile of Oil A appears to be distinct from that of oils B and C which was similarly observed in our preliminary study [112].

The unworn microstructure of the steel disk (speriodized AISI 52100 steel) consists of cementite particles (FeC) embedded in large ferrite grains (See Figure 5.10a). The subsurface microstructure of the unworn and worn surfaces were investigated with the aid of FIB preparation technique combined with ion channelling contrast imaging within an SEM. For spheroidised AISI 52100 steel material, dislocations are generated and accumulate in the near surface structure during boundary lubrication sliding. Further sliding increases the dislocation density and the dislocations begin to form tangles and dense dislocation walls (DDWs). Intersecting DDW divide the large ferrite grains into smaller cells with small misorientation between them. The extent of grain refinement is largely determined by the amount of plastic strain energy imparted into the subsurface microstructure during sliding test.

The cross-sectional microstructure for Oil A generated at different temperatures (Figure 5.10) shows that the extent of grain refinement extends much deeper into the material as temperature increased to 80 °C and 120 °C. In addition, the near-surface microstructure integrity appears compromised by the formation of voids. For the structure generated at 30 °C, the ferrite grains have been refined significantly to a large depth of about 4 μm below the surface, below which some of the original ferrite grains appear fairly intact. However, at 80 °C and 120 °C, grain refinement extent much deeper than the area captured (> 6 μm). The higher magnification microstructural images in Figure 5.11 show that the refined ferrite grains and carbide particles, although slightly difficult to distinguish in some areas. Some voids appear very near the surface for the structure generated at 80 °C. However, for the structure at 120 °C, some cracks appear to form at the interface of the refined ferrite grain and hard carbide particles.

Again, the depth of grain refinement of the subsurface structure generated with Oil B (Figure 5.12) appears to increases with temperature; although the depth of deformation appears to be less when compared to those of Oil A at different temperatures. In addition, the near-surface integrity is also relatively intact. The subsurface microstructure generated at 30 °C contains large ferrite grains with barely any evidence of grain refinement suggesting that the surface was barely

deformed during the sliding test. However for the surfaces generated at 80 °C and 120 °C the microstructures were deformed to some extent as evidenced by the refinement of the ferrite grain. The depth of the refined layer is about 2 μm for the surface generated at 80 °C and about 3 μm for the surface generated at 120 °C. Higher magification of the cross-sectional microstructures (Figure 5.13) shows that the near surface microstructure generated at 30 °C contains particles embedded in the ferrite grains with no evidence of grain refinement. However grain refinement is observed with the surfaces generated at 80 °C and 120 °C.

The subsurface microstructures generated with Oil C are shown in Figure 5.14. Similar to the results of oils A and B, the extent of grain refinement is greater for the test conducted at 80 °C and 120 °C. Closer examination of the very near surface shows that the integrity of the microstructure for the 80 °C and 120 °C is severly compromised when compared to those of oils A and B. The microstructure generated with oil temperature of 30 °C show a thin layer of refined grains (< 1 μm) sitting on large ferrite grains that appear barely deformed. Whereas for the microstructures generated at 80 °C and 120 °C, grain refinement is extensive with depth greater than the capture area (> 6 μm). The higher magnification images of the near-surface (Figure 5.15) show clear distinct between the surfaces generated at different temperatures. The near surface microstructure generated at 30 °C shows refinement of the ferrite grain with no voids or crack. The structure generated at 80 °C shows grain refinement of the ferrite grain but also rupture of the ferrite matrix and troughs probably generated due to wear of the weak ferrite matrix. The trough appears black and is likely filled with tribofilm generated on the surface. The microstructure generated at 120 °C shows evidence of extreme damage including: severe grain refinement, cracks and weak ferrite matrix and troughs containing what appears to be likely tribofilm generated on the surface during slidng. Extreme grain refinement observed for the microstructure generated at 120 °C might explain the relatively high surface hardening with Oil C at 120 °C in Figure 5.9c.

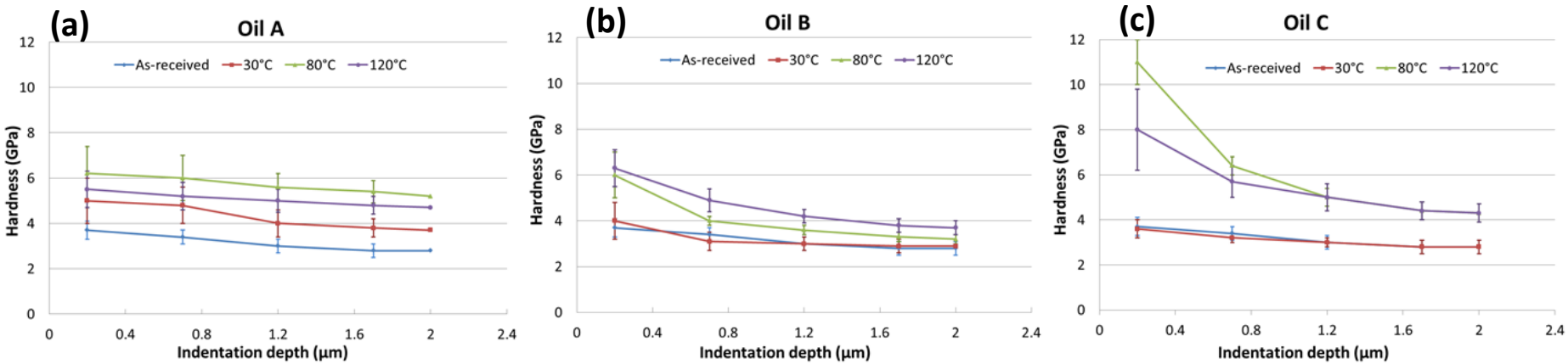

Figure 5.9: Effect of temperature on hardness-depth variation for oils A, B and C. Each data point on graphs (a), (b) and (c) represents average hardness (N = 8 – 15) across the wear scar with at least 50 µm spacing between any two locations of measurement. The error bars represent the standard deviation.

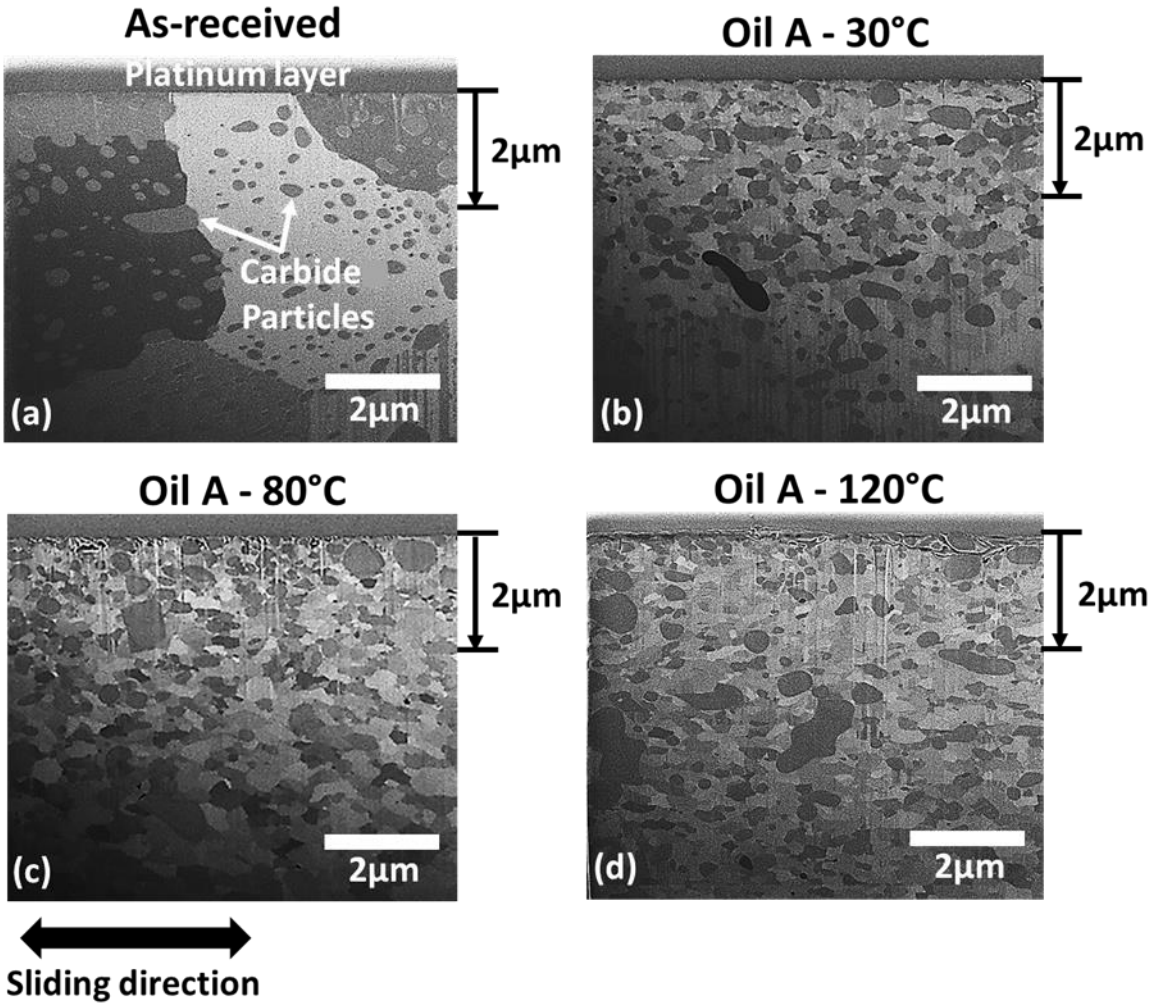

Figure 5.10: Subsurface microstructures of the (a) as-received material and after 2 hour sliding test with Oil A at (b) 30 °C (c) 80 °C (d) 120 °C and contact pressure of 0.94 GPa

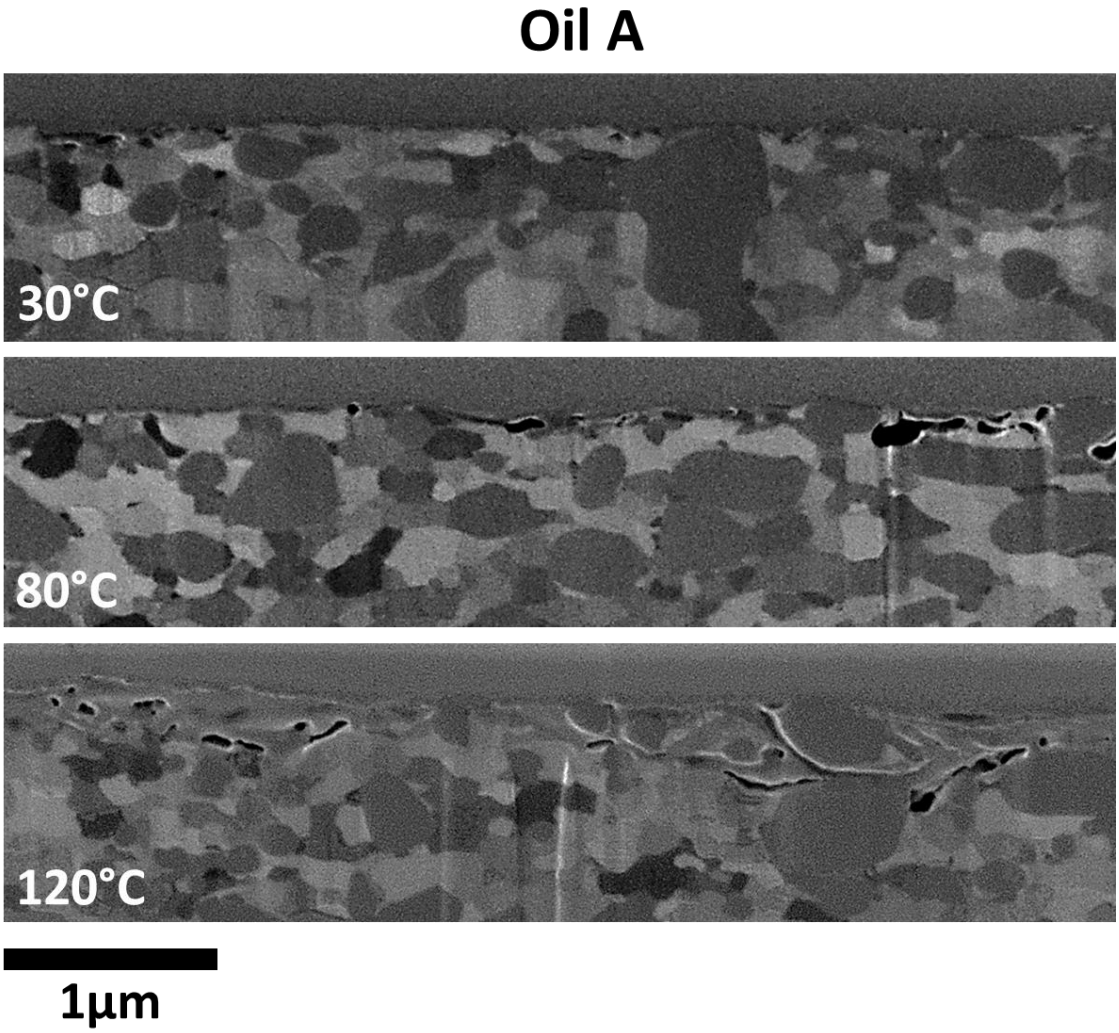

Figure 5.11: Higher magnification of the cross-sectional microstructures generated with Oil A at 30 °C, 80 °C and 120 °C

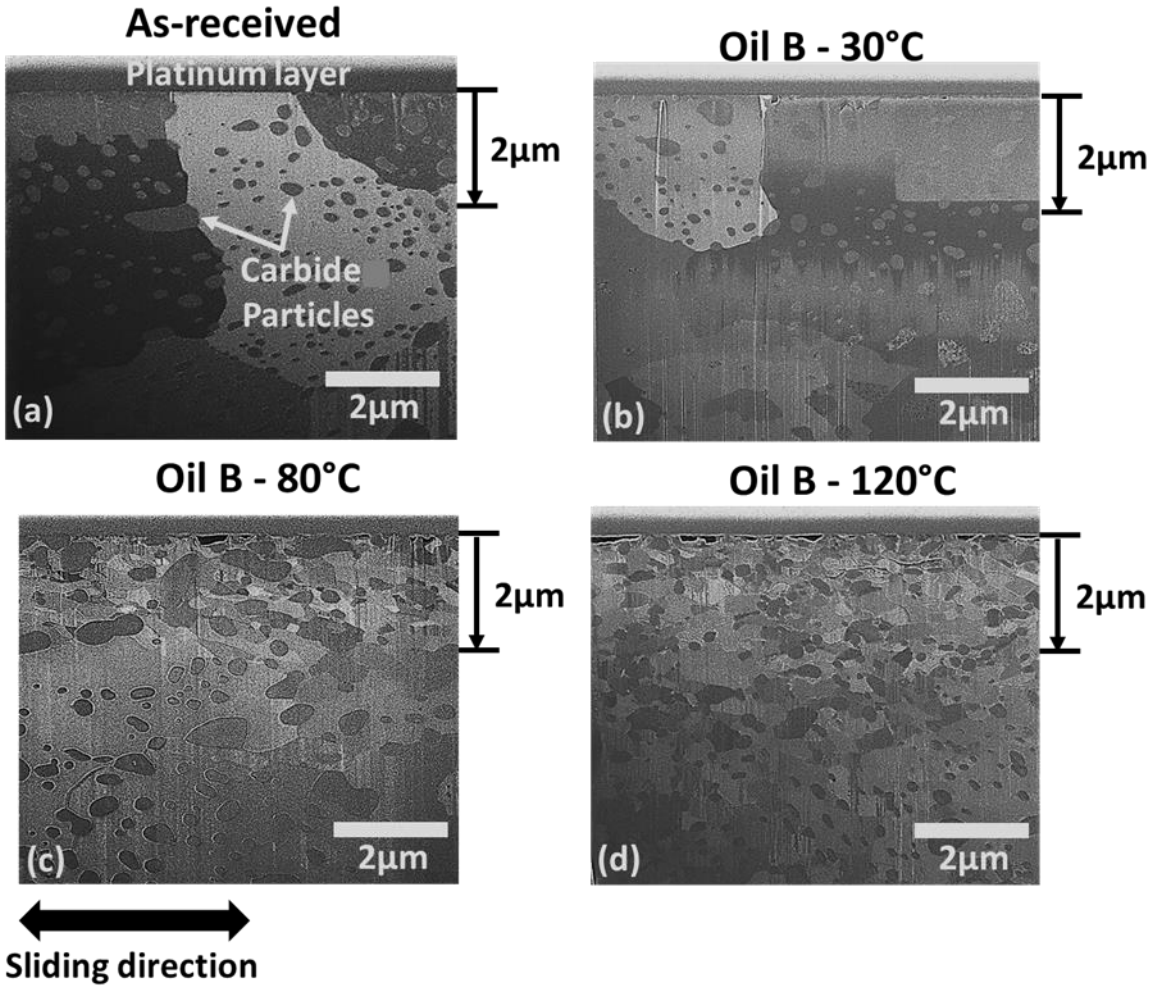

Figure 5.12: Subsurface microstructures of the (a) as-received material and after 2 hour sliding with Oil B at (b) 30 °C (c) 80 °C (d) 120 °C and contact pressure of 0.94 GPa

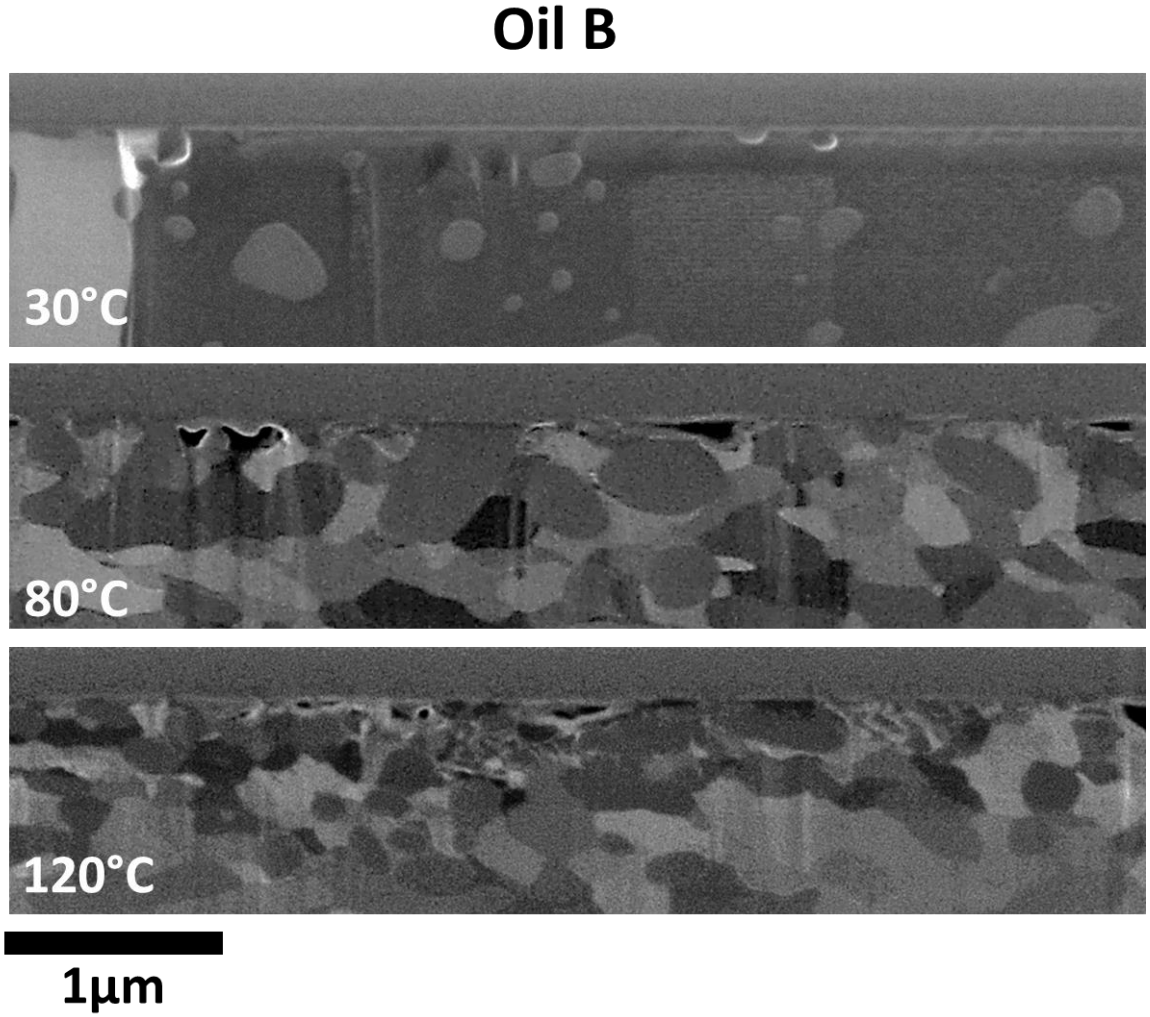

Figure 5.13: Higher magnification of the cross-sectional microstructures generated with Oil B at 30 °C, 80 °C and 120 °C

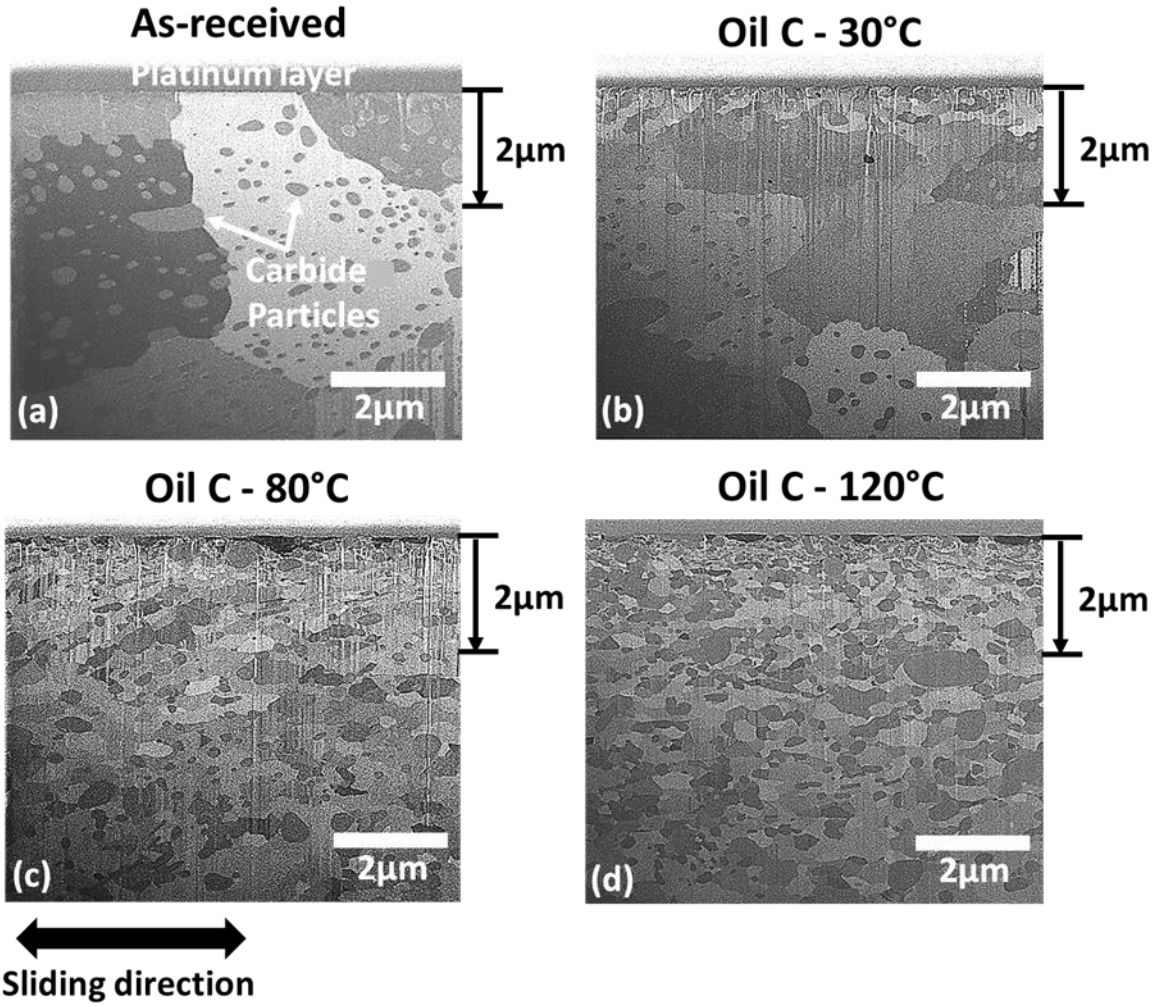

Figure 5.14: Subsurface microstructures of the (a) as-received material and after 2 hour sliding test with Oil C at (b) 30 °C (c) 80 °C (d) 120 °C and contact pressure of 0.94 GPa

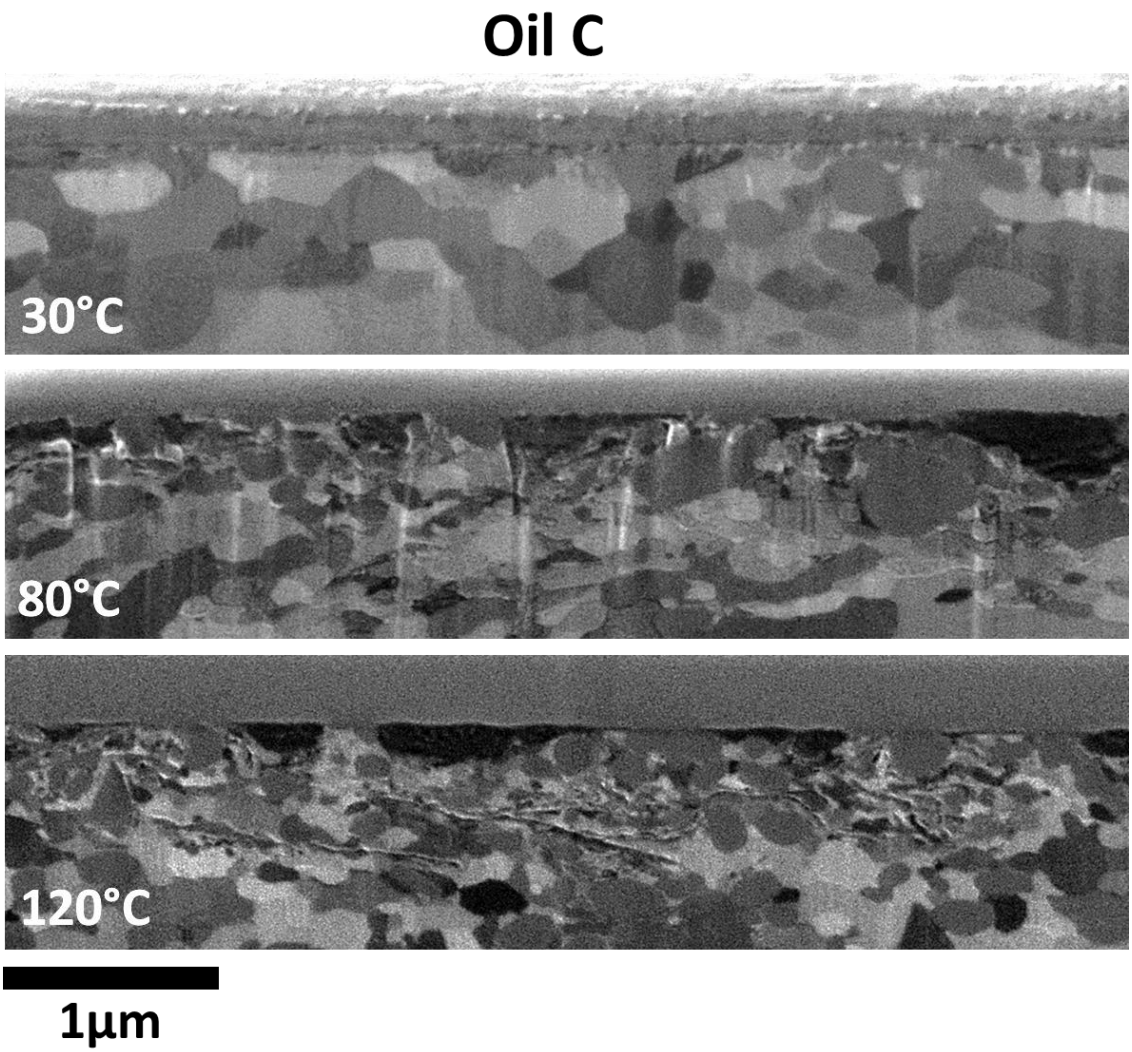

Figure 5.15: Higher magnification of the cross-sectional microstructures generated with Oil C at 30 °C, 80 °C and 120 °C

5.3.2.2 Influence of contact pressure

The effect of contact pressure on the hardness-depth profiles for oils A, B and C are shown in Figure 5.16. The extent of surface hardening increased significantly with increase in contact pressure particularly with oils A and C, whereas with Oil B, the hardness-depth profile did not change significantly at higher contact pressures. For Oil A, the hardness-depth profile is fairly uniform up to the measured depth of 2 µm. Conversely, for oils B and C, there is a gradient in the hardness-profile such that the hardness of the near-surface structure increases towards the surface. The extent of surface hardening in the near-surface region (< 0.8 µm) is relatively high

with Oil C (particularly for the tests at 80 °C and 120 °C), with values at the surface (9-11 μm) exceeding twice the value of the unworn surface (approx. 4 μm).

Figure 5.17 shows the cross-sectional microstructures generated with Oil A at different contact pressures. For the test conducted at 0.44 GPa, the microstructure shows grain refinement up to about 3 μm below the surface. Below 3μm, large ferrite grains appear undeformed. The microstructure generated at 0.75 and 0.94 GPa shows extensive grain refinement to a depth beyond the captured area (> 6 μm). For the microstructure generated at 0.94 GPa, it appears that there is a gradient in the grain size with increasingly bigger grains with depth. Higher magnification images of the cross-sectional mictrostructures are shown in Figure 5.18. Grain refinement of the ferrite matrix is evident from the microstructures generated at 0.44 GPa, 0.75 GPa and 0.94 GPa. However, voids near the surface only appear on the microstructure generated with contact load of 0.94 GPa.

From the cross-sectional microstructures for Oil B (Figure 5.19), the depth of the refined ferrite grain is limited to about 2 μm for the test at different contact pressures; whereas with Oil A, the depth of grain refinement exceeds 6 μm for the 0.75 GPa and 0.94 GPa microstructures. The layer of refined ferrite grain seats on large ferrite grains that appear intact and undeformed. This suggests that plastic strain accumulated during sliding is largely limited to the near surface (≤ 2 μm). Higher magnification images of the near-surface structures (Figure 5.20) shows refined ferrite grains with voids/cracks except for the microstructure at 0.94 GPa were a few voids can be seen.

The subsurface microstructure generated with Oil C at different contact pressures are shown in Figure 5.21. There's evidence of increased plastic strain accumulation with increasing contact pressure. To begin with, the depth of grain refinement increased with contact pressure from about 2 μm for both the 0.44 GPa and 0.75 GPa microstructure to about 5 μm for the 0.94 GPa microstructure. Closer observation of the near surface microstructure (Figure 5.22) shows that with the microstructure generated at 0.44 GPa, the ferrite grain is refined but the surface is intact with no voids or cracks. Whereas with the microstructure generated at 0.75

GPa, some of the grains appear elongated, there's evidence of delamination of the ferrite matrix and generation of troughs contain black matter which is likely tribofilm generated at the surface. For the microstructure generated at 0.94 GPa, troughs are also generated as well as the formation of cracks aligned in the sliding direction.

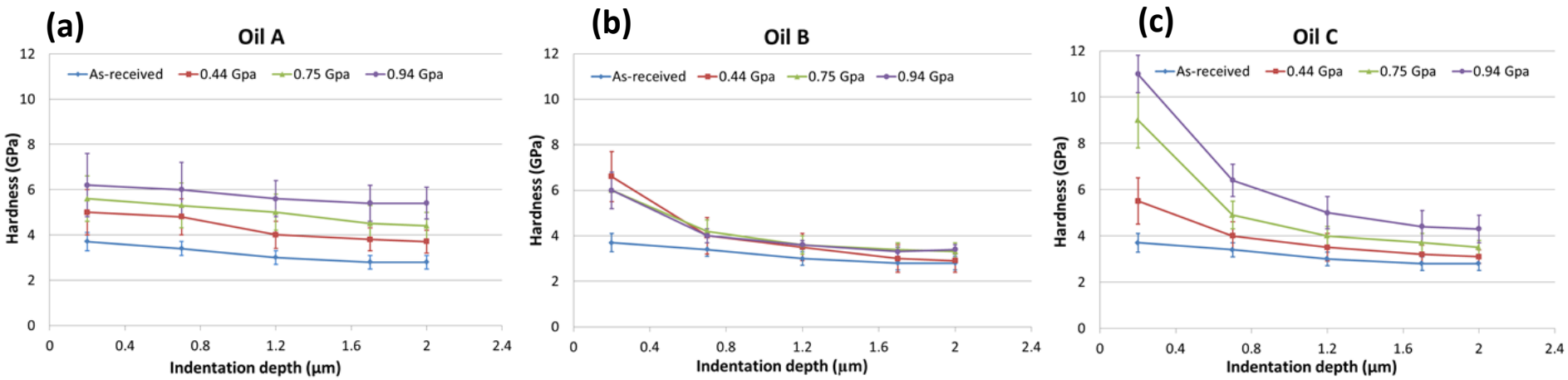

Figure 5.16: Effect of contact pressure on hardness-depth variation for oils A, B and C. Each data point on graphs (a), (b) and (c) represents average hardness (N = 8 – 15) across the wear scar with at least 50 µm spacing between any two locations of measurement. The error bars represent the standard deviation.

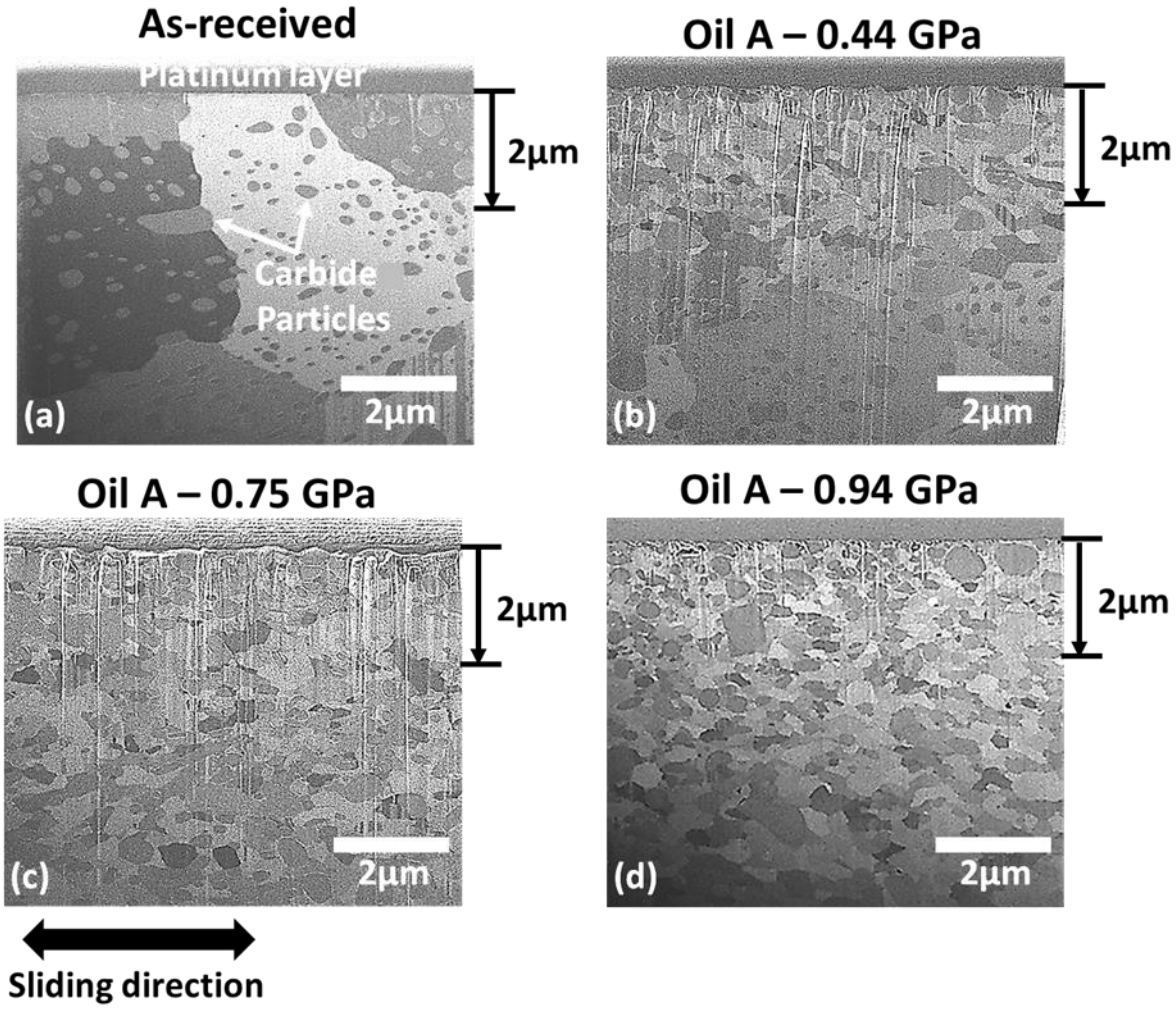

Figure 5.17: Subsurface microstructures of the (a) as-received material and after 2 hour sliding test with Oil A at (b) 0.44 GPa (c) 0.75 GPa (d) 0.94 GPa and temperature of 80 °C

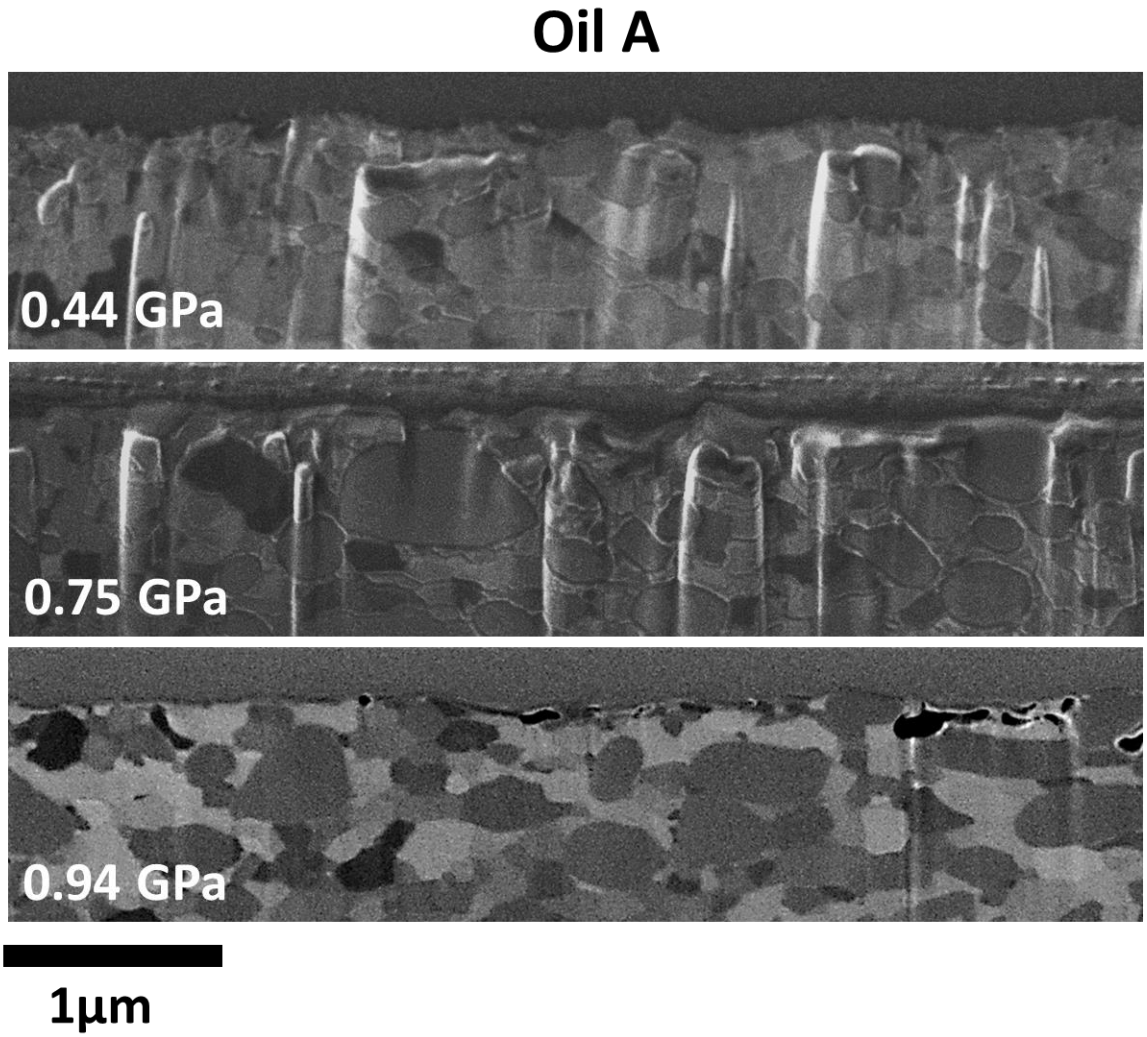

Figure 5.18: Higher magnification of the cross-sectional microstructures generated with Oil A at 0.44 GPa, 0.75 GPa and 0.94 GPa all tested at 80 °C

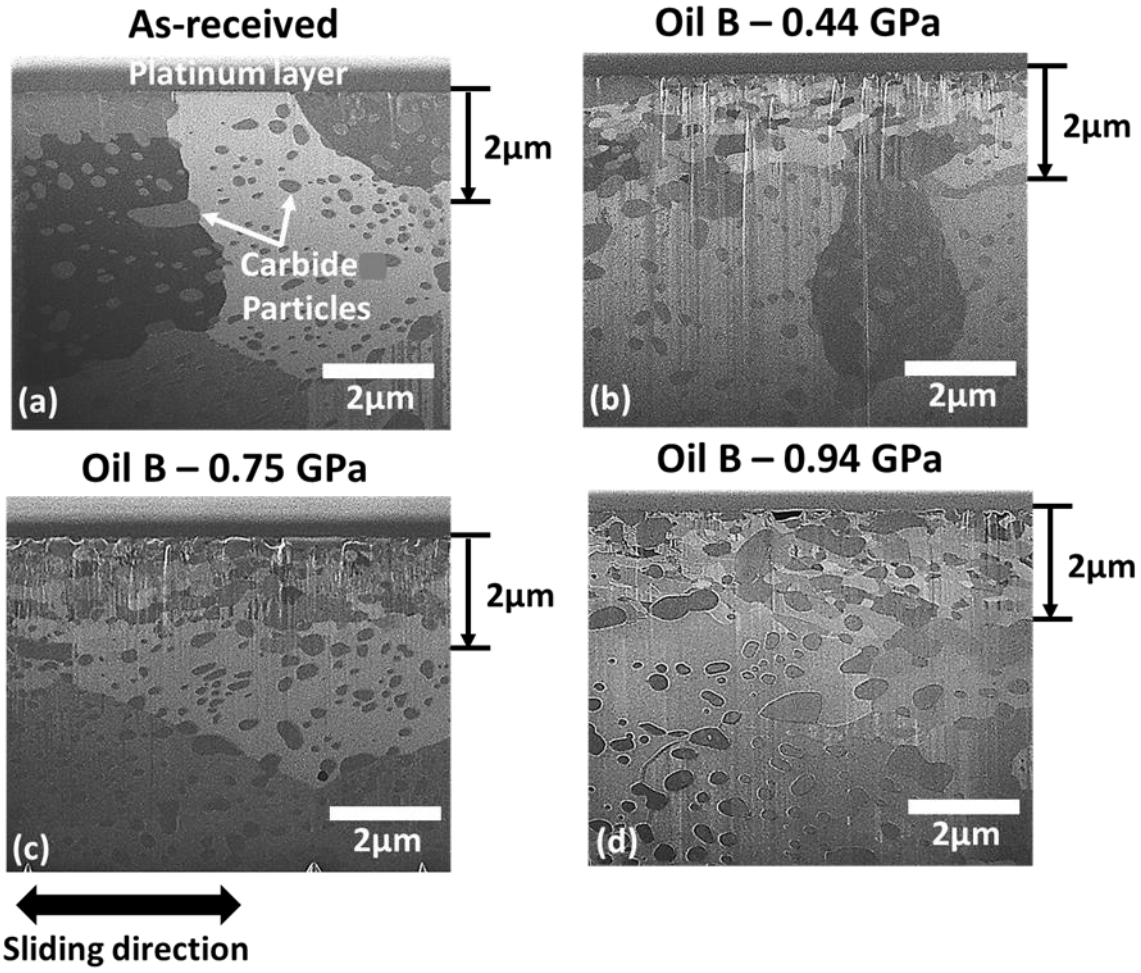

Figure 5.19: Subsurface microstructures of the (a) as-received material and after 2 hour sliding test with Oil B at (b) 0.44 GPa (c) 0.75 GPa (d) 0.94 GPa and temperature of 80 °C

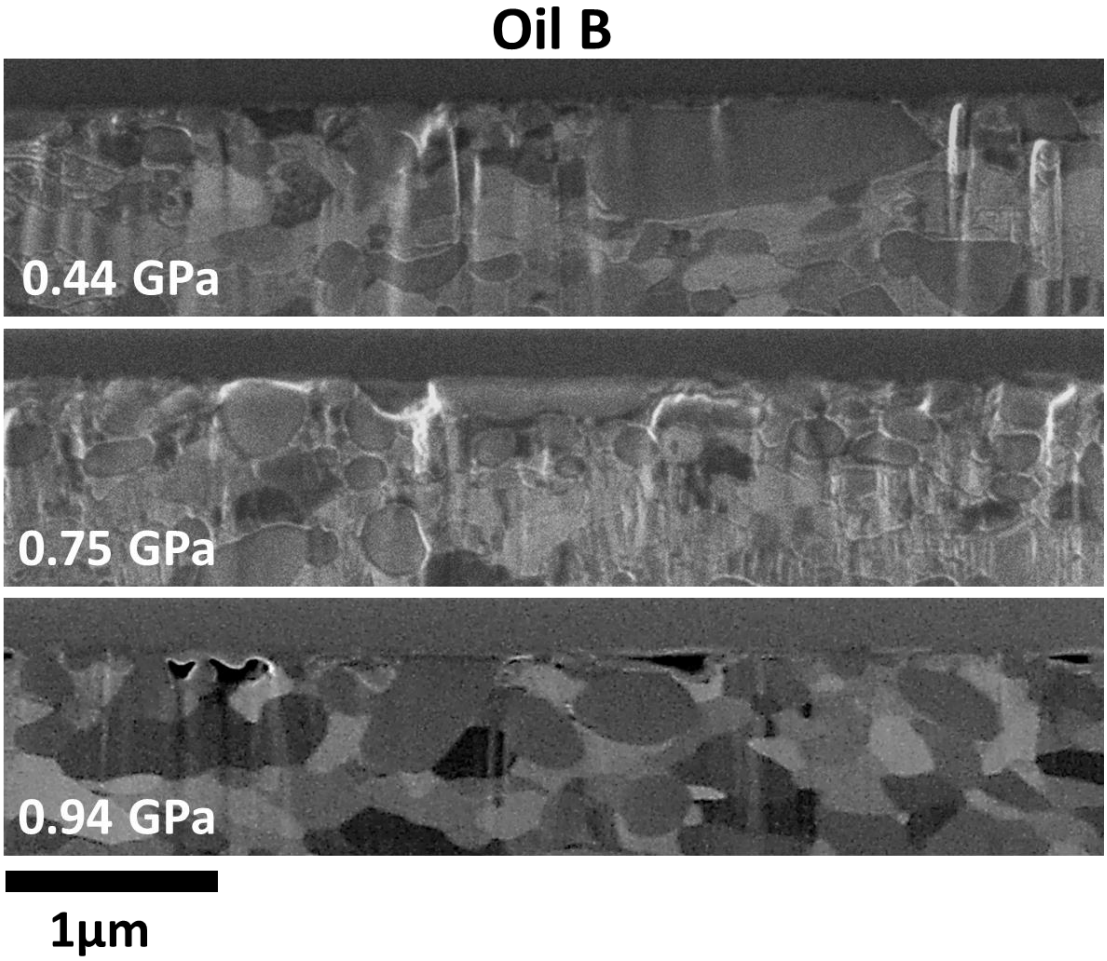

Figure 5.20: Higher magnification of the cross-sectional microstructures generated with Oil B at 0.44 GPa, 0.75 GPa and 0.94 GPa all tested at 80 °C

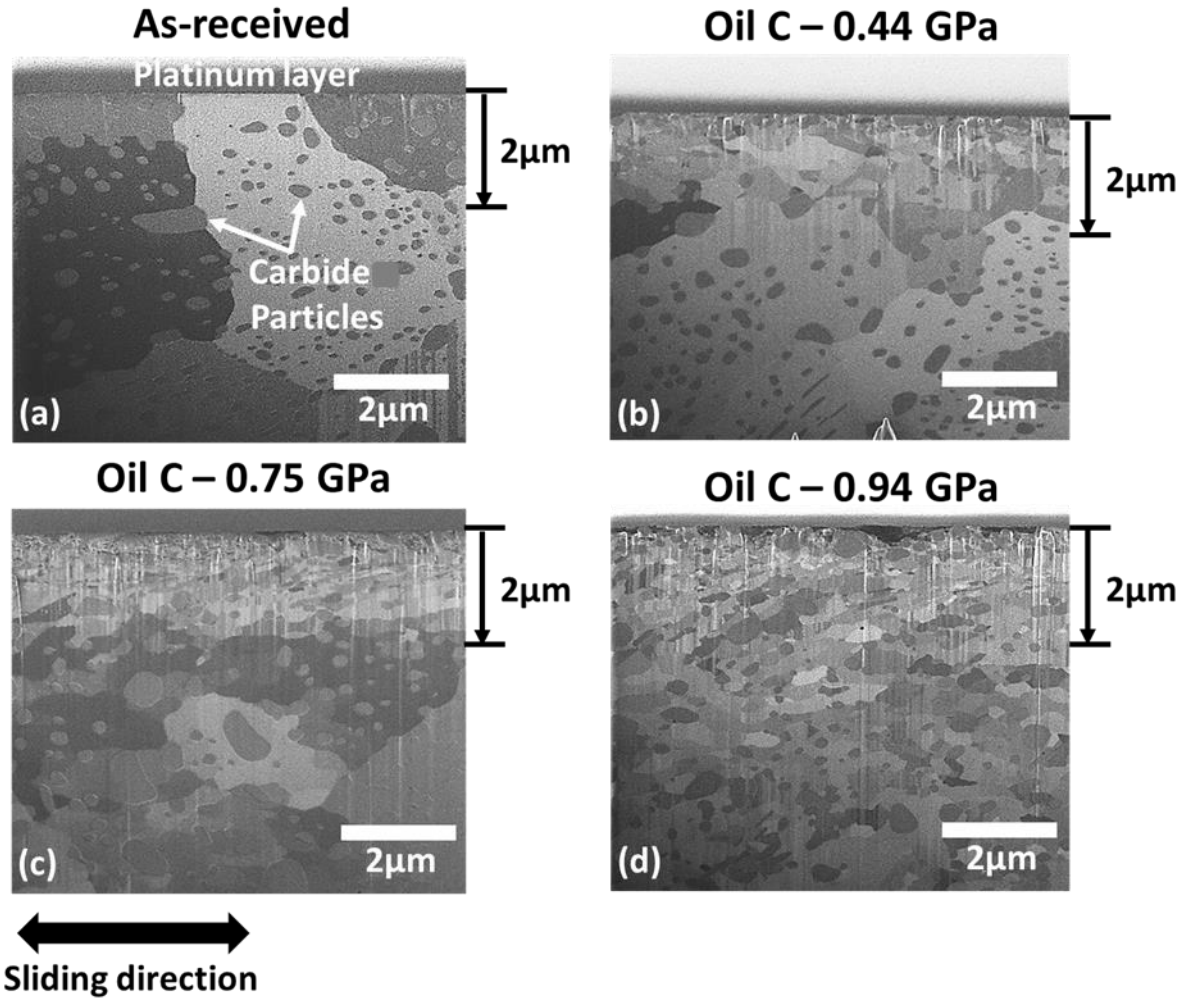

Figure 5.21: Subsurface microstructures of the (a) as-received material and after 2 hour sliding with Oil C at (b) 0.44 GPa (c) 0.75 GPa (d) 0.94 GPa and temperature of 80 °C

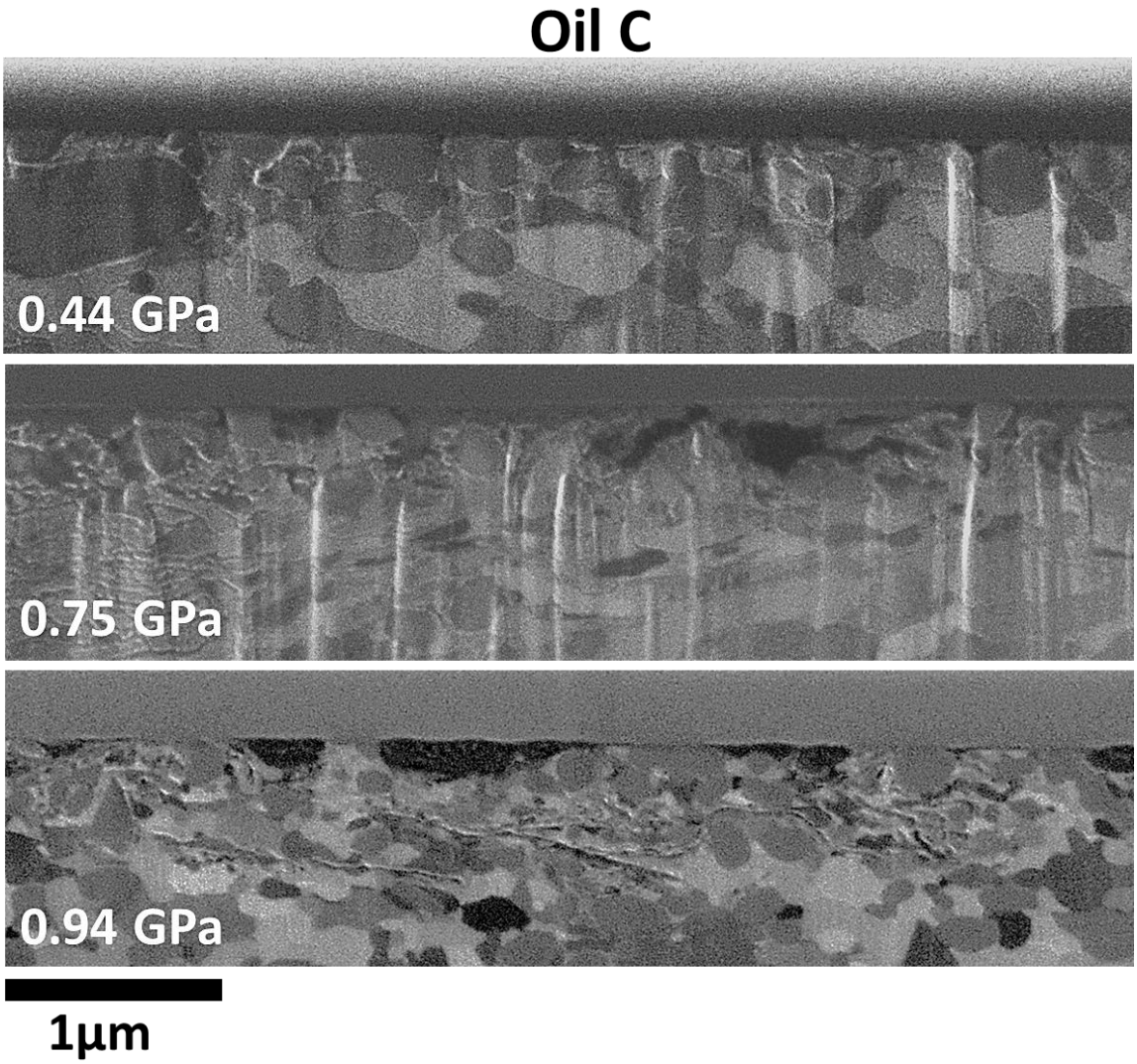

Figure 5.22: Higher magnification of the cross-sectional microstructures generated with Oil C at 0.44 GPa, 0.75 GPa and 0.94 GPa all tested at 80 °C

5.3.3 Subsurface transformation: differences between the oils

Oils A, B and C were tested under the same sliding conditions using the HFRR tribometer; however there are differences in the subsurface mechanical and microstructural responses. The three Oils have different base oil-additive combination and were specifically selected to provide different tribofilms and tribological performance. The nature of tribofilm formed and subsurface changes for the oils A, B and C has been discussed in Sections 5.3.1 and 5.3.2 respectively. In this section, we highlight and discuss the differences and similarities in subsurface transformation for the different oils. The results (Figure 5.23 and Figure 5.24) from the tests conducted at temperature of 80 °C and contact pressure of 0.94 GPa have be use to facilitate the discussion.

From the cross-sectional microstructures (Figure 5.24), it evident that the depth of the grain-refined layer for Oil B is relatively shorter and is less than 2 µm, whereas with oils A and C, it extends much deeper into the material and extends up to 6µm below the surface for Oil A and about 5 µm for Oil C. This corresponds with the hardness-depth results (Figure 5.23) which shows that with Oil B there is less hardening of the subsurface structure in the mid-section (0.8 µm – 2 µm), followed by Oil C and then Oil A. Although both Oils A and B contain different Mo-based friction modifiers, they both form tribofilms containing low friction MoS_2 (See Figures. 5.3 and 5.7); yet their subsurface responses are different under the same tribological testing conditions. Less strain hardening and shallower depth of refined ferrite grains observed with Oil B suggest that under the same operating conditions in sliding test, the nature of the tribofilm formed provides better surface protection and hence is able to minimize the amount of plastic strain introduced into the subsurface structure. There are a few aspects of the tribofilm formation that might explain the peculiarity observed with Oil B, this includes: how quickly the tribofilm forms, its stability once formed and its mechanical properties (shear strength and hardness). Oil B contains ZDDP additives which typically forms a tribofilm made up of iron and zinc phosphate matrix containing sulphides species [120]. This films form relatively quickly [51,45], are very stable (chemically and mechanically) once formed [125,48]. This attributes can help minimise direct contact between the

sliding surfaces and as such limit plastic deformation at the surface and strain accumulation in the subsurface structure.

Another major difference in the subsurface transformation for the oils is evident from the hardness-depth profiles (Figure 5.23). The hardness profile for Oil A is relatively uniform with depth (up to 2 μm). However with oils B and C, There is a gradient in the hardness profile, with hardness increasing towards the surface. Although with oils B and C there is a gradient in hardness, it is clear that the near surface hardness (0.8 μm) of Oil C is much higher than that of Oil B. The cross-sectional microstructures (from Figure 5.24) for oils B and C are also distinct particularly very near the surface. Higher magnification of the near surfaces (Figure 5.25) shows evidence of grain refinement for Oil B and Oil C; however it appears that the ferrite grains are more refined (smaller grains) with Oil C. The smaller ferrite grains could explain the higher hardness. Going by the Hall-Petch theory of grain-boundary strengthening [126], we would expect strengthening of the near-surface structure as the grains become smaller. Although it is still not clear, why it appear that strain localisation exist with oils B and C, and not with Oil A.

Relatively high surface hardening observed with Oil C (Figure 5.23) localised very near the surface corresponds with very fine grains near the surface (Figure 5.25) and might explain the relatively high wear measured with Oil C (Figure 5.2 and Figure 5.6). Subsurface nanocrystalline layer plays a role in the generation of wear particles [99] and the extent of wear [6,100]. Plastic strain accumulation and localization near the surface leads to increasingly smaller grain. Buscher et al. [99] in their study of subsurface nanocrystalline layer and its relationship with wear showed that wear debris size correlates to the nanocrystalline grain size. Hence they postulate that wear debris is generated from torn out nanocrystals in the near surface. The cementite particles in the AISI 52100 steel are much harder than the ferrite matrix. The interface between the grains and the particles can act as a stress concentration point and region of ferrite grain delamination. This is supported by the result of Oil C (Figure 5.25) where cracks are clearly observed.

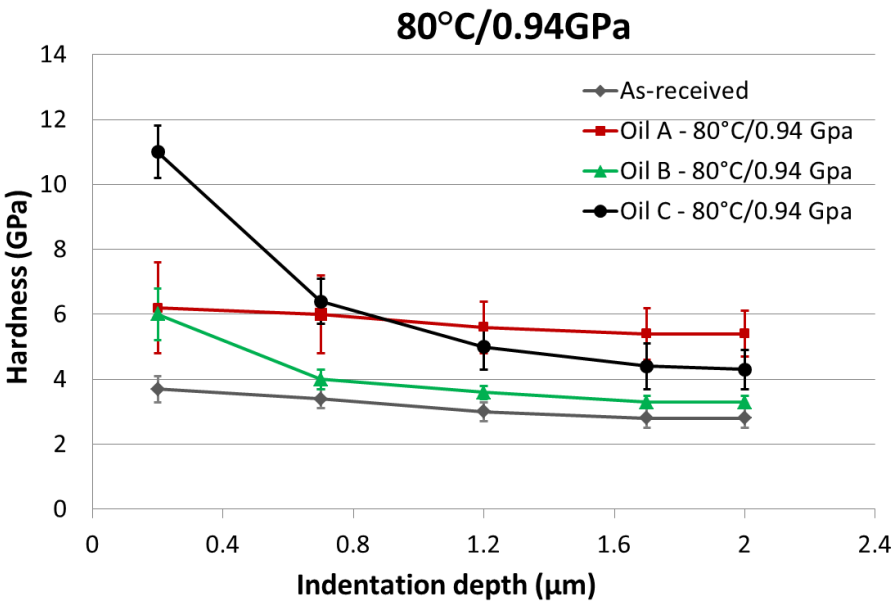

Figure 5.23: Hardness-depth variation of Oils A, B and C at 80°C/0.94 GPa. Each data point on graphs (a), (b) and (c) represents average hardness (N = 8 – 15) across the wear scar with at least 50 µm spacing between any two locations of measurement. The error bars represent the standard deviation.

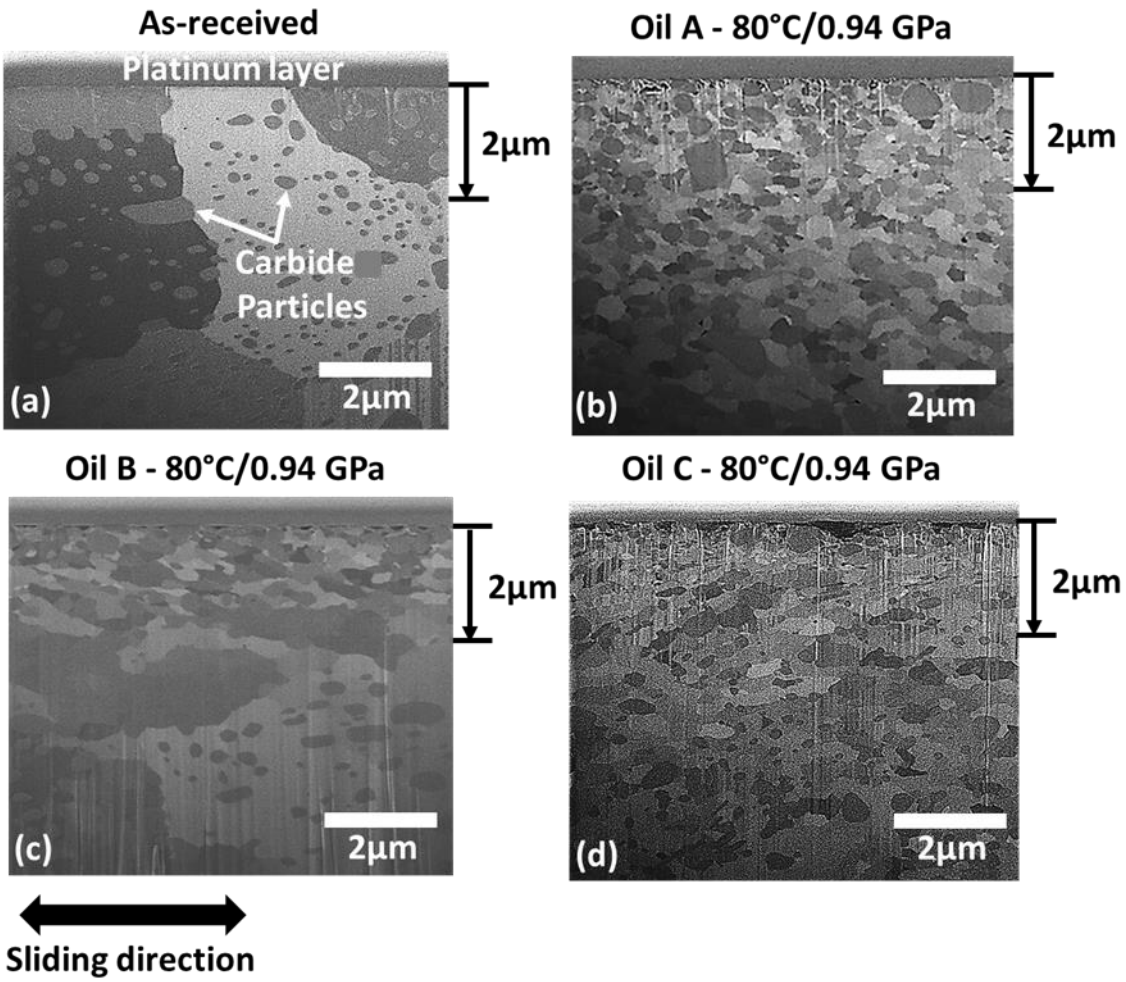

Figure 5.24: Subsurface microstructures of the (a) as-received material (b) Oil A (c) Oil B (d) Oil C after sliding test at 80°C/0.94 GPa.

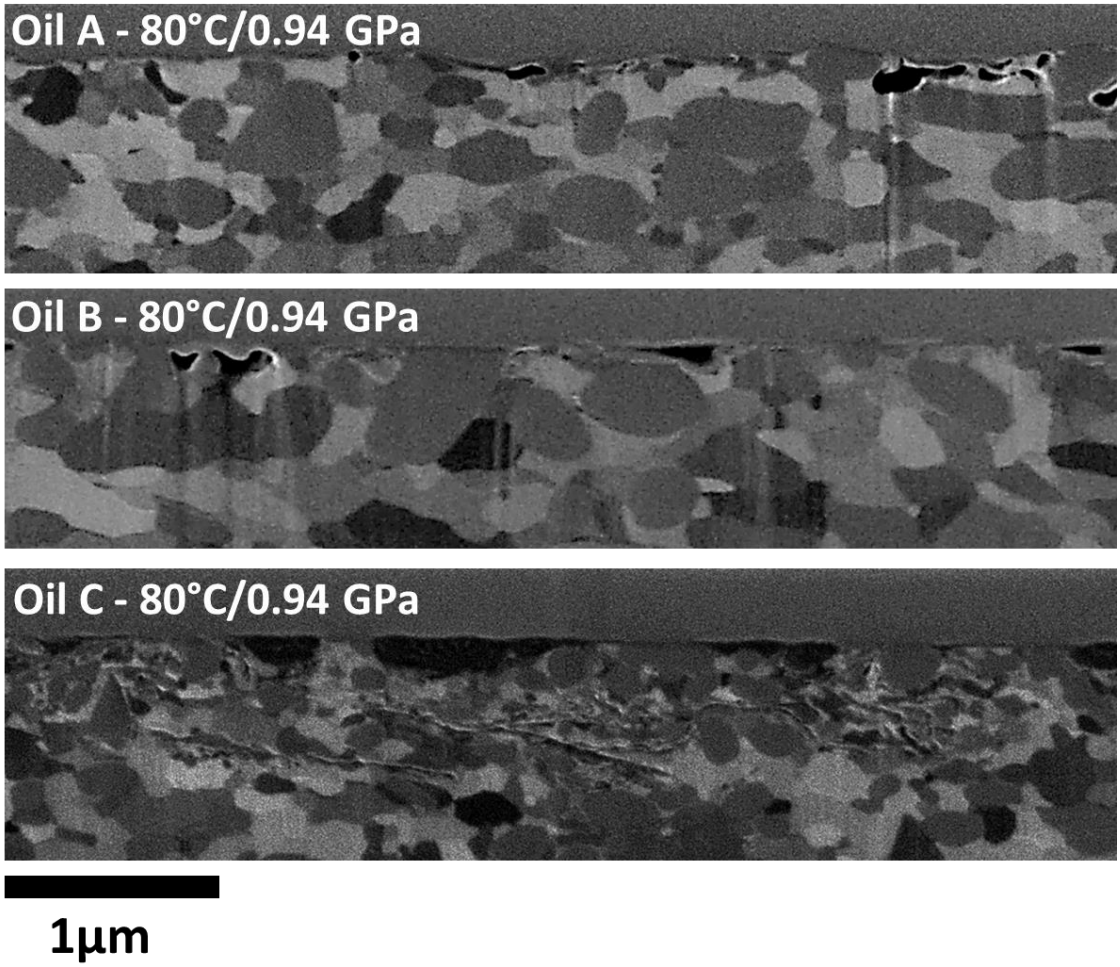

Figure 5.25: Higher magnification of the cross-sectional microstructures generated with Oils A, B and C at 80°C/0.94 GPa.

5.4 Conclusions

This paper investigated the influence of oil temperature and contact pressure on the tribological performance of three industrial gear oils (Oils A, B and C), the

nature of the tribofilm formed and subsurface (mechanical and microstructural) changes. The following conclusions are drawn:

The extent of friction and wear protection provided by gear oils is significantly influenced by the oil temperature and contact pressure. At higher temperature and contact pressure, frictional performance is improved as surface-additive interaction increases and friction-reducing tribofilms are formed. However wear performance deteriorates.

Investigating the influence of oil temperature and contact pressure on subsurface changes provided insight into the gear oil performance. Higher temperature and contact pressure promotes near-surface hardening and degradation of near-surface microstructural integrity by extensive deformation; this corresponds to lower wear performance.

Although Oil A and Oil B both contain molybdenum based friction modifiers, the extent of strain-hardening and the depth of grain refinement in the near surface is significantly reduced with Oil B which also contains antiwear additive (ZDDP) and corresponds to its superior wear performance in comparison to Oil A and Oil C.

The nature of strain-hardening is distinct with Oil A which has a uniform hardness-depth profile whereas there was a gradient hardness-depth profiles for oils B and C in the near surface region (< 2 μm below the surface).

The additive mix contained in a gear oil influences the nature of tribofilm formed but also the nature of subsurface changes. The results of this study emphasize the benefit of combining surface characterisation with subsurface analysis in the tribological performance of lubricants

Acknowledgements

The authors' would like to thank the Engineering Physical Sciences Research Council (EPSRC) for financing this project through the Advanced Metallic systems Centre of

Doctoral training (CDT). The authors would also like to thank the BP International Centre for Advanced Materials (BP-ICAM) for their financial support. Appreciation also goes to Dr. Chris Warrens and Andrew Forrests for their kind assistance in conducting the pressure-viscosity and nano-indentation experiments respectively.

Chapter 6

Paper 3: Industrial gear oils: sliding contact condition and tribo-pair hardness ratio on tribological performance and subsurface transformation of hardened AISI 52100 steel

This paper has not been published yet but has been written up with the intention of publishing it in 'Tribology International' Journal.

Contributions:

Aduragbemi Adebogun – is the lead author of this article and conducted all the experiments, analysed and interpreted the results.
Robert Hudson, Allan Matthews and Philip Withers gave advice on the experimental design, gave suggestions on data interpretation and also contributed to reviewing the article.

6 Industrial gear oils: Influence of sliding contact condition and tribo-pair hardness ratio on tribological performance and subsurface transformation of hardened AISI 52100 steel

Aduragbemi Adebogun[1, 2], Robert Hudson[3], Allan Matthews[1, 2, a], Philip J. Withers[2]

[1] International Centre for Advanced Materials (ICAM, Manchester Hub), School of Materials, M13 9PL

[2] School of Materials, The University of Manchester, Manchester, M13 9PL, United Kingdom

[3] BP Europa SE - Castrol Industrial Monchengladbach, Germany

[a] **Corresponding Author**: Allan Matthews,

allan.matthews@manchester.ac.uk

Abstract

We investigated the influence of contact severity and tribo-pair hardness ratio on the tribological performance of three gear oils and examined how their performance influences the extent of deformation in hardened AISI 52100 steel. Oil A contains molybdenum dithiophosphate additive friction modifier, Oil B contains amine molybdate complex friction modifier and zinc dithiophosphate antiwear additive. Oil C contains antiwear/extreme pressure phosphonate additive combined with a commercial gear oil package. Sliding tests were conducted using a SRV (Schwing-Reib-Verschleiss) tribometer with a contact pressure range of 1.3 GPa - 2.8 GPa and tribo-pair hardness ratio ≈ 1. This was followed by wear measurements and subsurface characterisation of the worn surface using X-ray diffraction and nanoindentation alongside scanning electron microscopy (SEM) in combination with a focused ion beam (FIB) preparation technique. By comparing the results from this study to previous HFRR results at lower contact pressures, we have established that the gear oils' frictional response to a more severe (SRV) contact is distinctive. While frictional performance improves with Oil B, it declines with Oil C and remains unchanged with Oil A. The results show wear rate is significantly lower in the SRV test with a higher tribo-pair hardness ratio (≈ 1). The wear rate remained low with increasing contact pressure, except for Oil B at 2.8

GPa. Characterisation of the sub-surface structure indicated a decrease in the plastic strain and/or increase in crystallite size, and the formation of adiabatic shear bands, which form under high local deformation and temperature. It is likely that the tribofilm formed for Oil B at a very high contact pressure of 2.8 GPa was unstable and unable to provide adequate surface protection leading to extensive deformation, temperature rise and thermal softening of the near surface.

6.1 Introduction

A tribosystem typically consists of two surfaces (tribo-pair) or more in relative motion, the interfacial element (i.e. lubricant), and the environment. The performance of formulated lubricants is strongly dependent on the input (operating conditions) into the system such as operating temperature and applied contact load/pressure. However, the properties of the tribo-pair themselves such as their hardness ratio, surface roughness etc. also have a strong influence as does the lubricant's base oil and additive combination.

The operating temperature and contact pressure applied to a tribosystem can significantly influence tribofilm formation. These variables have been shown to lower the thermal activation energy of zinc dithiophosphate (ZDDP) and molybdenum dithiocarbamate (MoDTC) tribofilms and hence increase the rate of formation [43,55,109]; in addition this also promotes complete decomposition of the friction modifier additive MoDTC. Complete decomposition leads to the formation of low friction MoS_2 in the tribofilm and ensures that the high friction compound $FeMoO_4$ is not formed [55]. In a recent article published by Spikes [127], the role of applied stress was highlighted and from several studies cited, it was concluded that applied contact pressure often increases the rate of chemical processes on rubbing surfaces. However, whilst sufficient applied load/pressure can promote chemical reactivity at the rubbing surfaces, Gabi et al [128] showed that excessively high contact pressure can promote premature breakdown of a ZDDP tribofilm. The ability of a formulated oil to effectively minimise friction and wear in a boundary lubricated contact is also highly dependent on the additive mix contained in the base oil.

The wear resistance of traditional metals is generally improved by increasing their hardness in keeping with Archard's classic equation [129] which is why mechanical elements such as gears and bearing steels are usually significantly case-hardened. Several studies [130-132] have shown that the best wear resistance is obtained from tribo-pairs with a hardness ratio close to unity. Most industrial lubricants are designed and tested to be used in specific applications. Hence when there is a material change to mechanical elements or the application of a new coating to existing elements, this can change the tribo-pair properties, such as the hardness ratio. In such cases, it is important to evaluate the lubricant's friction and wear performance with the new tribo-pair.

To better understand how formulated oils minimise wear, it can be beneficial to understand how they influence the near-surface layer. This was highlighted in our previous study [112]. There we concluded that industrial gear oils influence the extent of subsurface deformation in the near-surface via the tribofilm they form. Other researchers [61-63,77] have also studied the influence of formulated oils on subsurface deformation. The near-surface layer has been shown to have a direct impact on the wear process and wear particle generation [133,134]. In boundary lubrication, depending on the applied pressure, plastic deformation of surface asperities can occur in which case, dislocations accumulate near-surface with each sliding cycle increasing the amount of residual plastic strain. Most polycrystalline metals are work-hardened and experience the formation of nano-crystalline grains through a process of grain refinement [61-63]. Under very high local deformation inducing high surface temperature and high strain rates, martensitic steels such as hardened AISI 52100 steel have been reported to form white layers and adiabatic shear bands [135,136]. The primary metallurgical process in the formation of adiabatic shear bands has been reported to be dynamic recovery, which leads to local thermal softening near the surface [137,138,135,139]. This could potentially have a negative impact on wear performance.

In our previous study, the contact pressure range (0.44 GPa – 0.94 GPa) and tribo-pair hardness ratio (0.28) from HFRR sliding test were relatively low and did not reflect the operating conditions typical of the industrial context in which these

industrial gear oils operate in. Therefore, the current study aims to investigate the effect of contact severity (higher contact pressure range) and tribo-pair hardness ratio on the friction and wear performance of the gear oils, but also how the gear oils influence the near-surface of hardened AISI 52100 steel following friction sliding tests with an SRV tribometer.

6.2 Materials and methods

6.2.1 Lubricants

The tested lubricants are ISO VG 320 industrial gear oils with kinematic viscosity of 320 ± 32 mm^2/s at 40 °C. Oil A is used in wind power gearboxes, Oil B is used in heavy industrial application (such as mining gearboxes), while Oil C is a multifunctional gear oil used in different applications. The three oils have different base oil-additive mixes and are expected to form different types of surface film and hence perform differently with regards to friction and wear. Oil A and B both contain organomolybdenum friction modifiers molybdenum dithiophosphate (MoDTP) and amine molybdate complex respectively. In addition, Oil B also contains zinc dialkyldithiophosphate (ZDDP) and a sulphurised extreme pressure additive. Oil C contains extreme pressure/antiwear additives consisting of phosphonate and a commercial gear oil package. The complete formulation of the lubricants includes the base oil and the complete additive mix are shown in Table 6.1.

Table 6.1: Industrial formulated oils and their base oil/additive combination.

	Oil A	Oil B	Oil C
Base oil	Polyalphaolefin (> 90%)	Group 1 base stock mix (> 85%)	Polyalphaolefin (> 80%) Alkylated Naphthalene (5-15%)
Additives	Molybdenum Dithiophosphate (MoDTP) - (< 5%)	Amine Molybdate complex (< 5%) ZDDP (< 5%) Sulphurised - extreme pressure additive	Phosphonate (< 1%) Commercial gear oil package (< 5%)

	Mixed sulphonates – corrosion inhibitor (< 0.5%) Copper - corrosion inhibitor (< 0.5%)	Sulphonate mix – corrosion inhibitor (< 5%)
	Antifoam –trace	Antioxidant (< 1%) Methacrylate polymer – pour point depressant (< 5%)
		Antifoam -trace

6.2.2 Tribotesting

Sliding friction tests were conducted using an Optimol Instruments SRV tribometer (Schwing-Reib-Verschleiss). The test configuration comprises a sliding ball on a stationary disk immersed in the test oil. The ball slides on the disk with a stroke length of 1.5 mm and frequency of 33 Hz for a duration of two hours. The average sliding speed of the ball was 0.156 m/s. Two major sets of experiments were carried out; namely temperature and pressure variation tests. For the temperature variation test, the sliding tests were conducted at 30 °C, 80 °C and 120 °C. The contact load used was 600N which corresponds to a contact pressure of 1.9 GPa. For the pressure variation tests, the loads used were 200 N, 600 N and 2000 N which correspond to contact pressures of 1.3 GPa, 1.9 GPa and 2.8 GPa respectively. The pressure variation tests were carried out at temperature of 80°C.

6.2.3 Ball and Disc

The test ball and disks used were both made of AISI 52100 steel with hardness value of 11.3 ± 1 GPa, elastic modulus and Poisson's ratio of 210 GPa and 0.3 respectively. The ball diameter was 17.3 mm and the disk had a diameter of 24 ± 0.5 mm, with a height of 7.8 ± 0.5 mm. The surface roughness of the ball and disk were 0.75 ± 0.06 μm and 0.46 ± 0.14 μm respectively as measured by the confocal laser microscope described in Section 6.2.4. Prior to testing, the ball and disk were degreased with ethanol and after the sliding test they were cleaned with heptane to remove the excess oil.

6.2.4 Wear scar measurement

Wear scar measurements were carried out using a KEYENCE VK- X200 3D confocal laser microscope. The result was then post-processed using KEYENCE VK Analyser software. The first processing step was to correct for any slight tilt of the sample on the microscope stage. The wear measurement was carried out on the ball by measuring the wear diameter, followed by calculation of wear volume and specific wear rate. The specific wear rate was calculated by dividing the wear volume by the applied load and average sliding distance of 713 m.

6.2.5 Raman spectroscopy

A Renishaw 1000 microscope was used to characterise the tribofilm formed on the worn surfaces. The system uses an Argon laser source with wavelength of 514 nm. A 50 × objective lens was used to scan the wear scar with laser spot size of about 1µm. The exposure time was limited to 1 s to prevent excessive heating of the surface and subsequent transformation of the surface chemistry. The signal-noise ratio was reduced by taking 20 accumulations for each measurement.

6.2.6 Scanning electron microscopy – energy dispersive spectroscopy (SEM – EDX)

A FEI Quanta 650 FEG scanning electron microscope (SEM) equipped with energy dispersive X-ray (EDX) spectroscopy was used to image the surface and map out the elemental constituents of the tribofilm on the worn surfaces. Surface imaging and elemental mapping were carried out with acceleration voltages of 5 and 15 kV respectively.

6.2.7 X-ray diffraction (XRD) characterisation

To evaluate the residual plastic strain on the test ball, X-ray diffraction measurements were carried out using Proto iXRD Combo testing machine (Proto Manufacturing Inv. Taylor, MI USA), equipped with a two detector system. The complete XRD measurement parameters are shown in Table 6.2. Measurements were carried out on the test ball outside and within the worn scar using a chromium k_α radiation tube (wavelength, λ= 2.291 Å) at 20 kV, 4 mA to acquire the martensitic 211 (hkl) diffraction peak at Bragg's angle 2θ = 156.4 °. Prior to the test, the X-ray

diffraction system was calibrated with a stress-free (powder) standard and a stressed standard to accurately determine the stress-peak position. The stress-free and stressed standards were ferrite steel samples provided by the manufacturer (Proto Manufacturing). A multiple exposure technique with 11 measurements was used to obtain inter-planar d-spacing measurements. The full width half maximum (FWHM) of the peak intensities for each measurement point measured inside and outside worn surfaces were obtained using Proto iXRD Combo software.

Table 6.2: X-ray diffraction measurement parameter

Parameters	
X- ray type	Chromium-K_α
Wavelength (Å)	2.291
Source voltage (kV), current (mA)	20, 4
Diffraction plane	(211)
Bragg angle, 2θ	156.4°
Aperture size (mm)	0.5
β Angles	27
Number of β angles	11
β oscillation angle (°)	3
Phil angles (°)	0 an 90
Exposure time(s)	2
Number of exposure profiles	10
Number of exposure gain	40
X-ray elastic constant $S_1^{(hkl)}$ (MPa)	-1.2 x 10^{-6}
X-ray elastic constant $^1/_2\, S_2{}^{(hkl)}$ (MPa)	5.95 x 10^{-6}
Peak fit	Gaussian 80%

6.2.8 Nanoindentation

Hardness measurements were carried out using an MTS Nano Indenter XP system. The system was used to measure the hardness of the unworn ball and disk, but also to measure the near surface hardness of the worn surfaces using continuous stiffness measurement [68]. With this approach, it is possible to continuously measure mechanical response with depth as the diamond Berkovich indenter penetrates the surface at a constant strain rate of 0.05 s^{-1} to a depth of about 2 µm.

6.2.9 Scanning electron microscopy – focused ion beam (SEM-FIB)

The subsurface microstructures below the unworn and worn surfaces were revealed using a dual beam scanning electron microscope (SEM) FEI Nova NanoLab equipped with focused ion beam (FIB). A platinum layer is deposited on the surface to preserve the edge and prevent rounding-off during milling. An ion beam is used to mill out a trench through which the subsurface microstructure is revealed and imaged. Ion beam imaging was carried out with accelerating voltage of 30 kV and beam current of 9.7 pA.

6.2.10 Calculation of lambda ratio

To calculate the lambda ratio (λ), the minimum film thickness (h_{min}) was calculated using the empirical formula proposed by Dowson and Hamrock[113]:

$$\frac{h_{min}}{R'} = 3.63\left(\frac{U\eta_0}{E'R'}\right)^{0.68}(\alpha E')^{0.49}\left(\frac{W}{E'R'^2}\right)^{-0.073}\left(1 - e^{-0.68k}\right) \qquad \textbf{Equation 6.1}$$

Where R' is reduced radius of curvature, U is the speed, η_0 is dynamic viscosity, E' is reduced Young's modulus, α is pressure-viscosity coefficient, W is normal load. The relevant lubricant properties at 80 °C and 120 °C are presented in Table 6.3 below.

Table 6.3: Rheological properties of the gear oils

		Oil A	Oil B	Oil C
Dynamic viscosity, η_0 (m Pas)	80 °C	51.07	41.85	52.57
	120 °C	16.41	12.25	16.92
Pressure coefficient, α (GPa^{-1})	80 °C	14.67	19.66	14.69
	120 °C	18.00	18.00	16.23

6.3 Results and discussion

6.3.1 Tribological performance and tribofilm formation

In our previous study [112], we evaluated the frictional performance of the gear oils (Oil A, Oil B and Oil C) using an HFRR tribometer, followed by wear analysis of the worn surfaces generated. In this study we have tested the oils using an SRV tribometer. Both the HFRR and SRV tribometers test the oils in full sliding contact with a ball on disk configuration. However the contact pressure ranges of the two

tests are different. With the HFRR tribometer, the oils were tested in the range of 0.44 GPa – 0.94 GPa, while they were tested in the range of 1.3 GPa – 2.8 GPa in the SRV tribometer. Another difference between the HFRR and SRV tests is the hardness ratio between the disk and ball (H_{disk}/H_{ball}). For the HFRR test, the ball was hardened AISI 52100 steel and was about 3 times harder than the disk which was made of soft spheroidised AISI 52100 steel, hence the hardness ratio ($H_{disk}/\ H_{ball}$) was 0.28. Whereas for the SRV test, both the ball and disk were made of hardened AISI 52100 steel therefore the hardness ratio was ≈1. The lambda ratio values of the oils in the HFRR and SRV test were calculated taking into account the lubricants' rheological properties, mechanical properties of the tribo-pair, the applied load and the composite roughness of the tribo-pair. The lambda ratio ranged between 0.38 – 0.93 for the HFRR test and between 0.028 – 0.068 for the SRV test. From this we can say that the gear oils were functioning under a more severe contact condition in the SRV test when compared to the HFRR test. This section examines how the contact severity influences the nature of the tribofilm formed for the three oils and the corresponding frictional performance. In addition, we investigate the role of hardness ratio on the wear response for the gear oils.

6.3.2 Effect of contact severity (contact pressure) on the friction coefficient (μ) - temperature relationship for the three gear oils

Figure 6.1 shows that the change in friction coefficient-temperature for the different oils as contact severity (contact pressure) increases from the HFRR test to the SRV test. For instance, Oil A and Oil B both contain molybdenum-based friction modifiers: MoDTP and amine molybdate respectively, yet the frictional performance of Oil B improves in the more severe (higher contact pressure) SRV test specifically at the lower temperatures (30 °C and 80 °C); whereas with Oil A, there was no improvement and barely any change in the μ-temperature relationship. With Oil C, the friction coefficient was higher in the more severe SRV test, particularly at lower temperatures (30 °C and 80 °C). The level of pressure/stress applied in boundary lubricated rubbing contacts influences the chemical processes taking place on the surface. Applied pressure can reduce the thermal activation energy for tribofilm formation [43]. Therefore, it is possible that

an improvement in frictional performance seen with Oil B in the higher pressure contact (SRV) test could be attributed to the reduction of the energy barrier needed to form the low wear tribofilm. It is also possible that higher applied pressure might have promoted complete decomposition of the molybdenum based friction modifier (amine molybdate), hence preventing the formation of the high friction compound, $FeMoO_4$ that was shown by Khaemba et al [55] to form due to incomplete decomposition of MoDTC additive. It is also possible that the combination of ZDDP additive with amine molybdate friction modifier in Oil B might have a synergistic effect at higher contact pressure, promoting the formation of a tribofilm with improved frictional performance as suggested by a study by Bec et al [41]. Their study found that contact pressure played a critical role in the excellent frictional performance from formulated oil containing both MoDTC and ZDTP additives in comparison to MoDTC alone. The tribofilm formed with MoDTC/ZDTP possessed the ability to accommodate high applied pressure by increasing its hardness. Improvement in frictional performance was believed to be due to favourable orientation of MoS_2 sheets in the tribofilm obtained when the contact pressure was sufficiently high.

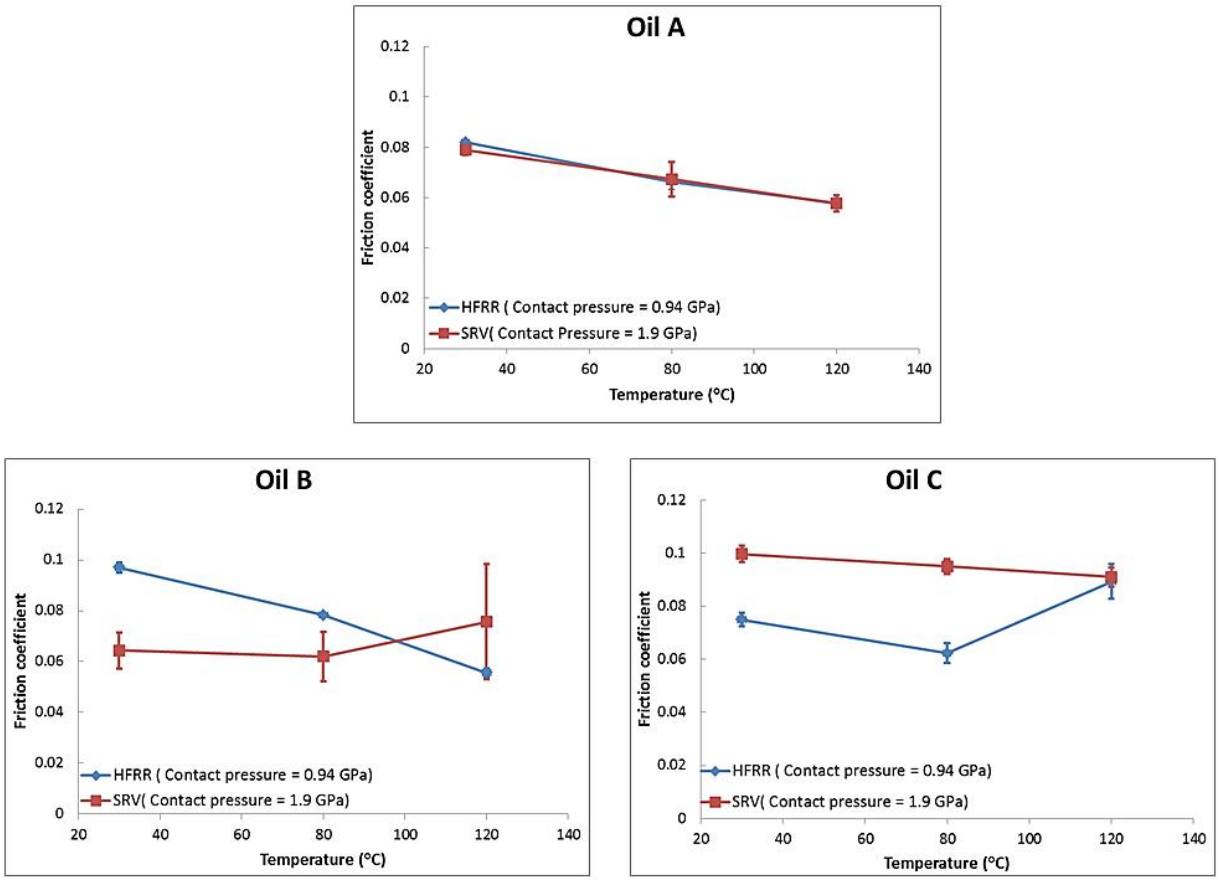

Figure 6.1: Influence of contact pressure (contact severity and test type) on μ-temperature relationship for oils A, B and C. Each data point shown on the graph represents the average friction coefficient (N = 3) and the error bars represent the standard deviation.

6.3.3 Influence of hardness ratio and contact pressure on wear performance.

Comparing the specific wear rate (SWR) for the HFRR and SRV tests, it is clear that the values are significantly higher in the HFRR test (0.065 – 4.3 x 10^{-8} mm^3/N.m) as shown in figure 6.2a compared to SRV test (0.14 - 1.63 x 10^{-8} mm^3/N.m) as shown in figure 6.2b. The significant drop in wear rate can be explained by the difference in hardness ratio between the ball and disk used in the HFRR and SRV tests. The hardness ratio between the ball and disk (H_{disk}/H_{ball}) in the HFRR test was 0.28, whereas that of the SRV test was ≈1. In the HFRR test, the softer disk was significantly worn as expected, with no significant wear of the ball [112]; whereas for the SRV test, since the hardness values of the tribo-pair components were the same both the disk and the ball were worn and the wear rate was significantly

lower. Tribo-pairs that generate the best wear resistance are usually those with hardness ratios close to unity [130-132].

The low hardness ratio of the HFRR test meant that it was a more sensitive test in investigating the ability of the oils in minimizing wear of the much softer spheroidised steel disk albeit in a lower contact pressure range compared to the SRV test. The wear rate in the HFRR test (figure 6.2a) generally increased with contact pressure and it is clear that Oil B provided the lowest wear rate while Oil C provided the highest. It is possible that the low wear rate provided by Oil B might be attributed to the inclusion of antiwear ZDDP additive in its formulation. However, in the SRV test, the wear rate was not very sensitive to an increase in contact pressure, although it can be seen that wear increased significantly with Oil B at the highest contact pressure of 2.8 GPa (figure 6b) and suggests a change in wear mechanism.

Figure 6.2c shows the variation of Lambda ratio with contact pressure in the HFRR and SRV test. The calculated values for the three oils shows that the HFRR contact went from mixed lubrication regime ($\lambda \approx 1.1$) at the lowest contact pressure of 0.44 GPa to boundary lubrication with lambda values of 0.97 ±0.1 and 0.97 ±0.1 at 0.75 GPa and 0.94 GPa respectively. The lambda ratio values calculated for the SRV contact were more than 10 times smaller than those of the HFRR contacts with values ranging from 0.061 to 0.074. This implies that in the SRV setup, the gear oils are operating under severe loading conditions. Failure of Oil B to maintain a low wear rate at 2.8 GPa suggests a failure of the tribofilm.

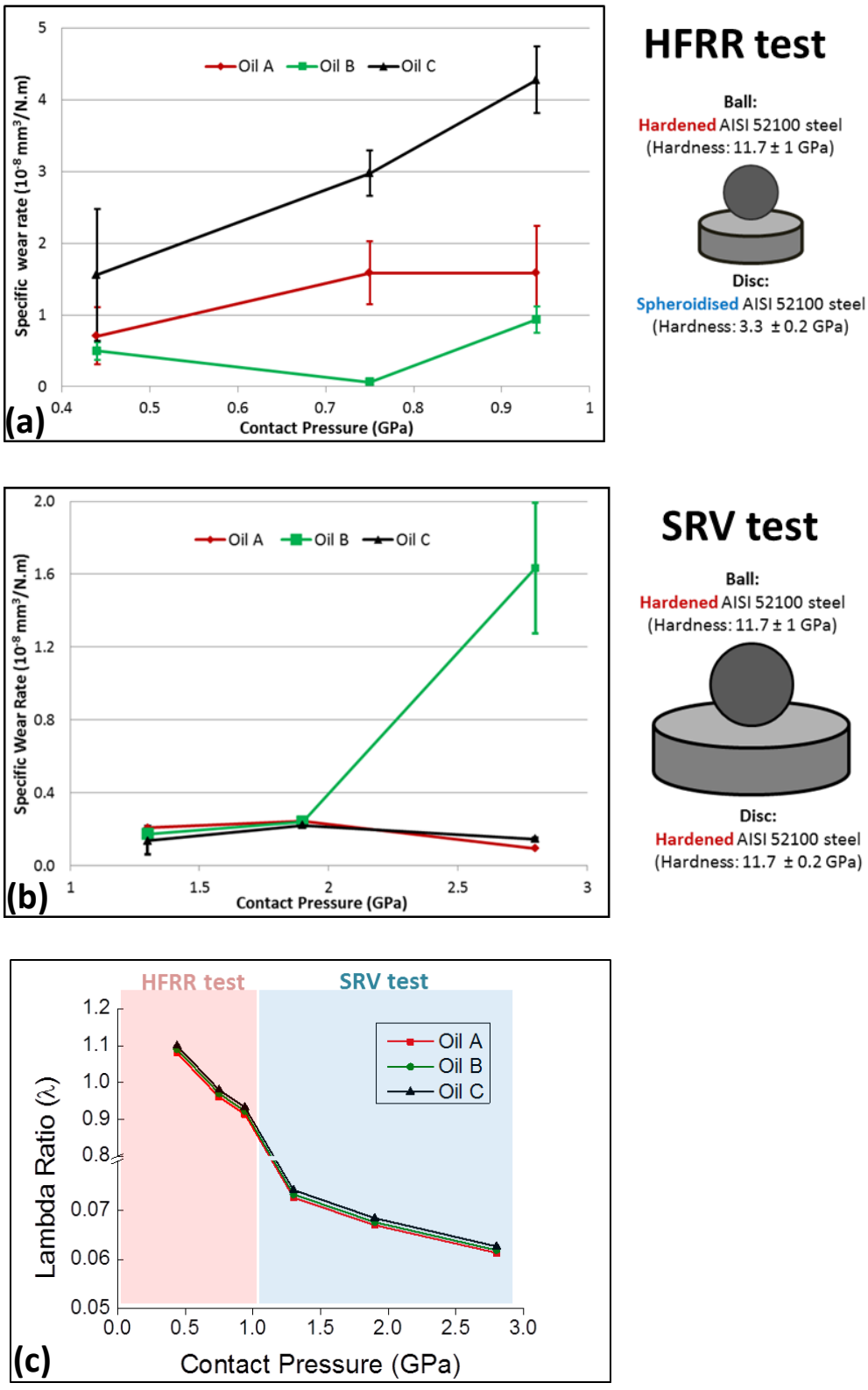

Figure 6.2: Specific Wear Rate vs. Contact Pressure for the different oils using the (a) HFRR and (b) SRV tribometers. (c) Shows the dependency of Lambda ratio on contact pressure. Each data point shown on graphs (a) and (b) represents the average friction coefficient (N = 3) and average specific wear rate (N = 3) respectively. The error bars represent the standard deviation.

6.3.4 Tribofilm formation

Raman and EDX characterisation of the worn surfaces generated with the SRV friction test at different temperatures are shown in figures 6.3 and 6.4 respectively. Chemical characterisation of the worn surfaces generated in the HFRR test (lower contact pressure) reported in our previous study [112] showed that iron oxide was predominantly measured on the worn surfaces generated at 30 °C. This suggested that the additive-surface interaction barely occurred at 30 °C. The additive chemistry was activated at 80 °C and 120 °C and was evidenced by the formation of MoS_2 with Oil A and Oil B and FeS_2 with Oil C. In this study, the oils were tested using higher contact pressure (but also higher tribo-pair hardness ratio and lower lambda ratio). The additive chemistry was activated even at the low temperature of 30°C. The EDX elemental map in figure 6.4 shows that sulphur and phosphorus are present on the worn surfaces generated (with Oil A, B and C) at 30 °C, 80 °C and 120 °C. In addition, calcium is also present on the surfaces worn using Oil A and zinc and magnesium elements are present on the surface worn using Oil B. Raman results in figure 6.3 also show that MoS_2 was detected on the surface worn using oils A and B even at the low temperature of 30 °C, and FeS_2 was detected on the surface using Oil C. This again suggests that under higher pressure (1.3 GPa – 2.8 GPa), the thermal activation energy required for the tribofilm formation can be reduced.

The high friction compound $FeMoO_4$ has been reported [55] to form when there is partial decomposition of MoDTC in a boundary lubrication contact. In the HFRR test, $FeMoO_4$ was detected on the surfaces worn with Oil A and B but only under low temperature (30°C) and contact pressure (0.44GPa) test conditions. Although Oil A and Oil B contain other Mo-based friction modifiers: MoDTP and amine molybdate compounds respectively, the presence of $FeMoO_4$ compound suggested partial decomposition of the friction modifiers and was associated with higher friction at low temperature and contact pressure. In this study, $FeMoO_4$ wasn't measured on the wear scars generated at all temperatures, perhaps due to the higher contact pressure promoting complete decomposition of the friction modifier

additives. Second order Raman peaks of MoS_2 were measured on the surfaces worn using Oils A and B (figure 6.3 and figure 6.5); one peak at 601 cm^{-1} (sometimes at 609 cm^{-1}) another at 774 cm^{-1} (sometimes at 767cm^{-1}). The peak at 601/609 cm^{-1} can likely be attributed to the $E^1_{2g}(M) + LA(M)$ [140] and the peak at 767/774 cm^{-1} can be attributed to either $2E^1_{2g}$ [141] at 750cm^{-1} or $A_{1g}(M) + E^1_{2g}(M)$ [141] at 780 cm^{-1}.

In the SRV test, surface-additive chemistry was active at the contact pressures of 1.3GPa, 1.9GPa and 2.8GPa, as evidenced by Raman and EDX results in figure 6.5 and figure 6.6 respectively. The EDX elemental maps show that sulphur and phosphorus elements are present on the worn surfaces generated with oils A, B and C. Oil A and Oil B contain detergent additives: calcium sulfonate and magnesium sulfonate, respectively. The elemental maps in figures 6.4 and 6.6 show that the tribofilm formed on the worn surface contains calcium for Oil A and magnesium for Oil B, which suggests that the detergent additives in the formulated oils contribute to the tribofilm formed and inevitably the tribological performance of the gear oils. Sulfonate additives can also be considered to be extreme pressure additives as they can react with iron metal surface to form a film that prevents metal-to-metal contact [142,143]. Topolovec-Miklozic and Forbus [142] reported that calcium sulphontate detergent formed a thick (100-150nm), pad-like calcium carbonate film effective in preventing wear.

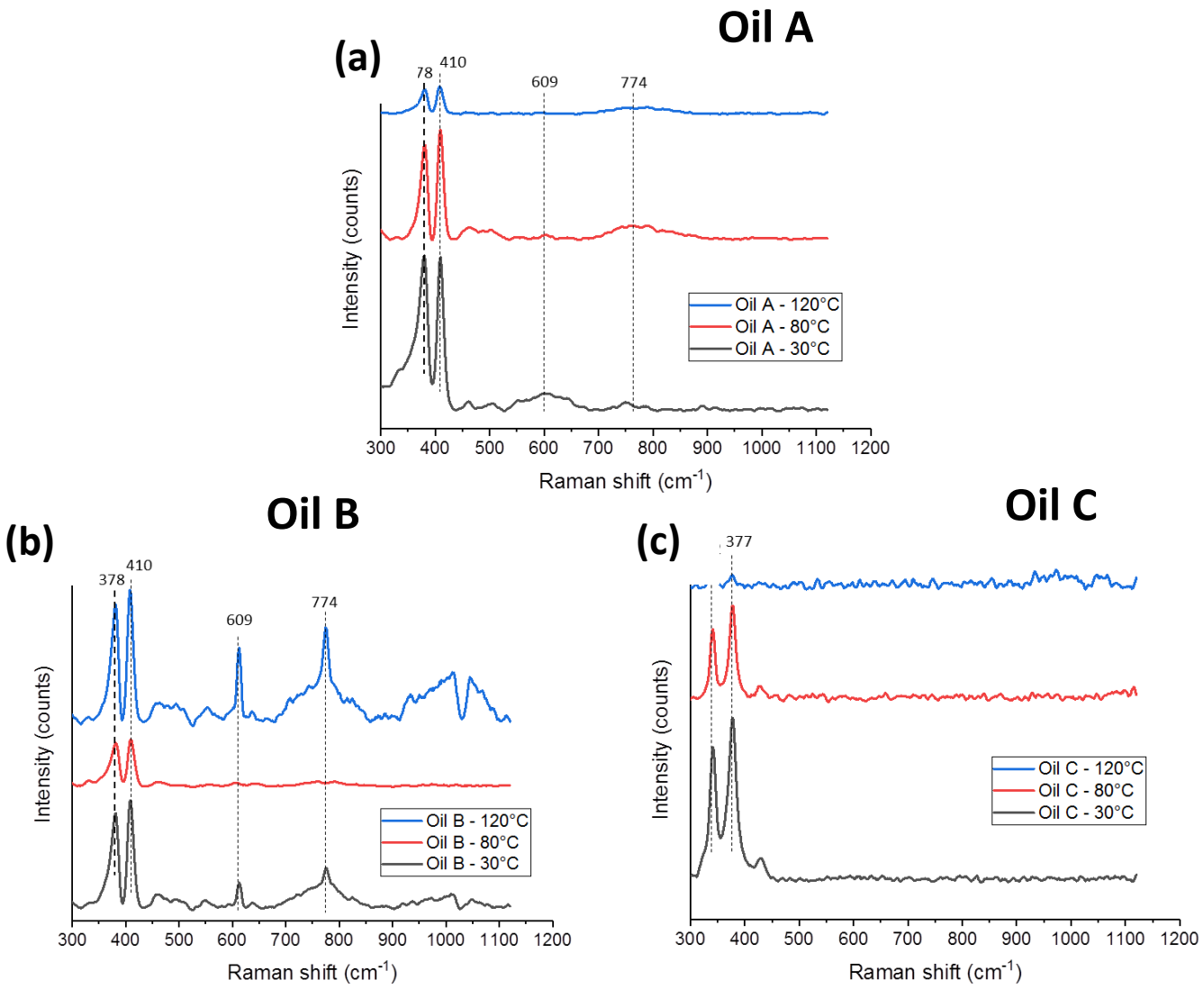

Figure 6.3: Effect of temperature on the Raman spectra measured on wear scars lubricated with (a) Oil A (b) Oil B (c) Oil C

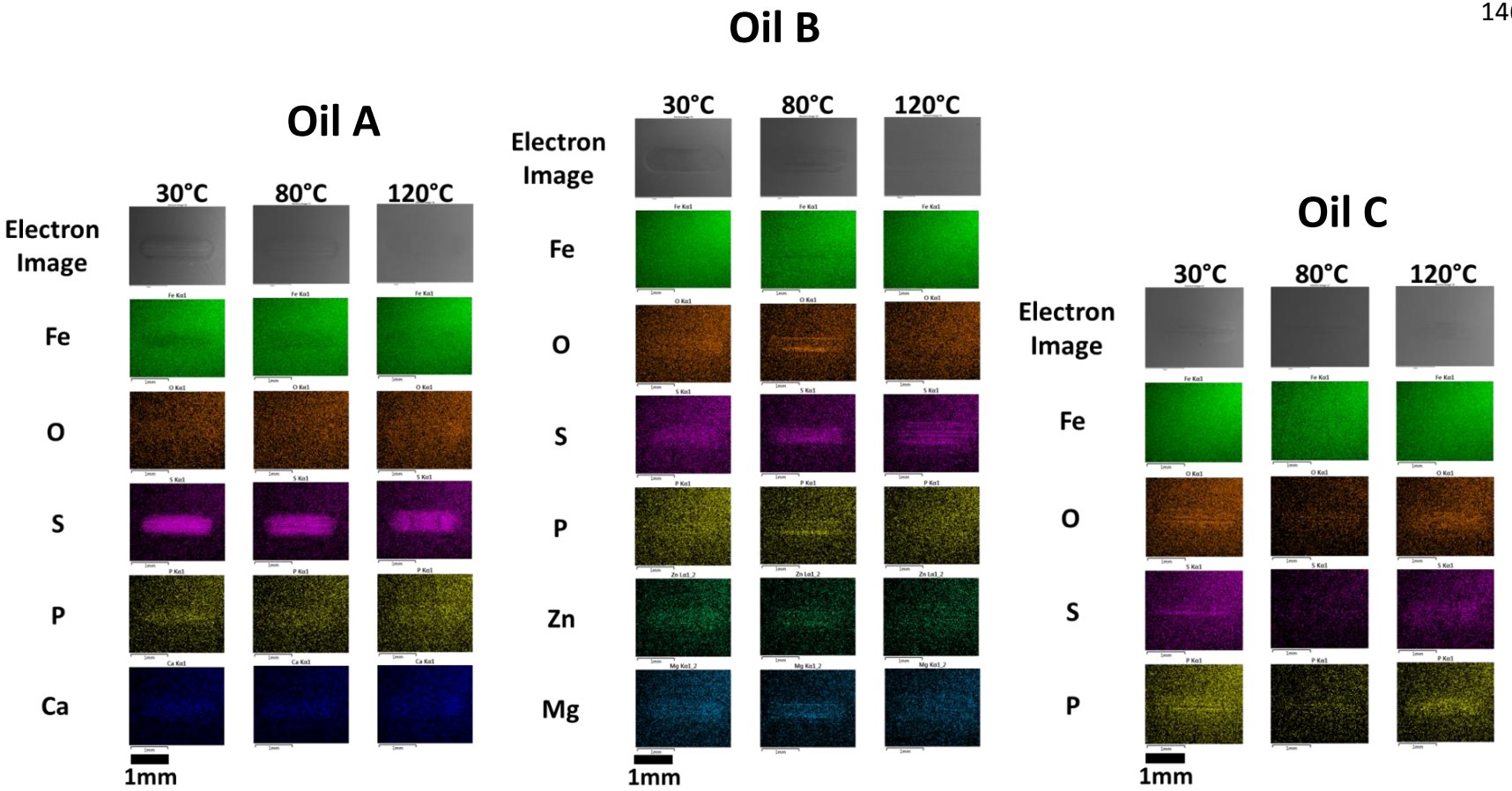

Figure 6.4: SRV test - SEM images and EDX maps of wear scars lubricated by oils A, B and C after sliding tests a 2 hour sliding test at temperatures of 30°C, 80°C and 120°C

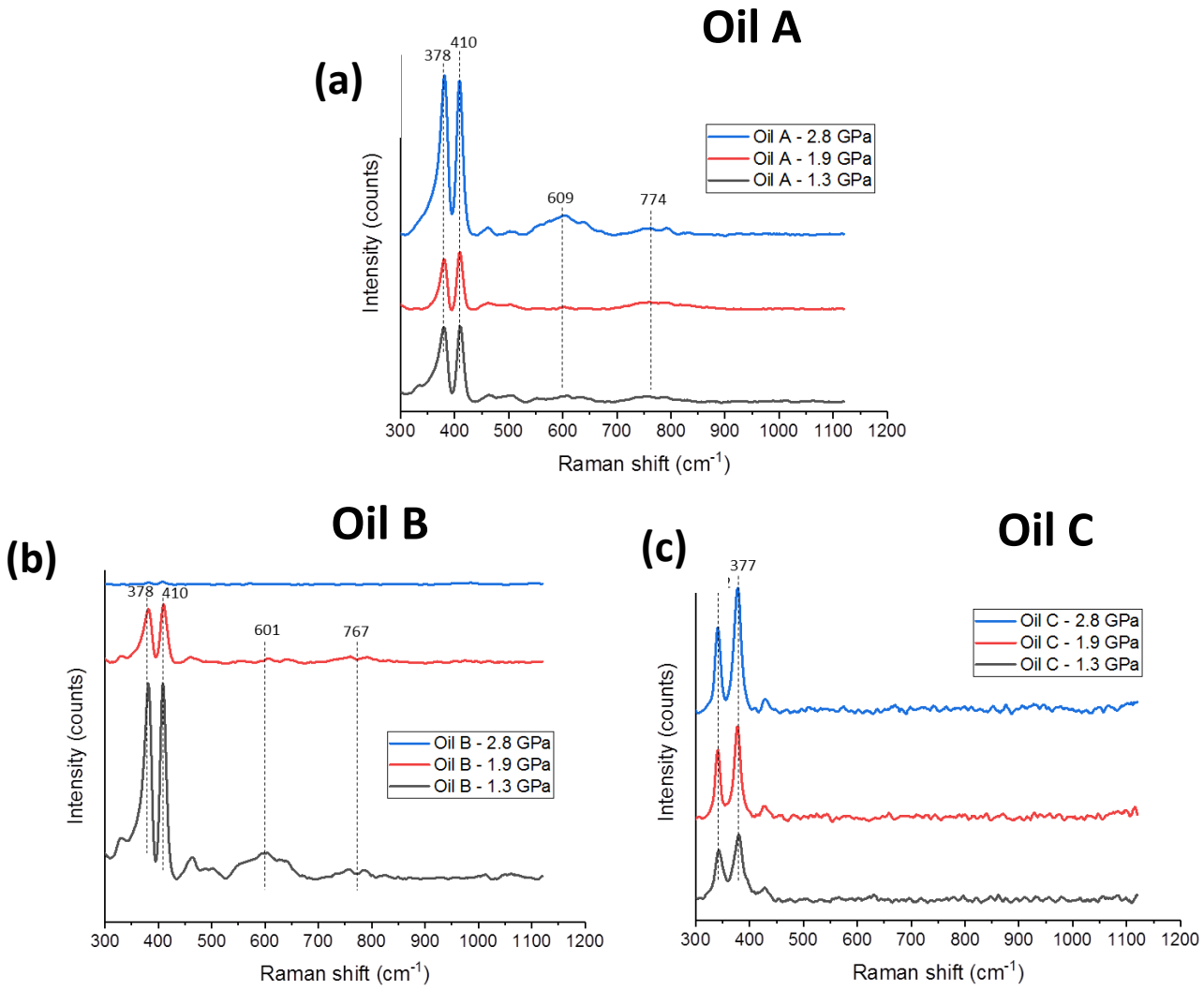

Figure 6.5: Effect of contact pressure on the Raman spectra measured on wear scars lubricated with (a) Oil A (b) Oil B (c) Oil C

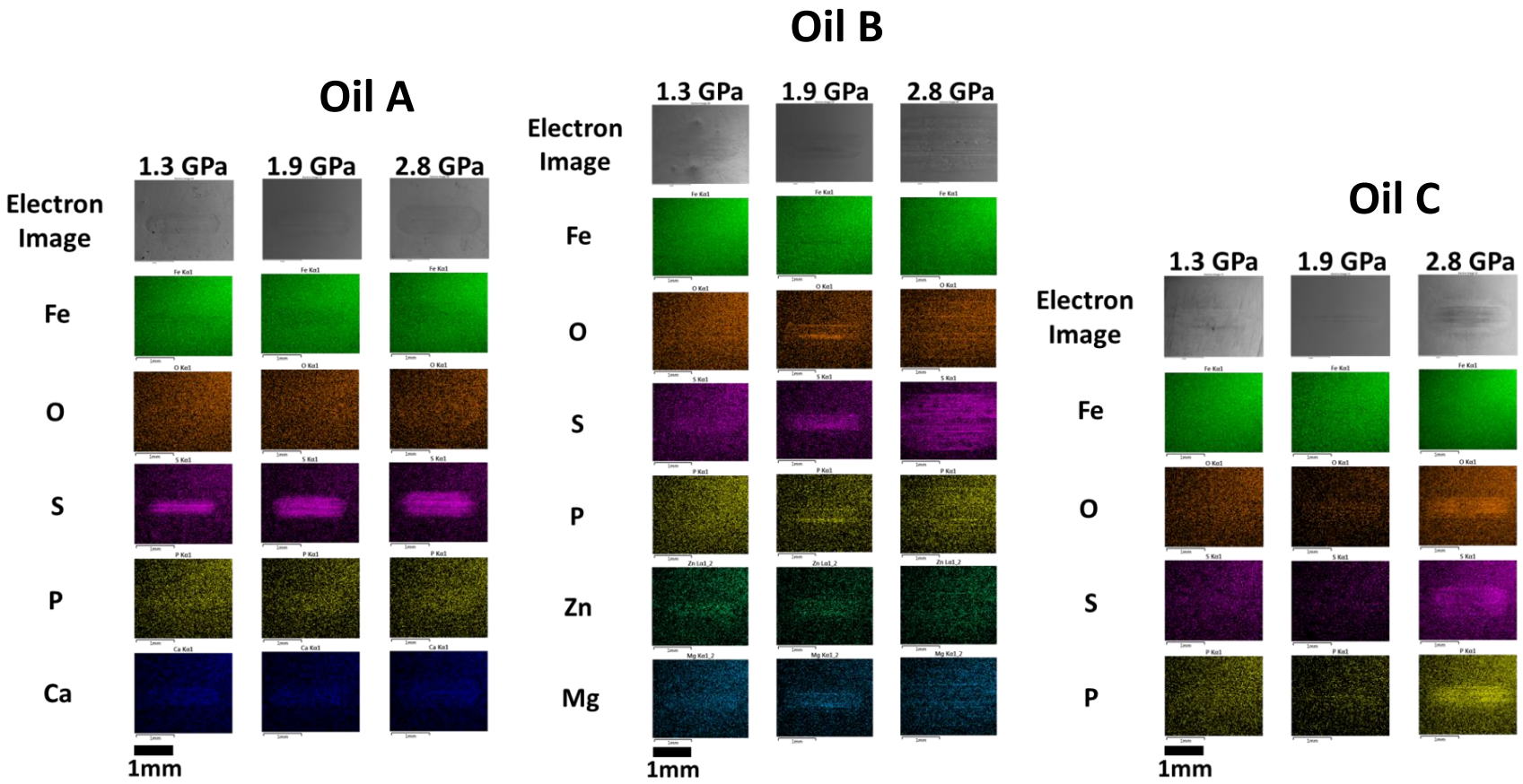

Figure 6.6: SEM images and EDX maps of wear scars lubricated by oils A, B and C after a 2 hour sliding test at contact pressures of 1.3 GPa, 1.9 GPa and 2.8 GPa

6.3.5 Subsurface transformation

Section 6.3.1 was focused on how a more severe contact condition might influence the nature of the tribofilm formed and the corresponding frictional performance, but also how the gear oils are able to minimize wear with tribo-pairs of different hardness ratios. In this section we establish and discuss the influence of the gear oil performance in the SRV test on the subsurface transformation (mechanical and microstructural). Our previous study [112] at lower contact pressures showed that the gear oils influence the extent of subsurface deformation on spheroidised AISI 52100 steel. In the previous study, wear measurement and subsurface characterisation was carried out on the softer disk following HFRR sliding test. However in this study, wear measurement and subsurface characterisation were carried out on the hardened AISI 52100 steel balls. Following SRV sliding test and wear characterisation, subsurface transformation below the worn surfaces generated was characterised by XRD and nanoindentation techniques to investigate the relative amount of plastic strain introduced into the near-surface metal layer. This was complemented with microstructural analysis below the wear scar. The XRD technique was used to investigate the change in the diffraction peak (broadness) of the 211 (hkl) plane of the worn martensitic steel surface. Full width half maximum (FWHM) was used as the measure to monitor any change of peak broadness and empirically determine the change in subsurface state. Using nanoindentation, we were also able to measure the near surface hardness of the worn surface up to a depth of 2 µm. Both the XRD diffraction characterisation and the hardness-depth measurement give us an idea of strain hardening or softening and/or changes to the grain size in comparison to the unworn surface which was also measured for comparison.

Figure 6.2b shows the variation of specific wear rate with increasing contact pressure. For the three oils, there was a slight increase in specific wear rate from 1.3 GPa to 1.9 GPa, followed by a slight decrease when the contact pressure increased to 2.8 GPa. However with Oil B, the specific wear rate increases tremendously at the extreme pressure of 2.8 GPa which suggests a change in wear regime from mild to severe. Therefore we chose to investigate surface

transformation below worn surfaces generated with contact pressures of 1.9 GPa and 2.8 GPa. In this manner we can establish the relationship between the extent of wear (mild or severe) and the nature of subsurface transformation (mechanical and microstructural).

The results of the hardness-depth measurements on the surfaces worn with Oils A, B and C are shown in figures 6.7a and figure 6.7b. The hardness profiles for Oil A and Oil B generated with contact pressure of 1.9 GPa (figure 6.7a) are lower than that of the as-received (AR) profile. This suggests that the near-surface layers might have been thermally softened during the sliding test. With Oil C, the standard deviation in the hardness values at different depths as shown by the error bars is quite large. This could mean that the hardness profile for Oil C is not significantly different from the unworn surface. Each point on the hardness-depth graph (figures 6.7a and 6.7b) is an average of 11-20 points on the worn surface. Therefore, it is possible that there might be large variation in the near-surface structure and hardness from the machining of the test substrate. In addition, it is possible that the condition at the interface during the sliding process might not be homogenous throughout, hence the high level of variation in the hardness profile across the worn surface. Tribofilm layers that form in boundary lubrication contacts in some cases are distributed evenly or patchy in nature [144,109,145]. Different levels of surface protection could give rise to inhomogeneous subsurface structures. The hardness profile for Oil B generated with a contact pressure of 2.8 GPa is significantly lower than the unworn surface hardness profile, even if the error bars are taken into account. The significant drop in the hardness profile with Oil B suggests thermo-mechanical annealing of the near-surface structure during the 2 hours sliding test.

The FWHM represents the extent of peak broadening of the martensitic 211 (hkl) plane from the sample's crystallite size and lattice strain, but also peak broadening contribution from the XRD instrument [146,147]. These three contributions have not been separated with results presented in figure 6.7c and figure 6.7d. However, the same instruments have been used for all the measurement and have been

calibrated using the same protocol; therefore the results reflect changes in crystallite size and lattice strain. A fall in the FWHM has been shown to correspond to an increase in crystallite size and/or decrease in lattice strain near the surface [148,149]. Thirteen measurements were taken across the wear scar generated on the ball as depicted in the image inserted in figure 6.7. There is barely any change in the FWHM measured inside and outside the wear scars generated with contact pressure of 1.9 GPa as shown in figure 6.7c. However, measurement on the surfaces worn using Oil B at 2.8 GPa (figure 6.7d) shows that the FWHM decreases significantly within the wear scar. Although there is a slight decrease in FWHM within the wear tracks generated using oils A and C, it is small compared to that generated using Oil B. We can thereby empirically infer lower plastic strain within the wear scar and/or increased crystallite size in the near surface microstructure. Peng et al [150] in their study showed a good agreement between hardness and FWHM, which we also see from this study, were lowering of the hardness depth profile for Oil B tested at 2.8 GPa corresponds to lowering of the FWHM within the wear scar generated.

The hardness-depth profile and XRD FWHM result both suggest a strong annealing effect on the surface worn using Oil B at 2.8 GPa and a relatively minute amount of annealing near the surface worn at 1.9 GPa. Subsurface microstructural analysis was conducted using SEM-FIB to complement XRD and hardness-depth profile results. Figure 6.8 shows the subsurface microstructure generated with contact pressure of 1.9 GPa. The subsurface microstructure generated by the oils appear similar and unchanged in comparison to the unworn microstructures (figure 6.8a) consisting of large carbide particles surrounded by martensitic lathes. However, the result of the subsurface microstructures generated at 2.8 GPa (figure 6.9) shows that the structure generated using Oil B produces a microstructure clearly different to those generated using oils A and C. Very near the surface (< 2.5 µm below the surface), the martensitic matrix appears to be elongated and significantly refined (divided into smaller grains). The microstructure appears similar to adiabatic shear bands formed in hardened steels. Adiabatic shear bands are typically formed under conditions of high local deformation at high strain rate giving rise to high local

temperature and local softening. Several studies [137,138,135,139] on the mechanism of adiabatic shear band formation have reported dynamic recovery to be the primary metallurgical process driving the process. The material within the shear band is usually characterised by elongated sub-grains and refined equiaxed grains [137,139]. Barry and Brye [138] reported a transition from dynamic recovery to dynamic recrystallization; however, there was no evidence of dynamic recrystallization as found in some other studies [137,139]. White layers which are typically associated with martensitic steel such as the AISI 52100 steel and have been shown to have a similar structures to adiabatic shear bands and are reported to form through a similar mechanisms [138,136].

The results of subsurface characterisation of the worn surface using XRD, nanoindentation and SEM-FIB to examine the cross-sectional microstructure have consistently shown evidence of thermal softening with the surface generated using Oil B at contact pressure of 2.8 GPa. The lower hardness-depth profile compared to the unworn surface, the decrease in the FWHM within the wear scar and the formation of adiabatic shear bands or white layers suggest softening of the structure in the top 2 µm - 2.5 µm of the worn surface. This was only observed with the surface worn using Oil B and might explain the significantly higher wear rate at the contact pressure of 2.8 GPa (figure 6.2b). For traditional metals, wear resistance is inversely proportional to surface hardness according to Archard [129]. Hence lowering of the surface hardness due to dynamic recovery and adiabatic band formation during sliding would promote wear of the softer surface by the harder counterface. In the boundary lubrication regime, the tribofilm formed at the contact plays a major role in preventing friction and wear. It’s likely that the higher contact pressure could have affected the stability or durability of the tribofilm formed with Oil B.

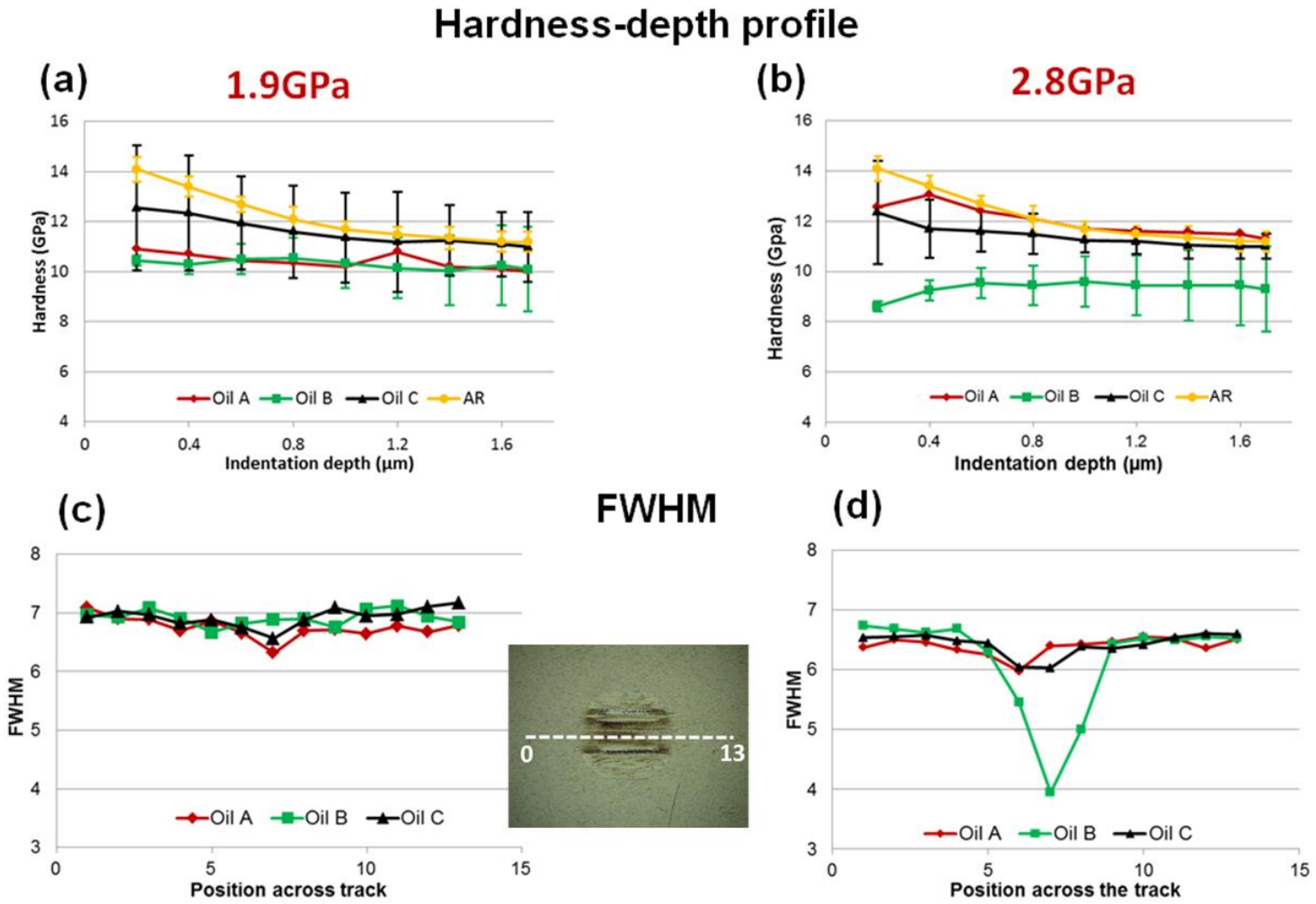

Figure 6.7**:** Hardness-depth profiles on the ball wear scars generated from the SRV test at contact pressures of (a) 1.9 GPa (b) 2.8 GPa and FWHM measurements across the ball wear scars at contact pressures of (c) 1.9 GPa (d) 2.8 GPa. Each data point on graphs (a) and (b) represents average hardness (N = 8 – 15) across the wear scar with at least 50 µm spacing between any two locations of measurement. The error bars represent the standard deviation.

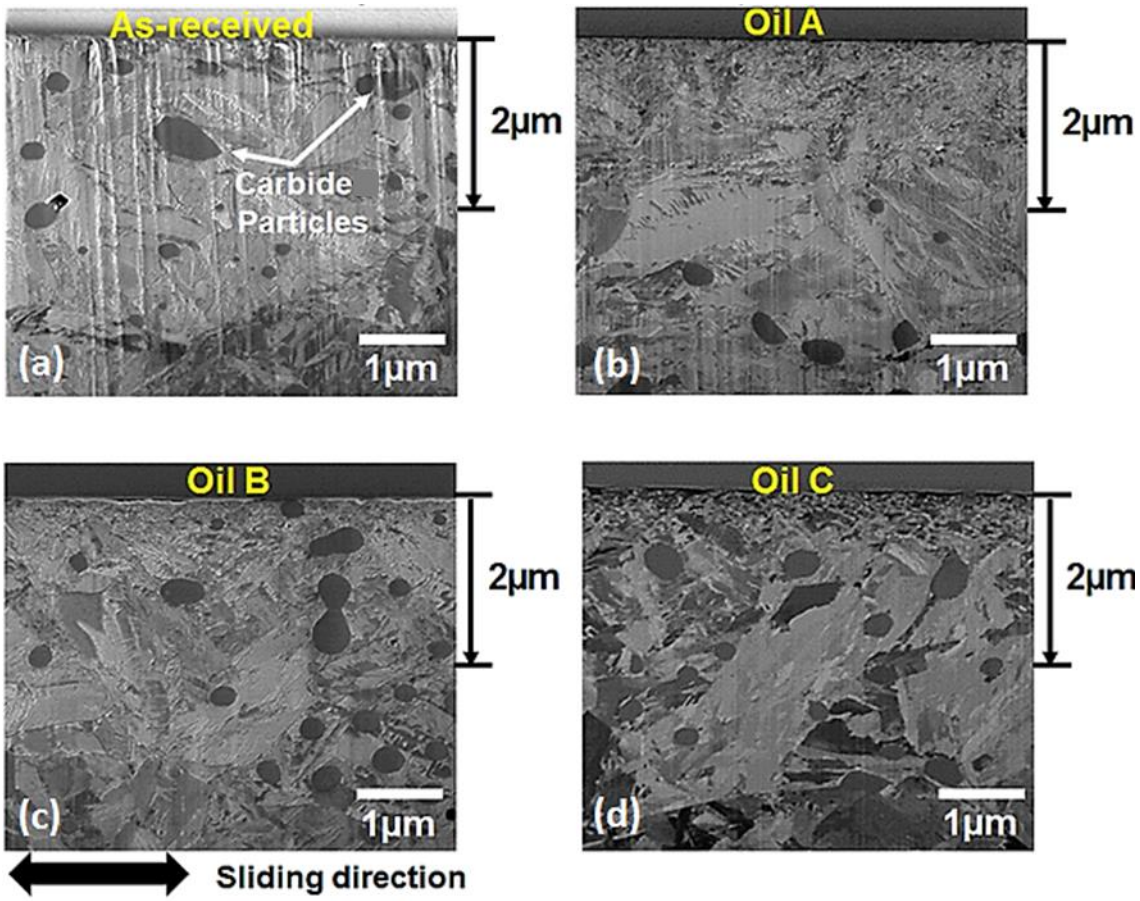

Figure 6.8: Subsurface microstructures (cross sections) generated in a SRV tests at 80°C and a contact pressure of 1.9 GPa

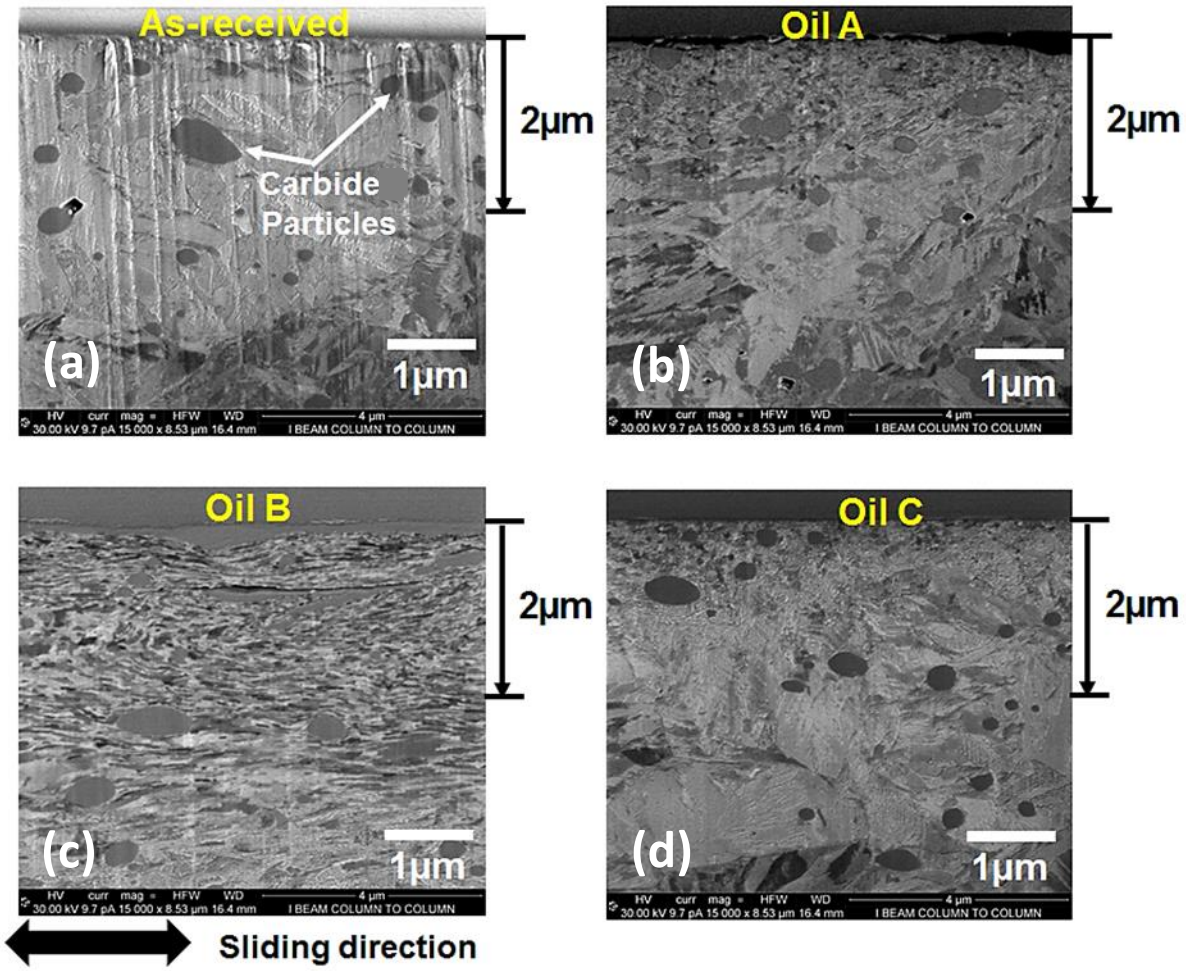

Figure 6.9: Subsurface microstructures (cross sections) generated in SRV tests at 80°C and contact pressure of 2.8 GPa

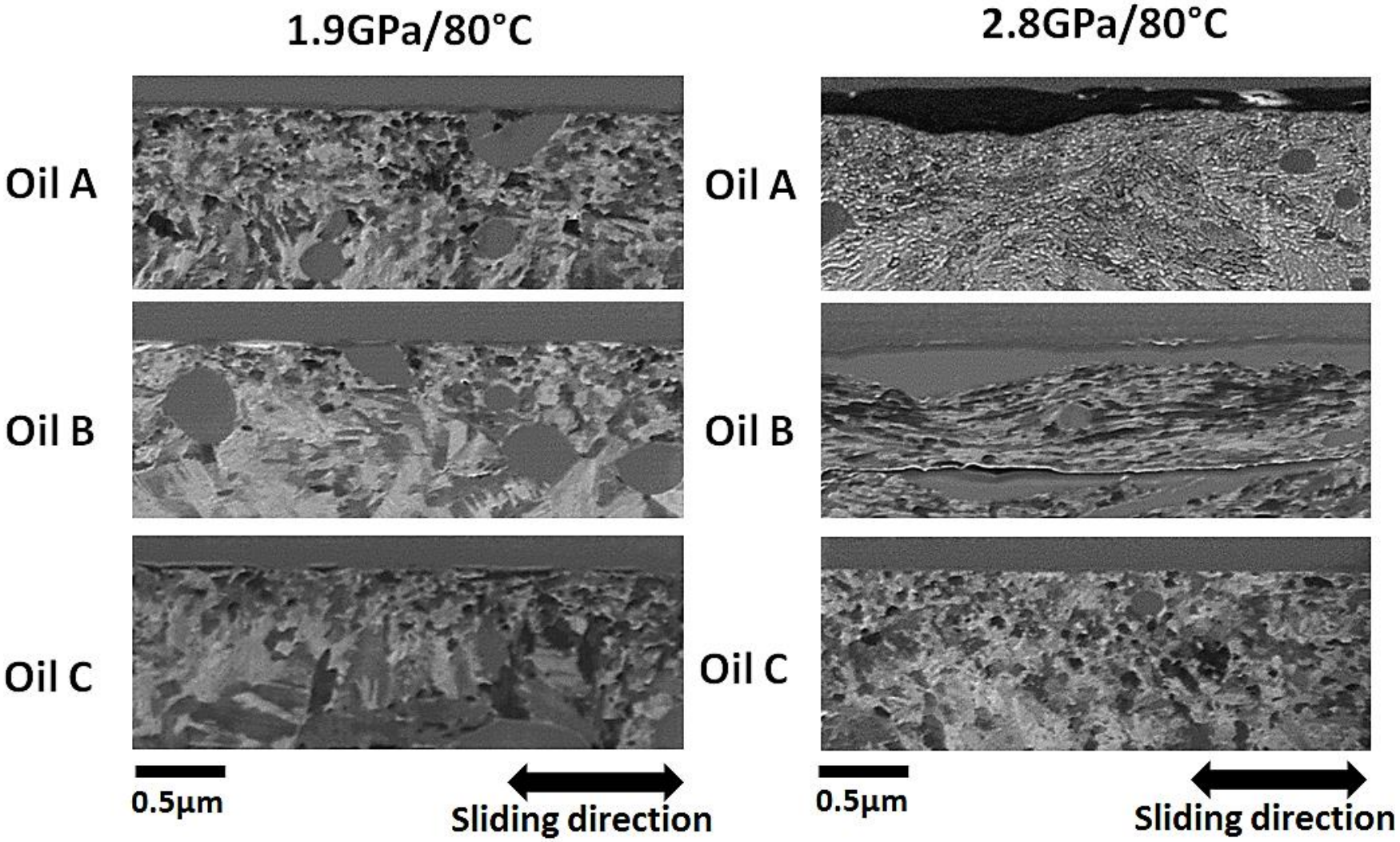

Figure 6.10: Subsurface microstructure (cross sections) generated in SRV tests at 80 °C and a contact pressure of 1.9 GPa (left) and 2.8 GPa (right)

6.4 Conclusions

We have studied the behaviour of three gear oils under boundary lubrication sliding condition in an SRV test.

- The differences in the three gear oil formulations (oils A, B and C) with distinct base oil and additive combinations is reflected in their differing relationships between contact severity (contact pressure) and frictional performance. Although Oil A and Oil B both contain molybdenum based friction modifiers, improvement in frictional performance was only observed with Oil B under the more severe test conditions, while frictional performance worsened with Oil C.
- Additive-surface interaction at a low temperature of 30 °C was increased in the more severe SRV test in comparison to the HFRR study carried out previously [112]. We suggest that the high contact pressure condition in the SRV test lowers the thermal activation barrier for the additive-surface chemical reaction.
- Wear rate dropped significantly when the hardness ratio of the tribo-pair was close to unity. However, a lower hardness ratio (0.28) provided more sensitive wear vs contact pressure behaviour. The results re-iterate the importance of testing formulated oils with operating conditions (contact pressure, temperature, tribo-pair hardness ratio etc.) similar to the industrial application.
- Subsurface characterisation of the worn surface provided a possible explanation for the high wear rate with Oil B at 2.8 GPa. The three techniques (XRD, nanoindentation and SEM-FIB) coherently suggest thermal softening of the near-surface structure. XRD FWHM and hardness-depth profile measurements indicated reduced plastic strain and/or increase in the crystallite size just beneath the worn surface (< 2.5 μm). Cross-sectional microstructural analysis showed a structure similar to adiabatic shear bands which are formed under conditions of high local deformation at high strain rates giving rise to high local temperatures and softening. Softening of the near surface compromises the wear resistance of the material.

Acknowledgements

The authors' would like to thank the Engineering Physical Sciences Research Council (EPSRC) for financing this project through the Advanced Metallic systems Centre of Doctoral training (CDT). The authors would also like to thank the BP International Centre for Advanced Materials (BP-ICAM) for their financial support. Appreciation also goes to Dr. Chris Warrens and Andrew Forrests for their kind assistance in conducting the pressure-viscosity and nano-indentation experiments respectively.

7 Conclusions and further work

7.1 Conclusions

In this thesis, three commercial gear oils (Oil A, Oil B and Oil C as described in thesis) were investigated in boundary lubricated sliding contact. The broad aim was to develop a better understanding of how they interact with steel surfaces to minimise friction and wear but more importantly how they influence the metal subsurface microstructure. The thesis attempts to answer three questions:

- Do the gear oils and the tribofilm they form influence the nature of transformation beneath the metal surface?
- How does bulk oil temperature and varying contact pressure influence the nature of tribofilm formed for the different gear oils and how does this influence the extent of subsurface transformation?
- Do the gear oils' tribological performances change when the contact pressure range and the tribo-pair hardness ratio is significantly increased? In addition, how does this affect the way they influence the transformation of the subsurface structure?

To answer the above questions, we investigated the friction and wear performance of the gear oils by carrying out friction sliding tests and wear measurements from the wear scars generated. To understand the nature of the tribofilms formed on the surface we utilized two complementary characterisation techniques EDX and Raman spectroscopy. To understand how the gear oils influence the subsurface metal layer, we investigated changes in the mechanical properties through nanoindentation hardness-depth measurement on the worn surfaces and microstructural changes using SEM-FIB to examine the cross-sectional microstructure. The following conclusions were drawn:

- The base oil-additive combination of a gear oil influences the nature of tribofilm formed during sliding contact conditions and affects the level of surface protection provided. This in turn determines the nature and extents of deformation induced below the surface; and consequently wear performance.

- In Chapters 4 and 5 where the tribo-pair of the friction tests consisted of a hardened AISI 52100 steel ball on a much softer spheroidised AISI 52100 steel disk, the extent of wear correlated with the degree of strain-hardening and grain refinement near the surface. Wear was much higher when the near-surface was significantly strain-hardened and the large microsized ferrite grains (characteristics of the unworn surface) were refined to nanometer sizes. Comparing the three gear oils near-surface properties, plastic strain hardening was relatively lower with Oil B which contains a friction modifier additive (amine molybdate) in combination with a ZDDP antiwear additive.

- The gear oils and the tribofilms they form also determine how plastic strain is distributed in the subsurface metal layer. Uniform strain-hardening with depth was consistently observed with Oil A, whereas with Oil B and Oil C, there was a gradient in the strain hardening with strain increasing significantly towards the surface especially with Oil C which generated the most severe case of strain hardening amongst the three oils.

- In Chapter 6 where the ball and disk used were both hardened AISI 52100 steel, severe wear corresponded to friction-induced softening of the near-surface metal layer.

- Higher oil temperatures and contact pressures increase the surface-additive interaction, giving rise to the formation of tribofilms with better frictional performance. However, higher temperatures and contact pressures also reduce the lubricant oil film thickness and increases direct metal contact between sliding surfaces. This consequently promotes near-surface hardening and degradation of the near-surface microstructural integrity and ultimately corresponds to worse wear performance.

  - The combination of relatively higher contact pressure and tribo-pair hardness ratio increases surface-additive interaction at low temperature (30 °C). In Chapter 5 mostly Iron oxide was measured on the worn surfaces when the three oils were tested with a contact pressure of 0.94GPa and

hardness ratio of 0.28. However, in Chapter 6 when the gear oils were tested with contact pressure of 1.9 GPa and tribo-pair hardness ratio of ≈ 1, low friction MoS_2 was measured on the surfaces lubricated by Oil A and Oil B, while FeS_2 was measured on the surface lubricated with Oil C.

- Combining the results of Chapters 4, 5 and 6, we hypothesise the level of wear protection from the gear oils depends on the materials used as the tribo-pair. It is influenced by the starting microstructure and its mechanical properties. Oil B provided the lowest wear rate under conditions of low contact pressures range between 0.44 GPa – 0.75 GPa; tribo-pair hardness ratio of 0.28 in the HFRR tests. In contrast, it failed to prevent severe wear under high contact pressure of 2.8 GPa; tribo-hardness ratio of≈ 1, whereas Oil A and Oil B maintained relatively low wear rate. Severe wear rate with Oil B was linked to significant softening of the near-surface structure of hardened AISI 52100 steel with the formation of adiabatic shear bands observed. This reiterates the importance of testing gear oils with operating conditions similar to those of their industrial application.

In summary this thesis highlights the importance of complementary surface and subsurface characterisation in the investigation of industrial gear oils.

7.2 Further work

- To better understand the relationship between gear oil formulations, their associated tribofilms, subsurface transformation and wear observed in this study, a greater understanding of the tribofilms generated is essential. This includes investigating:

  - The kinetics of tribofilm formation and their stability/durability during the tribo-process. A tribofilm that forms quickly and remains stable during the tribo-process is likely to minimise subsurface deformation and consequently wear. This would require finding a way to track the tribofilm formation in situ (during the tribo-process). Although the electrical contact resistance (ECR)

technique in-built into the HFRR tribometer was able to give some in situ information of the tribofilm, this technique could only track insulating films which means any conductive film formation is excluded from the result.

- Measuring the tribofilm chemistry in situ is still a challenge but remains vital to better understanding the exact mechanism of tribofilm formation. The exact mechanisms for many tribofilms still remain unknown or unclear. In this study and many others, the tribofilms are measured after the tribo-process and the residual oil has been removed. With this approach, it is challenging to accurately evaluate the intermediate chemical processes that occur.

- Time-of-Flight Secondary Ion Spectroscopy (ToF-SIMS) chemical characterisation technique would be useful for further study of the tribofilm chemistry. It is a surface-sensitive analytical method that can used to analyse elements and molecules present on the surface with high lateral resolution.

- The mechanical properties of the tribofilms (such as shear strength and hardness) as these are likely related to the extent of deformation induced into the subsurface.

- Measuring the stress-depth profile below the worn surfaces could potentially be useful in elucidating the differences in how the subsurface is strain-hardened or softened. In paper 2 (Chapter 5), the results showed that with Oil A strain hardening was consistently uniform with depth but with Oil B and Oil C, there was a gradient in strain-hardening.

References

1. Musial, W., Butterfield, S., McNiff, B.: Improving wind turbine gearbox reliability. In: European Wind Energy Conference, Milan, Italy 2007, pp. 7-10
2. Errichello, R.: Morphology of micropitting. Gear technology 4, 74-81 (2012).
3. Suh, N.P.: An overview of the delamination theory of wear. Wear 44(1), 1-16 (1977).
4. Jasim, K.M., Dwarakadasa, E.: Wear in Al-Si alloys under dry sliding conditions. Wear 119(1), 119-130 (1987).
5. Jahanmir, S., Suh, N.: Mechanics of subsurface void nucleation in delamination wear. wear 44(1), 17-38 (1977).
6. Kolubaev, A., Tarasov, S., Sizova, O., Kolubaev, E.: Scale-dependent subsurface deformation of metallic materials in sliding. Tribology International 43(4), 695-699 (2010).
7. Emge, A., Karthikeyan, S., Rigney, D.: The effects of sliding velocity and sliding time on nanocrystalline tribolayer development and properties in copper. Wear 267(1-4), 562-567 (2009).
8. Burghardt, G., Wächter, F., Jacobs, G., Hentschke, C.: Influence of run-in procedures and thermal surface treatment on the anti-wear performance of additive-free lubricant oils in rolling bearings. Wear 328, 309-317 (2015).
9. Hashimoto, F., Chaudhari, R.G., Melkote, S.N.: Characteristics and Performance of Surfaces Created by Various Finishing Methods. Procedia CIRP 45, 1-6 (2016).
10. Menezes, P.L., Kailas, S.V., Lovell, M.R.: Fundamentals of engineering surfaces. In: Tribology for Scientists and Engineers. pp. 3-41. Springer, (2013)
11. Bhushan, B.: Surface roughness analysis and measurement techniques. In: Modern Tribology Handbook, Two Volume Set. pp. 74-144. CRC press, (2000)
12. Gadelmawla, E., Koura, M., Maksoud, T., Elewa, I., Soliman, H.: Roughness parameters. Journal of Materials Processing Technology 123(1), 133-145 (2002).
13. Ai, X., Moyer, C.A.: Rolling element bearing. BRUSHAN, B. Modern Tribology handbook 2, 7.69-67.104 (2001).
14. Association, W.B.: Bearings and the Environment. http://www.bearingsandtheenvironment.com/portals/0/bearing-english.pdf (2008). Accessed 10th April 2015`
15. Bhadeshia, H.: Steels for bearings. Progress in materials Science 57(2), 268-435 (2012).
16. Song, W., von Appen, J., Choi, P., Dronskowski, R., Raabe, D., Bleck, W.: Atomic-scale investigation of ε and θ precipitates in bainite in 100Cr6 bearing steel by atom probe tomography and ab initio calculations. Acta Materialia 61(20), 7582-7590 (2013).
17. Song, W., Choi, P.-P., Inden, G., Prahl, U., Raabe, D., Bleck, W.: On the Spheroidized Carbide Dissolution and Elemental Partitioning in High Carbon Bearing Steel 100Cr6. Metallurgical and Materials Transactions A 45(2), 595-606 (2014).

18. Luzginova, N., Zhao, L., Sietsma, J.: The cementite spheroidization process in high-carbon steels with different chromium contents. Metallurgical and Materials Transactions A 39(3), 513-521 (2008).
19. Dossett, J., Totten, G.J.A.H.: Introduction to Surface Hardening of Steels. 4, 389-398 (2013).
20. Kuhn, M., Gold, P.W., Loos, J.: Wear and friction characteristics of PVD-coated roller bearings. Surface and Coatings Technology 177–178(0), 469-476 (2004). doi:http://dx.doi.org/10.1016/S0257-8972(03)00914-9
21. Akagaki, T., Kato, K.: Plastic flow process of surface layers in flow wear under boundary lubricated conditions. Wear 117(2), 179-196 (1987).
22. Komvopoulos, K., Saka, N., Suh, N.: The mechanism of friction in boundary lubrication. Journal of tribology 107(4), 452-462 (1985).
23. Komvopoulos, K., Suh, N.P., Saka, N.: Wear of boundary-lubricated metal surfaces. Wear 107(2), 107-132 (1986).
24. Jahanmir, S.: The relationship of tangential stress to wear particle formation mechanisms. Wear 103(3), 233-252 (1985).
25. Suh, N.P.J.W.: The delamination theory of wear. 25(1), 111-124 (1973).
26. Jahanmir, S., Suh, N., Abrahamson, E.J.W.: Microscopic observations of the wear sheet formation by delamination. 28(2), 235-249 (1974).
27. Saka, N., Suh, N.J.J.o.E.f.I.: Delamination wear of dispersion-hardened alloys. 99(2), 289-294 (1977).
28. Kotzalas, M.N., Doll, G.L.: Tribological advancements for reliable wind turbine performance. Philosophical Transactions of the Royal Society of London A: Mathematical, Physical and Engineering Sciences 368(1929), 4829-4850 (2010).
29. Moorthy, V., Shaw, B.: An observation on the initiation of micro-pitting damage in as-ground and coated gears during contact fatigue. Wear 297(1-2), 878-884 (2013).
30. Oila, A., Bull, S.: Assessment of the factors influencing micropitting in rolling/sliding contacts. Wear 258(10), 1510-1524 (2005).
31. Papay, A.: Antiwear and extreme-pressure additives in lubricants. Lubrication Science 10(3), 209-224 (1998).
32. Cizaire, L., Martin, J., Gresser, E., Dinh, N.T., Heau, C.: Tribochemistry of overbased calcium detergents studied by ToF-SIMS and other surface analyses. Tribology Letters 17(4), 715-721 (2004).
33. Spikes, H.: The history and mechanisms of ZDDP. Tribology letters 17(3), 469-489 (2004).
34. Fuller, M.L.S., Kasrai, M., Bancroft, G.M., Fyfe, K., Tan, K.H.: Solution decomposition of zinc dialkyl dithiophosphate and its effect on antiwear and thermal film formation studied by X-ray absorption spectroscopy. Tribology international 31(10), 627-644 (1998).
35. Fujita, H., Spikes, H.: The formation of zinc dithiophosphate antiwear films. Proceedings of the Institution of Mechanical Engineers, Part J: Journal of Engineering Tribology 218(4), 265-278 (2004).
36. Yin, Z., Kasrai, M., Fuller, M., Bancroft, G.M., Fyfe, K., Tan, K.H.: Application of soft X-ray absorption spectroscopy in chemical characterization of antiwear

films generated by ZDDP Part I: the effects of physical parameters. Wear 202(2), 172-191 (1997).
37. Martin, J.M., Grossiord, C., Le Mogne, T., Bec, S., Tonck, A.: The two-layer structure of Zndtp tribofilms: Part I: AES, XPS and XANES analyses. Tribology international 34(8), 523-530 (2001).
38. Martin, J., Minfray, C.: Antiwear chemistry in presence of ZDDP. In: World Tribology Congress III 2005, pp. 599-600. American Society of Mechanical Engineers
39. Bell, J., Delargy, K.: The composition and structure of model zinc dialkyldithiophosphate anti-wear films. In: Proc. 6th Inter. Congress on Tribology „Eurotrib 1993
40. Choa, S.-H., Ludema, K.C., Potter, G.E., Dekoven, B.M., Morgan, T.A., Kar, K.K.: A model of the dynamics of boundary film formation. Wear 177(1), 33-45 (1994). doi:http://dx.doi.org/10.1016/0043-1648(94)90115-5
41. Bec, S., Tonck, A., Georges, J.-M., Roper, G.W.: Synergistic effects of MoDTC and ZDTP on frictional behaviour of tribofilms at the nanometer scale. Tribology Letters 17(4), 797-809 (2004).
42. Dorgham, A., Neville, A., Ignatyev, K., Mosselmans, F., Morina, A.J.R.o.S.I.: An in situ synchrotron XAS methodology for surface analysis under high temperature, pressure, and shear. 88(1), 015101 (2017).
43. Zhang, J., Spikes, H.: On the mechanism of ZDDP antiwear film formation. Tribology Letters 63(2), 24 (2016).
44. Onodera, T., Martin, J.M., Minfray, C., Dassenoy, F., Miyamoto, A.J.T.L.: Antiwear chemistry of ZDDP: coupling classical MD and tight-binding quantum chemical MD methods (TB-QCMD). 50(1), 31-39 (2013).
45. Aktary, M., McDermott, M.T., McAlpine, G.A.: Morphology and nanomechanical properties of ZDDP antiwear films as a function of tribological contact time. Tribology letters 12(3), 155-162 (2002).
46. Ye, J., Kano, M., Yasuda, Y.: Evaluation of nanoscale friction depth distribution in ZDDP and MoDTC tribochemical reacted films using a nanoscratch method. Tribology Letters 16(1-2), 107-112 (2004).
47. Ye, J., Kano, M., Yasuda, Y.: Evaluation of local mechanical properties in depth in MoDTC/ZDDP and ZDDP tribochemical reacted films using nanoindentation. Tribology Letters 13(1), 41-47 (2002).
48. Morina, A., Neville, A.: Tribofilms: aspects of formation, stability and removal. Journal of Physics D: Applied Physics 40(18), 5476 (2007).
49. Parsaeian, P., Ghanbarzadeh, A., Van Eijk, M.C., Nedelcu, I., Neville, A., Morina, A.: A new insight into the interfacial mechanisms of the tribofilm formed by zinc dialkyl dithiophosphate. Applied Surface Science 403, 472-486 (2017).
50. Morina, A., Neville, A., Priest, M., Green, J.: ZDDP and MoDTC interactions in boundary lubrication—the effect of temperature and ZDDP/MoDTC ratio. Tribology international 39(12), 1545-1557 (2006).
51. Zhang, Z., Yamaguchi, E., Kasrai, M., Bancroft, G.: Tribofilms generated from ZDDP and DDP on steel surfaces: Part 1, growth, wear and morphology. Tribology Letters 19(3), 211-220 (2005).

52. Tang, Z., Li, S.: A review of recent developments of friction modifiers for liquid lubricants (2007–present). Current opinion in solid state and materials science 18(3), 119-139 (2014).
53. Spikes, H.: Friction modifier additives. Tribology Letters 60(1), 5 (2015).
54. Miklozic, K.T., Graham, J., Spikes, H.: Chemical and physical analysis of reaction films formed by molybdenum dialkyl-dithiocarbamate friction modifier additive using Raman and atomic force microscopy. Tribology Letters 11(2), 71-81 (2001).
55. Khaemba, D.N., Neville, A., Morina, A.: New insights on the decomposition mechanism of Molybdenum DialkyldiThioCarbamate (MoDTC): a Raman spectroscopic study. RSC Advances 6(45), 38637-38646 (2016).
56. Grossiord, C., Varlot, K., Martin, J.-M., Le Mogne, T., Esnouf, C., Inoue, K.: MoS2 single sheet lubrication by molybdenum dithiocarbamate. Tribology international 31(12), 737-743 (1998).
57. Unnikrishnan, R., Jain, M., Harinarayan, A., Mehta, A.: Additive–additive interaction: an XPS study of the effect of ZDDP on the AW/EP characteristics of molybdenum based additives. Wear 252(3-4), 240-249 (2002).
58. Muraki, M., Yanagi, Y., Sakaguchi, K.: Synergistic effect on frictional characteristics under rolling-sliding conditions due to a combination of molybdenum dialkyldithiocarbamate and zinc dialkyldithiophosphate. Tribology international 30(1), 69-75 (1997).
59. Rehbinder, P.: About influence of changing surface on cleavage hardness and other crystal properties. In: Proceedings of 6th Physical Congress, Moscow 1928
60. Buckley, D.H.: Effect of surface active media on friction, deformation, and fracture of calcium fluoride. (1969).
61. Cao, S., Sarasin, F., Cantoni, M., Mischler, S.: Effect of surface films on tribologically induced metallurgical transformations of steel in oil lubricated contacts. Wear 368, 75-83 (2016).
62. Reichelt, M., Gunst, U., Wolf, T., Mayer, J., Arlinghaus, H.F., Gold, P.W.: Nanoindentation, TEM and ToF-SIMS studies of the tribological layer system of cylindrical roller thrust bearings lubricated with different oil additive formulations. Wear 268(11-12), 1205-1213 (2010).
63. Qu, J., Bansal, D.G., Yu, B., Howe, J.Y., Luo, H., Dai, S., Li, H., Blau, P.J., Bunting, B.G., Mordukhovich, G.: Antiwear performance and mechanism of an oil-miscible ionic liquid as a lubricant additive. ACS applied materials & interfaces 4(2), 997-1002 (2012).
64. Wang, Z., Yan, Y., Su, Y., Qiao, L.: Effect of proteins on the surface microstructure evolution of a CoCrMo alloy in bio-tribocorrosion processes. Colloids and Surfaces B: Biointerfaces 145, 176-184 (2016).
65. Fouvry, S., Liskiewicz, T., Kapsa, P., Hannel, S., Sauger, E.: An energy description of wear mechanisms and its applications to oscillating sliding contacts. Wear 255(1-6), 287-298 (2003).
66. Specifications, G.P.: Surface Texture: Profile Method–Rules and Procedures for the Assessment of Surface Texture. EN ISO 4288 (2000).
67. Moore, M.: The relationship between the abrasive wear resistance, hardness and microstructure of ferritic materials. Wear 28(1), 59-68 (1974).

68. Li, X., Bhushan, B.: A review of nanoindentation continuous stiffness measurement technique and its applications. Materials characterization 48(1), 11-36 (2002).
69. Butler, H.J., Ashton, L., Bird, B., Cinque, G., Curtis, K., Dorney, J., Esmonde-White, K., Fullwood, N.J., Gardner, B., Martin-Hirsch, P.L.: Using Raman spectroscopy to characterize biological materials. Nature protocols 11(4), 664 (2016).
70. Inkson, B.: Scanning electron microscopy (SEM) and transmission electron microscopy (TEM) for materials characterization. In: Materials characterization using nondestructive evaluation (NDE) methods. pp. 17-43. Elsevier, (2016)
71. Spalvins, T.: A review of recent advances in solid film lubrication. Journal of Vacuum Science & Technology A: Vacuum, Surfaces, and Films 5(2), 212-219 (1987).
72. Guerret-Piécourt, C., Grossiord, C., Le Mogne, T., Martin, J., Palermo, T.: Tribochemical interactions between molybdenum dithiophosphate and succinimide additives. Surface and interface analysis 30(1), 646-650 (2000).
73. Yamamoto, Y., Gondo, S.: Friction and wear characteristics of molybdenum dithiocarbamate and molybdenum dithiophosphate. Tribology Transactions 32(2), 251-257 (1989).
74. Yamamoto, Y., Gondo, S.: Environmental Effects on the Composition of Surface Films Produced by an Organo-Molybdenum Compound©. Tribology transactions 37(1), 182-188 (1994).
75. Unnikrishnan, R., Jain, M.C., Harinarayan, A.K., Mehta, A.K.: Additive–additive interaction: an XPS study of the effect of ZDDP on the AW/EP characteristics of molybdenum based additives. Wear 252(3–4), 240-249 (2002). doi:http://dx.doi.org/10.1016/S0043-1648(01)00865-1
76. Grossiord, C., Varlot, K., Martin, J.M., Le Mogne, T., Esnouf, C., Inoue, K.: MoS2 single sheet lubrication by molybdenum dithiocarbamate. Tribology International 31(12), 737-743 (1998). doi:https://doi.org/10.1016/S0301-679X(98)00094-2
77. Evans, R.D., Doll, G.L., Hager, C., Howe, J.Y.: Influence of steel type on the propensity for tribochemical wear in boundary lubrication with a wind turbine gear oil. Tribology letters 38(1), 25-32 (2010).
78. Wieting, T.: Long-wavelength lattice vibrations of MoS2 and GaSe. Solid State Communications 12(9), 931-935 (1973).
79. Jahanmir, S.: Wear reduction and surface layer formation by a ZDDP additive. ASME, Transactions, Journal of Tribology 109, 577-586 (1987).
80. Rigney, D., Glaeser, W.: The significance of near surface microstructure in the wear process. Wear 46(1), 241-250 (1978).
81. Rice, S., Nowotny, H., Wayne, S.: A survey of the development of subsurface zones in the wear of materials. In: Key Engineering Materials 1989, pp. 77-100. Trans Tech Publ
82. Rehbinder, P.: About influence of changing surface on cleavage hardness and other crystal properties. In: Proc 6th Phys Congress. Moscow 1928
83. Kajdas, C., Majzner, M.: Boundary lubrication of low-sulphur diesel fuel in the presence of fatty acids. Lubrication science 14(1), 83-108 (2001).

84. Oliver, W.C., Pharr, G.M.: An improved technique for determining hardness and elastic modulus using load and displacement sensing indentation experiments. Journal of materials research 7(6), 1564-1583 (1992).
85. Suzuki, T., Endo, N., Shibata, M., Kamasaki, S., Ichinokawa, T.: Contrast differences between scanning ion and scanning electron microscope images. Journal of Vacuum Science & Technology A: Vacuum, Surfaces, and Films 22(1), 49-52 (2004).
86. Keller, R.R., Geiss, R.H.: Transmission EBSD from 10 nm domains in a scanning electron microscope. Journal of Microscopy 245(3), 245-251 (2012).
87. Mayer, J., Giannuzzi, L.A., Kamino, T., Michael, J.: TEM sample preparation and FIB-induced damage. MRS bulletin 32(5), 400-407 (2007).
88. Sarin, R., Tuli, D., Sureshbabu, A., Misra, A., Rai, M., Bhatnagar, A.: Molybdenum dialkylphosphorodithioates: synthesis and performance evaluation as multifunctional additives for lubricants. Tribology international 27(6), 379-386 (1994).
89. Khaemba, D.N., Neville, A., Morina, A.: A methodology for Raman characterisation of MoDTC tribofilms and its application in investigating the influence of surface chemistry on friction performance of MoDTC lubricants. Tribology Letters 59(3), 38 (2015).
90. Graham, J., Spikes, H., Korcek, S.: The friction reducing properties of molybdenum dialkyldithiocarbamate additives: part I—factors influencing friction reduction. Tribology Transactions 44(4), 626-636 (2001).
91. Bowden, F., Ridler, K.: Physical properties of surfaces-III—The surface temperature of sliding metals-The temperature of lubricated surfaces. In: Proc. R. Soc. Lond. A 1936, vol. 883, pp. 640-656. The Royal Society
92. Klamecki, B.E.: Energy dissipation in sliding. Wear 77(1), 115-128 (1982).
93. Huq, M., Celis, J.-P.: Expressing wear rate in sliding contacts based on dissipated energy. Wear 252(5-6), 375-383 (2002).
94. Tao, N.R., Wang, Z.B., Tong, W.P., Sui, M.L., Lu, J., Lu, K.: An investigation of surface nanocrystallization mechanism in Fe induced by surface mechanical attrition treatment. Acta Materialia 50(18), 4603-4616 (2002). doi:https://doi.org/10.1016/S1359-6454(02)00310-5
95. Zhou, L., Liu, G., Ma, X., Lu, K.: Strain-induced refinement in a steel with spheroidal cementite subjected to surface mechanical attrition treatment. Acta Materialia 56(1), 78-87 (2008).
96. Buckley, D.H.: Influence of surface active agents on friction, deformation, and fracture of lithium fluoride. (1964).
97. Tangena, A.G.: Tribology of thin film systems. (1987).
98. Croft, M., Jisrawi, N., Zhong, Z., Horvath, K., Holtz, R.L., Shepard, M., Lakshmipathy, M., Sadananda, K., Skaritka, J., Shukla, V., Sadangi, R.K., Tsakalakos, T.: Stress Gradient Induced Strain Localization in Metals: High Resolution Strain Cross Sectioning via Synchrotron X-Ray Diffraction. Journal of Engineering Materials and Technology 130(2), 021005-021005-021010 (2008). doi:10.1115/1.2840962
99. Büscher, R., Täger, G., Dudzinski, W., Gleising, B., Wimmer, M., Fischer, A.: Subsurface microstructure of metal-on-metal hip joints and its relationship

to wear particle generation. Journal of Biomedical Materials Research Part B: Applied Biomaterials 72(1), 206-214 (2005).
100. Panin, V., Kolubaev, A., Tarasov, S., Popov, V.: Subsurface layer formation during sliding friction. Wear 249(10-11), 860-867 (2001).
101. Hashimoto, C., Okubo, H., Tadokoro, C., Sasaki, S.: Correlation between nano-mechanical and macro-tribological properties of tribofilms derived from organic phosphoric additives. Tribology Online 11(5), 632-638 (2016).
102. Landauer, A.K., Barnhill, W.C., Qu, J.: Correlating mechanical properties and anti-wear performance of tribofilms formed by ionic liquids, ZDDP and their combinations. Wear 354, 78-82 (2016).
103. Tung, S.C., Gao, H.: A study of break-in film development with different piston ring coatings and correlation with electrical contact resistance measurements. Tribology transactions 46(3), 326-331 (2003).
104. Fujita, H., Glovnea, R., Spikes, H.: Study of zinc dialkydithiophosphate antiwear film formation and removal processes, part I: experimental. Tribology transactions 48(4), 558-566 (2005).
105. Ji, H., Nicholls, M.A., Norton, P.R., Kasrai, M., Capehart, T.W., Perry, T.A., Cheng, Y.-T.: Zinc-dialkyl-dithiophosphate antiwear films: dependence on contact pressure and sliding speed. Wear 258(5-6), 789-799 (2005).
106. Morina, A., Neville, A.: Understanding the composition and low friction tribofilm formation/removal in boundary lubrication. Tribology International 40(10-12), 1696-1704 (2007).
107. Komvopoulos, K., Chiaro, V., Pakter, B., Yamaguchi, E., Ryason, P.: Antiwear tribofilm formation on steel surfaces lubricated with gear oil containing borate, phosphorus, and sulfur additives. Tribology transactions 45(4), 568-575 (2002).
108. Minfray, C., Martin, J.-M., Lubrecht, T., Belin, M., Le Mogne, T.: A novel experimental analysis of the rheology of ZDDP tribofilms. In: Tribology Series, vol. 41. pp. 807-817. Elsevier, (2003)
109. Gosvami, N., Bares, J., Mangolini, F., Konicek, A., Yablon, D., Carpick, R.: Mechanisms of antiwear tribofilm growth revealed in situ by single-asperity sliding contacts. Science 348(6230), 102-106 (2015).
110. Martin, J.M., Grossiord, C., Varlot, K., Vacher, B., Igarashi, J.: Synergistic effects in binary systems of lubricant additives: a chemical hardness approach. Tribology Letters 8(4), 193-201 (2000).
111. Morina, A., Neville, A., Priest, M., Green, J.: ZDDP and MoDTC interactions and their effect on tribological performance–tribofilm characteristics and its evolution. Tribology Letters 24(3), 243-256 (2006).
112. Adebogun, A., Hudson, R., Breakspear, A., Warrens, C., Gholinia, A., Matthews, A., Withers, P.: Industrial Gear Oils: Tribological Performance and Subsurface Changes. Tribology Letters 66(2), 65 (2018).
113. Hamrock, B.J., Dowson, D.: Minimum film thickness in elliptical contacts for different regimes of fluid-film lubrication. (1978).
114. Thibeau, R.J., Brown, C.W., Heidersbach, R.H.: Raman spectra of possible corrosion products of iron. Applied Spectroscopy 32(6), 532-535 (1978).

115. Vogt, H., Chattopadhyay, T., Stolz, H.: Complete first-order Raman spectra of the pyrite structure compounds FeS2, MnS2 and SiP2. Journal of Physics and Chemistry of Solids 44(9), 869-873 (1983).
116. Najman, M., Kasrai, M., Bancroft, G.: X-ray absorption spectroscopy and atomic force microscopy of films generated from organosulfur extreme-pressure (EP) oil additives. Tribology Letters 14(4), 225-235 (2003).
117. Miyajima, M., Kitamura, K., Matsumoto, K.: Characterization of Tribofilm with the Remaining Lubricating Oil by Raman Spectroscopy. Tribology Online 10(3), 225-231 (2015).
118. Costello, M.T., Urrego, R.A.: Study of surface films of the ZDDP and the MoDTC with crystalline and amorphous overbased calcium sulfonates by XPS. Tribology transactions 50(2), 217-226 (2007).
119. Wei, D., Song, H., Wang, R.: An investigation of the effects of some motor oil additives on the friction and wear behaviour of oil-soluble organomolybdenum compounds. Lubrication Science 4(1), 51-72 (1991).
120. Minfray, C., Martin, J., De Barros, M., Le Mogne, T., Kersting, R., Hagenhoff, B.: Chemistry of ZDDP tribofilm by ToF-SIMS. Tribology Letters 17(3), 351-357 (2004).
121. Komvopoulos, K., Do, V., Yamaguchi, E., Yeh, S., Ryason, P.: X-ray photoelectron spectroscopy analysis of antiwear tribofilms produced on boundary-lubricated steel surfaces from sulfur-and phosphorus-containing additives and metal deactivator additive. Tribology transactions 47(3), 321-327 (2004).
122. Evans, R.D., More, K.L., Darragh, C.V., Nixon, H.P.: Transmission electron microscopy of boundary-lubricated bearing surfaces. Part II: Mineral oil lubricant with sulfur-and phosphorus-containing gear oil additives. Tribology Transactions 48(3), 299-307 (2005).
123. Sakamoto, T., Uetz, H., Föhl, J., Khosrawi, M.: The reaction layer formed on steel by additives based on sulphur and phosphorus compounds under conditions of boundary lubrication. Wear 77(2), 139-157 (1982).
124. Yamamoto, Y., Gondo, S., Kamakura, T., Tanaka, N.: Frictional characteristics of molybdenum dithiophosphates. Wear 112(1), 79-87 (1986).
125. Bancroft, G., Kasrai, M., Fuller, M., Yin, Z., Fyfe, K., Tan, K.H.: Mechanisms of tribochemical film formation: stabilityof tribo-and thermally-generated ZDDP films. Tribology Letters 3(1), 47-51 (1997).
126. Weertman, J.: Hall-Petch strengthening in nanocrystalline metals. Materials Science and Engineering: A 166(1-2), 161-167 (1993).
127. Spikes, H.: Stress-augmented thermal activation: Tribology feels the force. Friction 6(1), 1-31 (2018). doi:10.1007/s40544-018-0201-2
128. Nehme, G., Mourhatch, R., Aswath, P.B.: Effect of contact load and lubricant volume on the properties of tribofilms formed under boundary lubrication in a fully formulated oil under extreme load conditions. Wear 268(9-10), 1129-1147 (2010).
129. Archard, J.: Contact and rubbing of flat surfaces. Journal of applied physics 24(8), 981-988 (1953).
130. Rigney, D.: The roles of hardness in the sliding behavior of materials. Wear 175(1-2), 63-69 (1994).

131. Razhkovskiy, A., Bunkova, T., Petrakova, A., Gateluk, O.: Optimization of hardness ratio in rail–wheel friction pair. Journal of Friction and Wear 36(4), 334-341 (2015).
132. Zhai, W., Shi, X., Ibrahim, A.M.M., Xu, Z., Yang, K., Zhang, Q.: Effect of hardness ratio on the wear performance and subsurface evolution of Ni3Al matrix composites. Tribology Transactions 60(5), 902-912 (2017).
133. Büscher, R., Täger, G., Dudzinski, W., Gleising, B., Wimmer, M., Fischer, A.: Subsurface microstructure of metal-on-metal hip joints and its relationship to wear particle generation. Journal of Biomedical Materials Research Part B: Applied Biomaterials: An Official Journal of The Society for Biomaterials, The Japanese Society for Biomaterials, and The Australian Society for Biomaterials and the Korean Society for Biomaterials 72(1), 206-214 (2005).
134. Shakhvorostov, D., Gleising, B., Büscher, R., Dudzinski, W., Fischer, A., Scherge, M.: Microstructure of tribologically induced nanolayers produced at ultra-low wear rates. Wear 263(7-12), 1259-1265 (2007).
135. Zhang, B., Shen, W., Liu, Y., Tang, X., Wang, Y.: Microstructures of surface white layer and internal white adiabatic shear band. Wear 211(2), 164-168 (1997).
136. Habak, M., Lebrun, J.L., Morel, A.: A study of the influence of the metallurgical state on shear band and white layer generation in 100Cr6 steel: application to machining. In: AIP Conference Proceedings 2007, vol. 1, pp. 691-696. AIP
137. Mgbokwere, C., Nutt, S., Duffy, J.: Shear band formation in 4340 steel: A TEM study. Mechanics of materials 17(2-3), 97-110 (1994).
138. Barry, J., Byrne, G.: TEM study on the surface white layer in two turned hardened steels. Materials Science and Engineering: A 325(1-2), 356-364 (2002).
139. Cho, K.-M., Lee, S., Nutt, S., Duffy, J.: Adiabatic shear band formation during dynamic torsional deformation of an HY-100 steel. Acta Metallurgica et Materialia 41(3), 923-932 (1993).
140. Stacy, A., Hodul, D.: Raman spectra of IVB and VIB transition metal disulfides using laser energies near the absorption edges. Journal of Physics and Chemistry of Solids 46(4), 405-409 (1985).
141. Chen, J., Wang, C.: Second order Raman spectrum of MoS2. Solid State Communications 14(9), 857-860 (1974).
142. Topolovec-Miklozic, K., Forbus, T.R., Spikes, H.: Film forming and friction properties of overbased calcium sulphonate detergents. Tribology Letters 29(1), 33-44 (2008).
143. Zhongyi, H., Liping, X., Sheng, H., Aixi, C., Jianwei, Q., Xisheng, F.: Tribological and antioxidation synergistic effect study of sulfonate-modified nano calcium carbonate. PLoS One 8(5), e62050 (2013).
144. Rai, Y., Neville, A., Morina, A.: Transient processes of MoS2 tribofilm formation under boundary lubrication. Lubrication Science 28(7), 449-471 (2016).
145. Haque, T., Morina, A., Neville, A., Arrowsmith, S.: Tribochemical interactions of friction modifier and antiwear additives with CrN coating under boundary lubrication conditions. Journal of Tribology 130(4), 042302 (2008).

146. Mote, V., Purushotham, Y., Dole, B.: Williamson-Hall analysis in estimation of lattice strain in nanometer-sized ZnO particles. Journal of Theoretical and Applied Physics 6(1), 6 (2012).
147. Zak, A.K., Majid, W.A., Abrishami, M.E., Yousefi, R.: X-ray analysis of ZnO nanoparticles by Williamson–Hall and size–strain plot methods. Solid State Sciences 13(1), 251-256 (2011).
148. Fu, P., Jiang, C.: Residual stress relaxation and micro-structural development of the surface layer of 18CrNiMo7-6 steel after shot peening during isothermal annealing. Materials & Design (1980-2015) 56, 1034-1038 (2014).
149. Malek, M.F., Mamat, M.H., Musa, M.Z., Khusaimi, Z., Sahdan, M.Z., Suriani, A.B., Ishak, A., Saurdi, I., Rahman, S.A., Rusop, M.: Thermal annealing-induced formation of ZnO nanoparticles: Minimum strain and stress ameliorate preferred c-axis orientation and crystal-growth properties. Journal of Alloys and Compounds 610, 575-588 (2014). doi:https://doi.org/10.1016/j.jallcom.2014.05.036
150. Fu, P., Chu, R., Xu, Z., Ding, G., Jiang, C.: Relation of hardness with FWHM and residual stress of GCr15 steel after shot peening. Applied Surface Science 431, 165-169 (2018).

BLANK